Color appearance of extreme fine stimuli: effect of optical and neural factors

(微細刺激の色の見えに寄与する眼光学と神経的要因)

January 2022

Doctor of Philosophy (Engineering)

Tama Kanematsu
兼松　圭

Toyohashi University of Technology

別紙４－１（課程博士（英文））

Date of Submission（month day, year）: January 7th, 2022

Department of Computer Science of Engineering	Student ID Number	D131304
Applicant's name	Tama Kanematsu	

Supervisors	Kowa Koida Shigeki Nakauchi

Abstract（Doctor）

Title of Thesis	Color appearance of extreme fine stimuli: effect of optical and neural factors

Approx. 800 words

The colors of fine details are essential in our lives. For example, fabrics are made of various colored threads, and facial emotions are expressed by faint colors of the cheeks and lips. The importance of fine color details has increased in the era of high-resolution displays. It is known that a surrounding area influences the color appearance of a center area, and the influence becomes critical for detailed images. It is also known that the optical artifacts of the human eye, such as blurring and chromatic aberrations, degrade fine details and the colors of images. These neural and optical effects are integrated via the visual system and form our perception. Thus, it is important to differentiate these effects to understand how our color vision works.

This thesis focuses on the Monnier-Shevell illusion, which induces a significant color shift of a center stimulus according to two surrounding, spatially alternating complementary colors. The illusion is evident for S-cone colors (blue–yellow pairs) but not for L/M-cone colors (red-green pairs) for unknown reasons. It is thought that the effect works better for S-cone colors because the illusion is due to a synergistic effect of assimilation from the proximal colors and contrast from the distantly surrounding colors, and known spatial representation of colors in the early visual system is comparable for both S-cone and L/M-cone colors except for its spatial resolution. Here, I report a new spatial context of the Monnier-Shevell illusion, in which a thin gray line (test line) flanked with white lines (contour) appears reddish when surrounded by a uniform cyan. Psychological experiments and simulations excluded the possibility of the illusion being induced by optical artifacts. Experiment 2 showed that a chromatic (as opposed to an achromatic) contour modified color shifts, indicating linear summation of the color induction effect, chroma of the contour, and chroma of the test. In Experiment 3, I investigated the effect of line widths of the illusion and found that maximum effects for the L/M-cone colors were 0.9 and 1.9 min of visual angle for the contour and the test line. These widths corresponded to the width of a single photoreceptor and were eight times thinner than optimal widths for the S-cone colors. Observed differences of the optimal widths between two colors could reflect the known difference in spatial property between two colors.

Experiment 4 examined the effect of luminance contrast of the contour and found that a black contour instead of a white one diminished the illusory effect, indicating the importance of the white contour, and simple spatial organization along the chromatic axis failed to explain the illusion.

Simulation of the chromatic shift due to optical artifacts predicted the large chromatic shift at the retina; however, perceived color closely matched the actual chromaticity of the stimuli. This indicates that the human color system seems to provide veridical perception of color using some type of compensation, which could be attained through contrast enhancement from distant surroundings. This compensation works well for simple uniform backgrounds, but patterned backgrounds, such as our stimuli of flanking white contours and the original Monnier-Shevell illusion, induce an unexpectedly large color shift because the flanking white contours break the balance between the proximal assimilation and distant contrast effects. This interpretation suggests the Monnier-Shevell illusion is the side effect of removing chromatic shifts by the optical artifacts. This thesis describes the color appearances of fine stimuli and the effect of the complex spatial context. The neural mechanisms and models revealed here are useful for modern high-definition image-engineering applications.

Acknowledgements

I would like to thank my supervisor Kowa Koida for all the discussions, comments, and advice. I have taught him kindly that human vision science is full of interesting questions, and how to solve those. I also received generous support from the open and flat atmosphere in his Lab for six years.

I would like to thank two co-referees Shigeki Nakauchi and Tetsuto Minami for their useful comments and support. Their comments made my research sophisticated and their support gave me many chances to meet many other researchers in the vision science field.

I would like to thank our lab members for many questions and many helping me out in my research.

I would like to appreciate the support from KAKENHI Grant Number JP20J12600 (Japan Society for the Promotion of Science), and the scholarship and tuition fee exemption from Toyohashi University of Technology.

Finally, I am very grateful for my family members.

Contents

List of Figures

List of Tables

Chapter 1

Introduction

1.1 Fine color perception

Color appearance depends on spatial context. This dependence was discovered in the 19th century by the French chemist Michel-Eugëne Chevreul. He was named the director of Manufacture des Gobelins, which created dye products in Paris to establish dye quality. The factory created a tapestry (**Fig. 1.1A**) and furniture for royal, so the weave was drawn with complex illustrations and rich colors (**Fig. 1.1B**). Fine color details provide a subjective experience, such as some impression of the tapestry, so strict calibration is important to display an actual color.

He encountered the complaint that the light-blue, violet, gray, and black Gobelins weave tended to appear as low-quality (Chevreul 1839). He observed that black appeared less vivid when drawing a shadow in violet and blue draperies and revealed that the appearance was not due to dye quality. Therefore, the complaints of the black weave were due to human perception. He performed experiments and named the phenomenon simultaneous chromatic contrast. This phenomenon indicates that the surrounding chromaticity affects the appearance of fine stimuli.

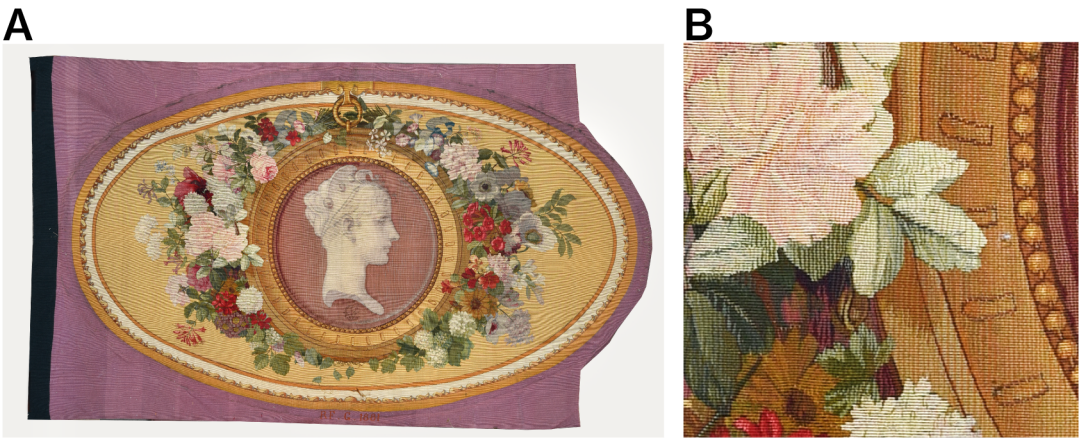

Figure 1.1 Example of a tapestry (**A**) and enlarged the example (**B**)
This tapestry is "TAPISSERIE DE LICE" hung at a door of Elysée Palace, created by Manufacture des Gobelins in 1889. The photograph was obtained from Collection du Mobilier national (https://collection.mobiliernational.culture.gouv.fr/).

Two factors affect the quality of spatial vision. The first is optics, which collects light from the surroundings. The collection ability is critical for spatial vision because the light reflects on surfaces in the surroundings and contains information about spatial changes. The second is the sampling function that receives the light. The sampling becomes finer if the sampling sensor lies densely on the focus plane of the light.

Human vision has a notable feature, spatial vision, compared to other species. Visual acuity is the ability to resolve static spatial detail. **Fig. 1.2** shows the comparison of the visual acuity between species. The vertical axis unit is cycles per degree (cpd), which indicates the resolved number of black and white stripes at a viewing angle of 1 deg. Therefore, the larger the cpd, the finer is the visual acuity. Human visual acuity is estimated to be approximately 60 cpd (top right in **Fig. 1.2)**, which is higher than that of most species (Caves, Brandley, & Johnsen 2018). Further, eye structure and retina support human visual acuity. The eye's optical system reduces diffraction compared to compound eyes, resulting in higher image quality. The number of image sensors that resolve the image determines the upper visual-resolution limit. A larger eye can pack several sensors. The image sensor on the retina is densely packed at the center of the gaze. Hence, the human vision of the gaze treats fine details that the optics restrict. Interestingly, the image sensors at the gaze specialize in color vision, not only spatial. Therefore, fine perception is an aspect of human color vision.

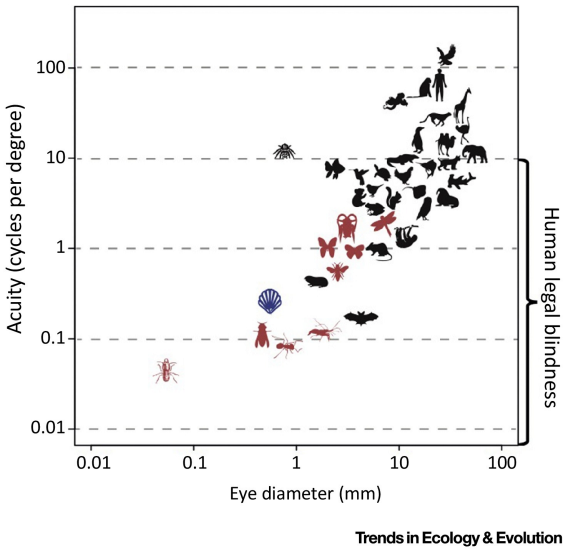

Figure 1.2 Visual acuity across species

The horizontal axis indicates the eye diameter of each species. The vertical axis indicates visual acuity. The higher the vertical axis, the better is the acuity. Each icon represents the acuity of a species. Black, red, and blue icons represent species with a camera, compound, and mirror eyes, respectively. This figure is obtained from Caves, Brandley, & Johnsen (2018). See the supplemental information for the actual values.

The human visual resolution has been well investigated. Contrastingly, studies on color appearance in fine stimuli have received little attention. Some studies have been conducted on the appearance of fine stimuli. However, broadening these studies was challenging because the apparatus could not show sufficient color depth or complicated fine shapes. Although it is possible to make coarse stimuli appear finer by increasing the viewing distance, this distance does not match the optimal focus position for humans. The longer the viewing distance, the more severe the human lens adjustment. The formerly advanced apparatus, the CRT monitor, was useful for showing fine color stimuli. However, it had a problem; the resolution was small. Another issue is that previous studies used unnatural stimuli to avoid artifacts. The stimuli in the experimental room cannot reveal what humans perceive, even if they can understand the neural mechanisms. Although many unnatural stimuli results have greatly advanced human visual science, investigations of the color perception of fine stimuli remain. Color vision science has insufficiently revealed why human vision has the color perception of fine stimuli.

Why should we understand the mechanism of color perception of fine stimuli? There are three reasons for this finding: The first of these is social communication. The second is to provide evidence to support rapid popularization. The third is using an efficient color perception of fine stimuli to create products.

First, they may be for the sake of social communication and health. Components of the human face can convey emotions, such as happiness, sadness, anger, and excitement. For example, the angle of the eyebrows or lips represents excitement or anger (**Fig. 1.3)**. The reddish lip suggests that they are in good health, and the bluish lip does not. Thus, the color perception of fine stimuli is needed to detect the emotions or health of others.

Figure 1.3 Examples of excited or angry faces
The images were from Multi-Task Facial Landmark dataset
(http://mmlab.ie.cuhk.edu.hk/projects/TCDCN.html).

Second, the industry seems to pay attention to the color perception of the fine stimuli of humans. Third, the maximum resolution of the monitor has sharply increased (**Fig. 1.4)**. The maximum resolution was less than 100 pixels per inch (PPI) in 2004 and now exceeds 300 PPI by 2021. Professionals used high-resolution monitors. Currently, there is a growing demand for high-resolution monitors for general use.

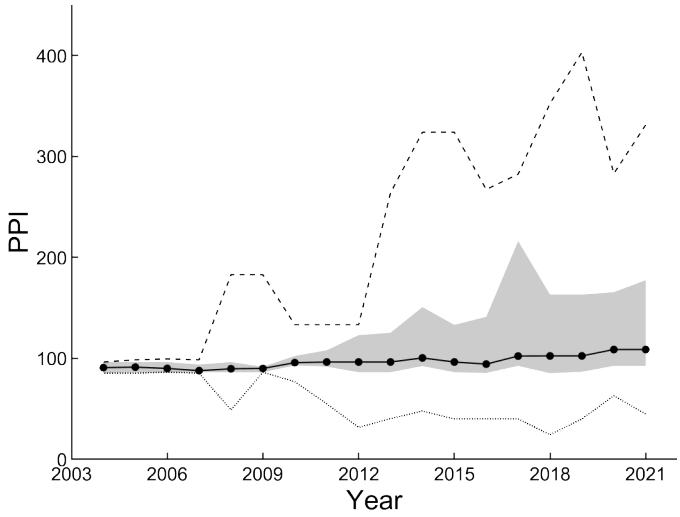

Figure 1.4 Changing the resolution of the PC and tablet monitors from 2004 to 2021

The solid, dashed, and dotted lines indicate the median, maximum, and minimum resolutions of the PC and tablet monitors each year. The gray area represents the quantiles from 25 % to 75 %. The vertical and horizontal axes represent the PPI and year of the launch date, respectively. The lacking of launch dates was replaced with their registered dates. All information (n = 1945) was obtained from https://kakaku.com in November 2021.

Third, the cosmetics industry makes products change their detailed color to give an attractive impression to others. The products for eyelashes have a variety of colors that provide different impressions. For example, black false eyelashes (left in **Fig. 1.5)** give an impression of a defined and strong eye. In contrast, the brown color (right in **Fig. 1.5)** gives the impression that eyelashes look more natural. Human vision detects such fine appearances and perceives subjective perceptions.

Figure 1.5 Two colors of fake eyelashes

A photo of false eyelashes of black (left) and brown (right) color.

Fine details and color appearance interact because fine details must have a spatial context, such as chromatic surroundings. Furthermore, human vision keeps the spatial details finer with the big eye and many image sensors, critical for optical artifacts. Therefore, to understand the

mechanism of the color appearance of fine stimuli, it is necessary to study from the aspect of the spatial context and optics. This thesis attempted to elucidate the mechanisms of fine color perception using stimuli with complex spatial contexts on a high-resolution monitor through psychophysical and computational methods.

1.2 Overview

This thesis comprises of eight chapters (**Fig. 1.6**). Chapter 1 explains why human vision prefers fine colors. Chapter 2 introduces knowledge and studies on color perceptions of fine stimuli from optics, physiology, and psychophysical methods and identifies points that have not been revealed. Chapter 3 presents a new spatial context of an illusion and validates whether optical artifacts cause an illusory effect. I show that the illusion could be a tool for elucidating mechanisms to perceive color appearance in fine stimuli. Chapter 4 presents the results of the color matching to show that the chromatic contrast in the spatial context affects the color appearance in the thin line by summing. Chapter 5 presents the optimal width for the spatial context that differs between the two-color axes in the human visual system using a psychophysical method. The effect of optical artifacts on color appearance was also validated using simulated data. Chapter 6 examined how luminance contrast modulated the illusory effect and suggested the summing is hard to explain color appearance in the spatial context. Moreover, I have summarized controversial theories regarding color illusions. Subsequently, Chapter 7 raises an assumption to correct the optical artifact in the spatial context and discusses the mechanism for color appearance in fine stimuli. Finally, Chapter 8 summarizes the results and concludes this thesis.

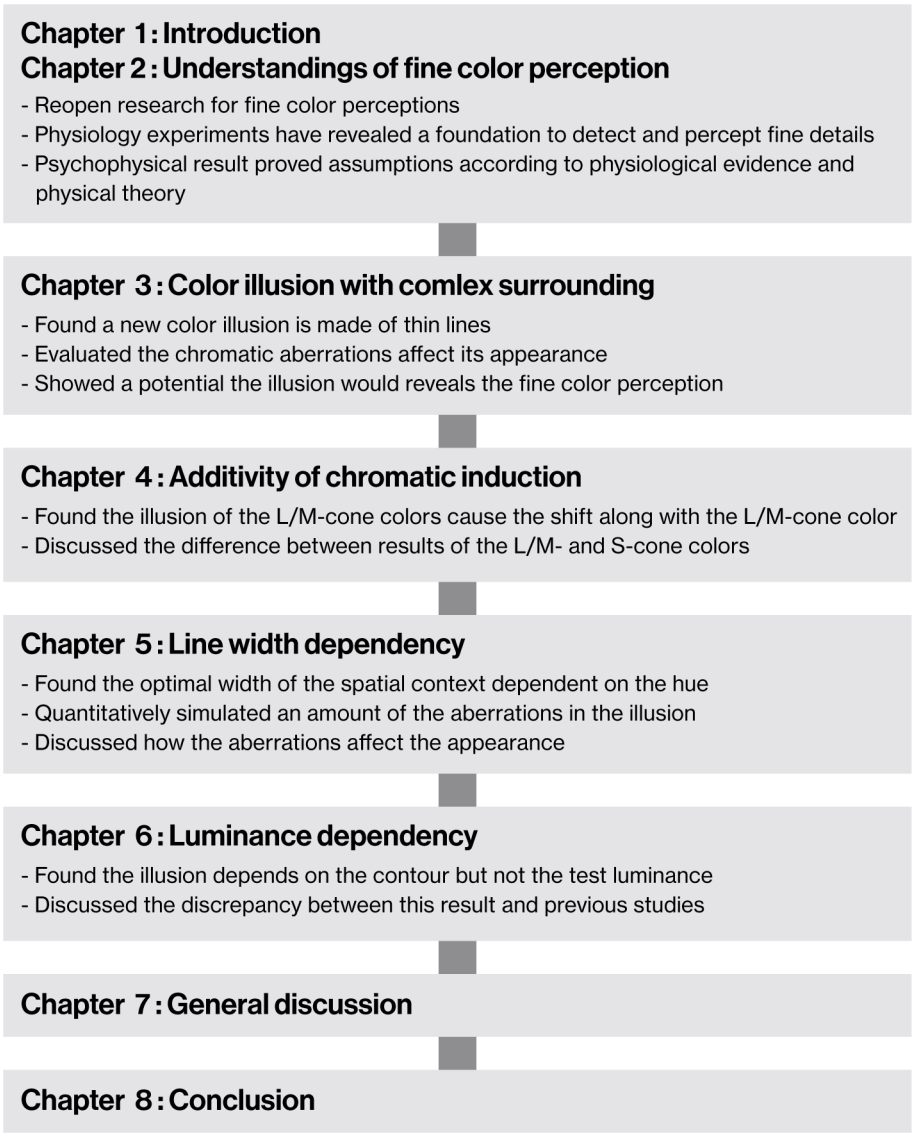

Figure 1.6 Overview of this thesis

Chapter 2

Understandings for color perception of fine stimuli

2.1 Introduction

The human visual system detects light in the eye, calculates and analyzes the spatial signal through the eye to the cortex, and then perceives color appearances. This chapter introduces the spatial coding of human color vision to address the questions for the color perception of fine stimuli. The introduction summarizes the evidence of eye optics, physiology, and psychopathology.

2.2 Optics

2.2.1 Human eye

The eye structure is illustrated in **Fig. 2.1.** Light is stopped and partially passed by the pupil of the iris's aperture, refracted by the lens, and imaged on the retina. The human eye is a camera that supports human spatial resolution. A camera eye is an optical system that is one lens that forms light on many image sensors. The camera eye has a higher resolution than the compound eye, which is an optical system composed of a single eye with one lens and image sensors (Caves, Brandley, & Johnsen 2018) because diffraction is severe for small lenses. Diffraction is a phenomenon in which a plane wave wraps around a small aperture. When the aperture is relatively small, less diffraction occurs. The human eye made the lens and its aperture larger and avoided lowering the image quality.

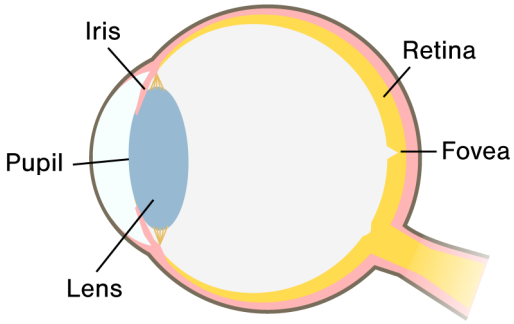

Figure 2.1 Structure of the human eye

The pupil and lens play an essential role in obtaining sharp incident light images. The pupil is circular, and its diameter changes to adjust the amount of light and focus depth. The diameter ranges from approximately 2 to 8 mm, depending on the amount of light, stimulus size, and age (Watson & Yellott 2012). The lens refracts light past the pupil and forms an image of the retina in the ocular globe. The lens is a biconvex lens with an accommodation function that focuses on an object by changing its curvature radius. The refractive power, a diopter, is defined by the inverse of the focal length (m) and is expressed in units of *D*. A small diopter indicates that the focal length is short because its refractive power is small. In contrast, a large diopter indicates a long focal length, owing to the ample refractive power.

2.2.2 Aberration

Ideally, the optics must focus on the light at one point. However, a human lens is not ideal and cannot focus on the light at one point. This phenomenon is called aberration and is classified into wavelength-dependent and wavelength-independent aberrations. Wavelength-dependent aberration is also known as chromatic aberration, subdivided into longitudinal and transverse chromatic aberrations according to a position shift in the focal light. Wavelength-independent aberration is also known as a monochromatic aberration, which has five primary types: spherical aberration, coma, astigmatism, field curvature, and distortion. Wavelength-dependent aberrations affect color appearances, whereas wavelength-independent aberrations mainly shape appearance. Pupil constriction reduces the aberrations of the incident light and improves image quality. Pupil size of 2–3 mm optimizes image quality (G. Smith & Atchison 2000).

Longitudinal chromatic aberration

Longitudinal chromatic aberration causes short-wavelength light to be focused closer to the lens, and long-wavelength light is focused away from the lens along the optical axis (**Fig. 2.2A**). Color fringes appear in the retinal image. **Fig. 2.3** shows a photograph of these fringe taken with a convex lens at two focal positions. The photograph of **Fig. 2.3A** is close to an image the human

sees because it was taken on the focus plane of the medium-wavelength light that the human lens usually focuses on. **Fig. 2.3B** shows the reddish fringes appearing in the dots' edge when the convex lens focuses on the focal plane of short-wavelength lights. When the lens focuses on the focal plane of long-wavelength light, the short-wavelength light is blurred such that bluish fringes appear at the edge of the dots (**Fig. 2.3C**). The difference in the refractive power is approximately 3.2 *D* between 750 and 365 nm (Thibos, Ye, et al. 1992; Wald & Griffin 1947). Longitudinal chromatic aberration is critical for fine color appearance.

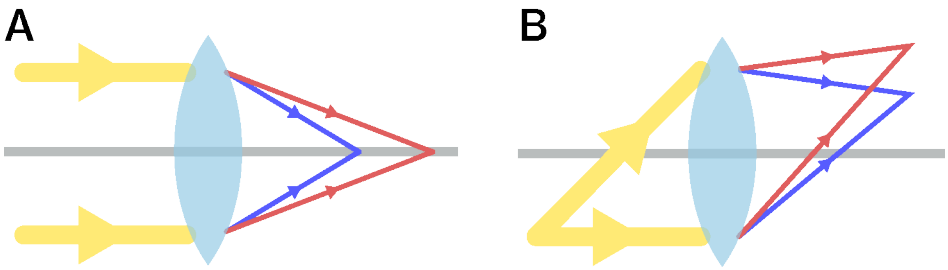

Figure 2.2 Schemas of (**A**) longitudinal and (**B**) transverse chromatic aberrations

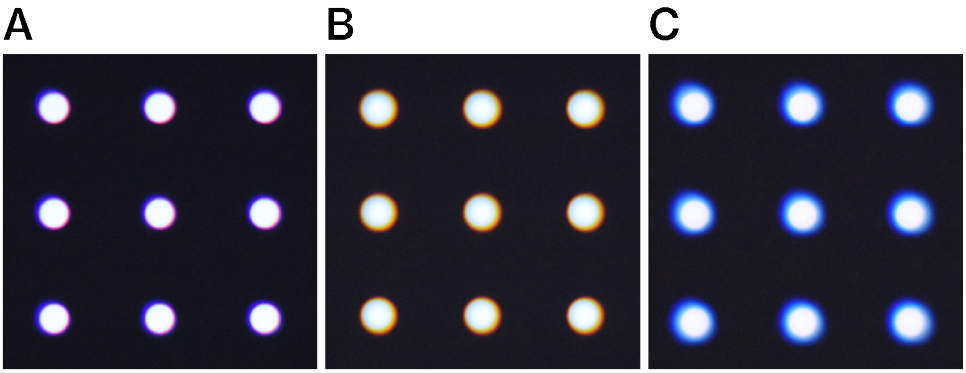

Figure 2.3 Color appearance of longitudinal chromatic aberration
A, **B**, and **C** are photographs that focus on medium-, short-, and long-wavelength light, respectively. See **Fig. 3.3** for this method.

Transverse chromatic aberration

The transverse chromatic aberration is the focus shifted away from the optical axis. For example, **Fig. 2.4** shows a photograph of its appearance taken with a convex lens at the left and right from the optical axis. Colored fringes emerge when a convex lens is turned to focus on a plane away from the optical axis. For instance, a bluish fringe appears at the left edges of the white dot when turning the convex lens to the right (**Fig. 2.4A**), whereas a reddish fringe appears

at the right edges, especially if the lens is turned to the left (**Fig. 2.4B**). For humans, the magnitude of the transverse chromatic aberration is 1.3 min at 5 degrees eccentricity (Thibos, Bradley, et al. 1990), which hardly affects the color perception on the optical axis.

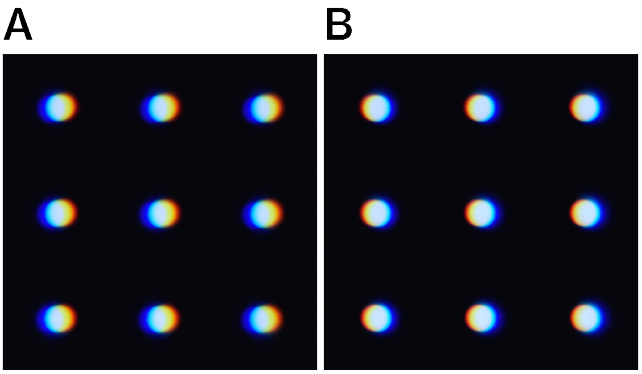

Figure 2.4 Color appearances of transverse chromatic aberration
A and **B** are photographs that focus on the left and right of the optical axis, respectively. The original image is the same as that in **Fig. 2.3.** See **Fig. 3.4** for this method.

2.3 Physiology and Anatomy

2.3.1 Retina

A partial area of the retina responds to an image of gaze. This area is called the fovea and has a diameter of approximately 1.5 mm (**Fig. 2.5A**). The fovea packs many photoreceptor cells specializing in fine details of color appearance. The approximately 5.5 mm centered on the fovea is called a macula with a yellow pigment. This pigment absorbs short-wavelength light and helps reduce chromatic aberrations. The parafovea is an area of approximately 2.5 mm centered on the fovea. The central 0.15 mm of the fovea is pitted and called the foveal pit. Each of these diameters corresponds to a viewing angle of 47, 21, 13, and 1 min, respectively, with a viewing distance of 40 cm (**Fig. 2.5A**). Cells of the foveal pit are the only photoreceptors that respond to light of different wavelengths and are called cone cells (Cuenca, Ortuño-Lizarán, & Pinilla 2018). The cone cell extends its axon and pedicle toward the outside of the pit (**Fig. 2.5B**) and transmits signals to the bipolar and ganglion cells.

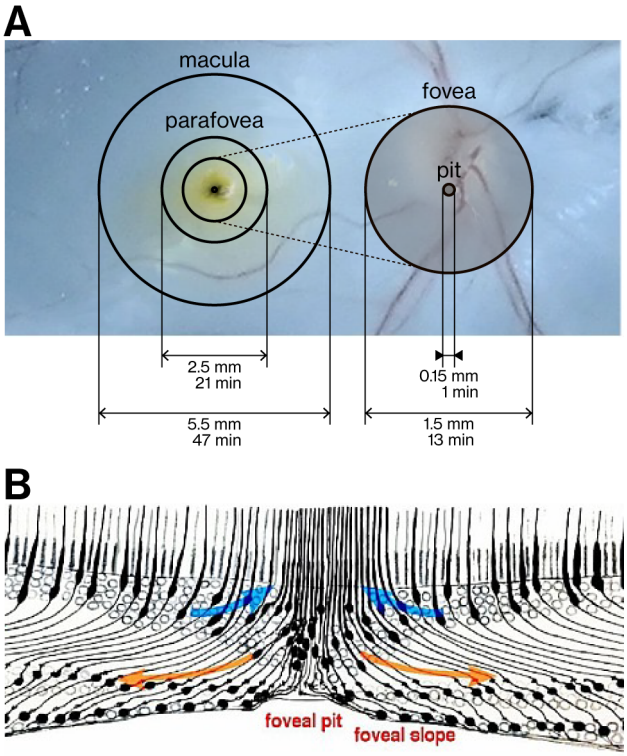

Figure 2.5 Map of the fovea (**A**) and drawing showing the cone axons and foveal pit (**B**)
These images have been modified from Kolb et al. (1995).

The cone cells are classified into three types according to their wavelength sensitivity. All of these are the basis of human color vision. The cone cells that respond to long-, medium- and short-wavelength light are the L, M, and S cones. L and M cones are distributed densely in the fovea and sparsely in the periphery (Curcio, Allen, et al. 1991; Curcio, Sloan, et al. 1990). The fovea within approximately 0.4 degrees has only the L and M cones, but not the S cones (Calkins 2001). The L and M cones are distributed throughout the retina, and their ratio depends on the individual (Hofer, Carroll, et al. 2005; A. Neitz et al. 2020; Roorda & D. R. Williams 1999). On average, the L and M cones are 67% and 28%, respectively. The distribution of the S cone is different from that of the other cones and peaks at 0.2 degrees eccentricity (Calkins 2001). The number of S cones is approximately only 5% of the total cones in the retina (Calkins 2001; Hofer, Carroll, et al. 2005; Roorda & D. R. Williams 1999). These distributions are the physical upper limits of the spatial resolution of human vision.

2.3.2 Retinal circuit

Midget bipolar cell is common in the fovea and mainly receives input from cone cells. This connection maintains a pathway in which human vision processes wavelength-dependent signals.

The response of the midget bipolar cell is of two types with different polarities. The cone's potential causes the ON midget bipolar cell to hyperpolarize and the OFF midget bipolar cell to depolarize. The ON and OFF midget bipolar cells at the fovea receive input from the cone (**Fig. 2.6,** Calkins, Schein, et al. 1994; Wool, Packer, et al. 2019; Zhang et al. 2020). This private line supports the high spatial resolution at the fovea (Patterson, M. Neitz, & J. Neitz 2019).

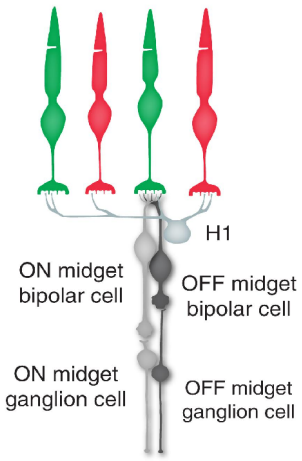

Figure 2.6 Retinal circuit for cone cells from Patterson, M. Neitz, & J. Neitz (2019)

The circuit of the S cone is different from those of the L and M cones. The S cone at the parafovea of macaques is connected to the S-OFF midget bipolar cell with the private line (Wool, Packer, et al. 2019). The ON bipolar cell of the S cone is called a blue cone bipolar cell, which receives inputs from the S cones, even near the fovea (Wool, Packer, et al. 2019). Thus, the S-cone pathway loses spatial detail information because the blue cone bipolar collects inputs over a more broad spatial area than the midget bipolar (Calkins 2001).

The cone cell is sensitive to wavelength and light intensity. Therefore, the cone response combines the wavelength and intensity information. To obtain the wavelength information, the subtraction between the cone cells which respond to different wavelengths is required. Retinal ganglion cells serve this difference signals. There are at least 17 types of retinal ganglion cells for primates (Grünert & Martin 2020), and two ganglion cells are involved in human color vision (Callaway 2005).

The midget ganglion cell responds to concentric-shaped stimuli. For example, the stimulus is similar to a red center and green concentric ring. A cell that responds to such spatial contrast is called an opponent cell. The opponent cell that responds to the example stimulus receives the L-ON and M-OFF cone inputs to its center and surroundings **Fig. 2.7A**. The midget ganglion cell receiving the M-ON and L-OFF inputs to the center and surroundings respond to green-red

modulation.

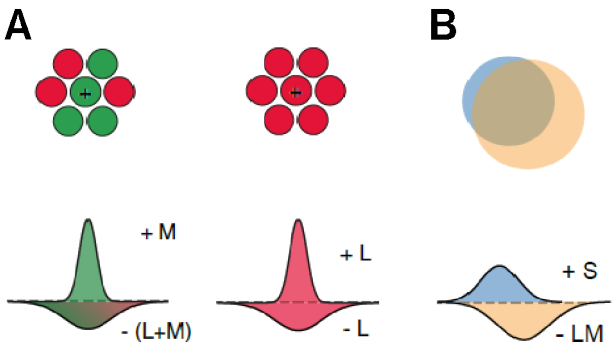

Figure 2.7 Spatial profile of the midget (**A**) and bistratified ganglion cells (**B**) The shema was from Patterson, M. Neitz, & J. Neitz (2019).

The midget ganglion cell at the fovea receives input from a single cone to the center of the receptive field. Hence, the midget ganglion provides fine details for human vision. In contrast, the surroundings of the midget cell receive a mixture of L and M cone inputs (**Fig. 2.7A**, Crook, Manookin, et al. 2011; Wool, Crook, et al. 2018). Therefore, the input ratio determines the degree of chromatic tuning of the midget ganglion cells (Wool, Crook, et al. 2018).

Since the midget ganglion cell is sensitive to the difference between the long- and medium-wavelength lights, its sensitivity also depends on the intensity differences between the cones. Therefore, the midget ganglion cell has a double duty to encode spatial contrast in both chromaticity and intensity (Patterson, M. Neitz, & J. Neitz 2019). Although the midget sensitivity varies, 90% of midget cells are more sensitive to white-black modulation than chromatic modulation (Wool, Crook, et al. 2018). This implies that the chromatic resolution is lower than the intensity resolution.

Blue bipolar cells project to the bistratified ganglion cells. The bistratified ganglion cell has an ambiguous profile and responds to uniform stimuli modulated by violet-yellow colors **Fig. 2.7B**. The spatial profile extends because, even near the fovea, the bistratified ganglion cell receives multiple S-cone inputs (Wool, Packer, et al. 2019). This extension is also facilitated by the broader dendrites of the bistratified ganglion cells (Calkins, Tsukamoto, & Sterling 1998; Crook, Davenport, et al. 2009; Dacey & Lee 1994). Therefore, the S-ON pathway loses a high spatial resolution for human vision.

2.3.3 Post-receptoral pathway

The axons of these ganglion cells pass through the thalamus and reach the cortex. The lateral geniculate nucleus (LGN) in the thalamus relies on the response of the retinal ganglion cells. Responses in the left and right visual fields project to the left and right LGN (**Fig. 2.8A**) in

parallel. As a result, ganglion axons in both eyes project parallel to the LGN. The LGN has six separate layers made of different cells (**Fig. 2.8B**). Layers 1 and 2 receive input from the parasol ganglion cell at the retina, responding to a large spatial contrast. Layers 4 to 6 are projected from the midget ganglion cells. Small cells are packed between each layer and receive inputs from the bistratified ganglion cells. Thus, the responses of each retinal ganglion cell remain to be treated in parallel. This is because each cell of the LGN is independent between the layers. Axons of LGN cells project to V1 of the early visual cortex, which processes visual signals.

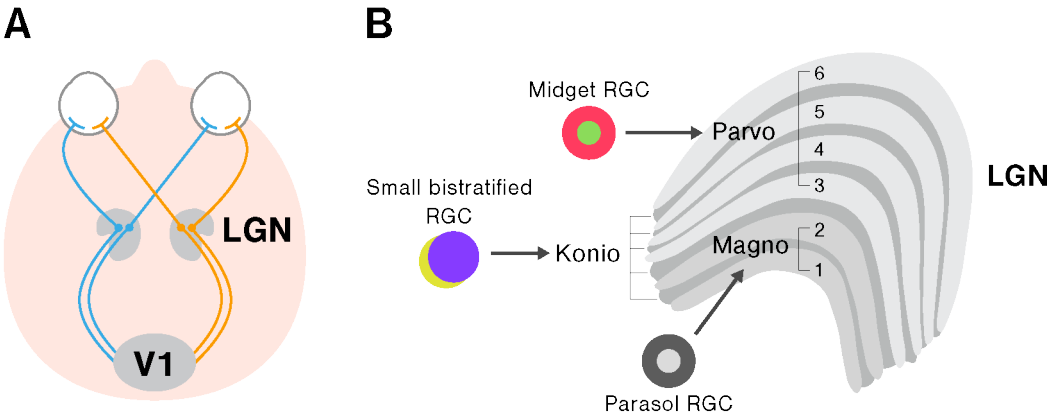

Figure 2.8 Shemas show retinal activity from the retina to the cortex
(**A**) Retinal responses pass through the LGN to the visual cortex V1 in parallel.
(**B**) Each retinal ganglion cells projects to different layers of the LGN.

2.4 Color representation

2.4.1 Opponent color system

Midget ganglion cells provide a red-green mechanism by combining different inputs from the L and M cones. Bistratified ganglion cells provide a violet-yellow mechanism by combining different inputs from the S and the sums of the L and M cones. These circuits at the retina are shown in **Fig. 2.9.** These responses represent the axes of the complementary color pairs in human perception. The color space of these axes is called the opponent color space. A pair of opponent colors cannot be perceived simultaneously, and various colors are made of a combination of opponent axes (Shevell & Martin 2017). The opponent system can represent the chromaticity of stimuli represented in the post-receptoral stage.

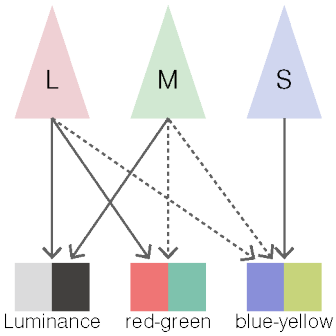

Figure 2.9 Opponent axes at the retina

2.4.2 MacLeod-Boynton chromaticity space

The Macleod-Boynton (MB) chromaticity space represents the chromatic signals of the post-receptor response (MacLeod & Boynton 1979). The MB space has two axes l and s, the relative activation of the L- and M-cones ($l = \mathrm{L}/(\mathrm{L}+\mathrm{M})$) and the activation of the S-cone ($s = \mathrm{S}/(\mathrm{L}+\mathrm{M})$) in an equiluminant plane, respectively. The plane combining the l and s axes is equiluminant because each axis is divided by the luminance signal (L + M). Because the MB space is a chromatic representation based on cone excitation, it is useful for examine the mechanism through the post-receptoral system, such as the retina and the LGN circuits.

2.5 Detection

2.5.1 Visual acuity

Visual acuity is an indicator of the ability to discriminate fine stimuli and is defined as the inverse of the visual angle (min) of the discriminated stimuli. 1.0 of a visual acuity indicates that 1 min of a stimulus could be detected. Visual acuity is measured by distinguishing the orientation of the Landolt ring gap or the letter E. Diffraction, aberrations, and cone density mainly limit the visual acuity (G. Smith & Atchison 1997).

Visual acuity usually refers to luminance visual acuity measured using a luminance contrast stimulus. Luminance visual acuity is well studied; background luminance, contrast, and artificial blurring all act additively (C. A. Johnson & Casson 1995). Although visual acuity is restricted by foveal optics, longitudinal chromatic aberration hardly contributes to luminance (Suchkov, Fernández, & Artal 2019). There are various findings on the visual acuity for chromatic stimuli. Color visual acuity, which is usually lower than luminance visual acuity, can be detected at the same degree as luminance acuity by increasing chromatic contrast (T. L. Chen & Yu 1996). These findings show that visual acuity is highly dependent on stimulus conditions.

2.5.2 Contrast sensitivity function

Since visual acuity is a detection index at a specific contrast, it is difficult to compare the difference between the various measurements of the visual acuity. Therefore, the detection performance was measured across contrasts under the same conditions, which is described as the contrast sensitivity function (CSF, **Fig. 2.10)**. The CSF is described by contrast sensitivity to the spatial frequency of the stimulus. Contrast sensitivity is the inverse of the contrast threshold of the detected grating stimulus. All spatial patterns can be theoretically represented by combining the spatial frequencies. Thus, CSF has been measured on the premise that the human visual system is linear.

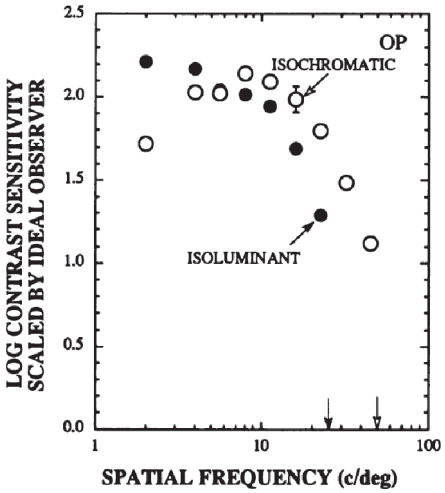

Figure 2.10 CSF curve shapes for chromatic (filled circles) and luminance (void circles)

The horizontal axis represents the spatial frequencies of the stimuli. The horizontal axis represents the contrast sensitivity. The solid and void arrows indicate the resolution limit for the chromatic and luminance gratings. The panel is from **williams1993**.

CSF shape is affected by factors such as eye movement, eye optics, macular pigment, cone blurring, cone distribution, and neural mechanisms in the retina and cortex (Geisler 1989; D. Williams, Sekiguchi, & D. Brainard 1993). Eye movement causes spatial phase changes, optics are less sensitive to high spatial frequencies (Campbell & Gubisch 1966; D. R. Williams, D. H. Brainard, et al. 1994), and the macula changes the spectral composition. The aperture of the cone causes Gaussian blur. Further, fine details of the stimulus are lost depending on the sampling of the cone distribution.

A significant constraint is cone sampling, which affects the upper resolution of the CSF because its distribution changes with eccentricity, and its response depends on the wavelength

selectivity. The spacing between the cones estimates that the upper resolution is 0.0084 deg (0.5 min, Wandell 1995). This spacing corresponds to 60 cpd. According to the sampling theorem, a complete perception can be obtained at the Nyquist frequency, which is half of the sampling frequency. However, the correct orientation of the fine patterns can be perceived at a spatial frequency approximately 1.5 times higher than the Nyquist frequency (D. R. Williams & Coletta 1987). The maximum spatial frequency for the detectable orientation was 50–60 cpd, excluding optical factors (Campbell & Green 1965; Campbell & Gubisch 1966). These results indicate that the theoretically derived Nyquist frequency is not the visual resolution limit.

The chromatic mechanism requires an input difference between the cones that respond to different wavelengths. Hence, cone sampling limits the chromatic CSF compared to the luminance CSF. The chromatic CSF is consistently low, and its critical fusion frequency is lower than that of luminance (**Fig. 2.10,** Mullen 1985; D. Williams, Sekiguchi, & D. Brainard 1993). The difference in the curve shape reflects the strategy of human vision; The luminance mechanism specializes in the mid-spatial frequency band to distinguish details, and the chromatic mechanism integrates chromatic signals to provide stable color appearances.

Cone sampling and eye optics are different for the L/M and S cones. Thus, the CSF differs between opponent color axes. According to theory and careful measurements, the CSF for the red-green and violet-yellow gratings did not exceed approximately 20 to 27 cpd (A. Neitz et al. 2020; Sekiguchi, D. R. Williams, & D. H. Brainard 1993) and 14 cpd, respectively. However, the experiment in which the optical factors were removed showed no difference in the CSF shapes and its critical fusion frequency between the red-green and violet-yellow gratings (Mullen 1985; Sekiguchi, D. R. Williams, & D. H. Brainard 1993). This indicates that the predicted effect of cone sampling appears to be less in the chromatic CSF. Experiments with insufficiently removed chromatic aberrations showed higher sensitivity at high spatial frequencies for the red-green grating than for the violet-yellow grating (Barboni et al. 2013; Mullen & Kingdom 2002; Webster, Switkes, & De Valois 1990). Natural observation causes the L-and M-cone gratings to be detected in finer detail than the S-cone grating.

2.6 Fine color perception

2.6.1 Aliasing

Human vision can detect stimuli with the upper limit of human visual resolution, but what perception do they see? If the spatial frequency of a grating stimulus is higher than the Nyquist frequency, sampling fails to reproduce the stimulus correctly. This failure is referred to as aliasing in the sampling theorem. Williams, Brainard, and colleagues confirmed that aliasing occurs in human perception by psychophysical methods. They reported participants perceived a zebra pattern (**Fig. 2.11B**) when the CSF was measured using a grating of 60–70 cpd of short-wavelength light (**Fig. 2.11A**). This was due to aliasing. Although short-wavelength gratings

cause aliasing (Zlatkova, Vassilev, & Anderson 2008), long- and medium-wavelength gratings hardly appear in the zebra pattern (D. R. Williams, Sekiguchi, et al. 1991). The zebra pattern in the longer-wavelength light might be compensated by the visual system or not permitted without short-wavelength light.

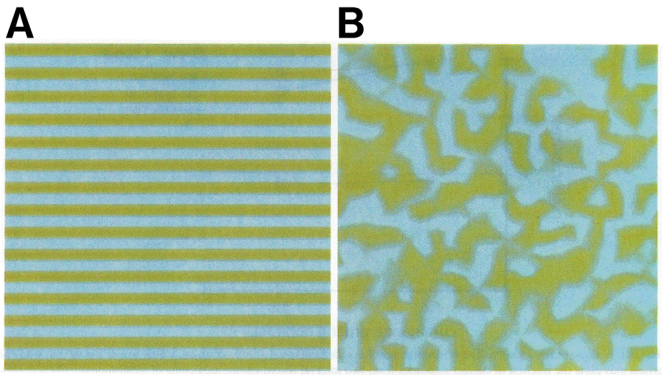

Figure 2.11 Grating (**A**) is perceived as the zebra pattern (**B**)
These images demonstrate the appearance of a zebra pattern in D. H. Brainard & D. R. Williams (1993).

Brewster's color is a phenomenon where red and green zebra patterns overlap when observing fine black and white stripes. Williams et al. examined the hypothesis that the aliasing of long- and medium-wavelength light causes a colored zebra appearance in Brewster's color. They experimented with quantifying the color appearance of the zebra pattern on black and white stripes using a CRT monitor and a defocused lens (D. R. Williams, Sekiguchi, et al. 1991). When the stripe's long- and medium-wavelength light was blurred, the zebra appeared violet and yellow along the s of the cardinal axis. By contrast, the zebra appears as a red-green color along the l of the cardinal axis when the lens is in focus. Therefore, the multispectral stripe causes aliasing in long- and medium-wavelength light.

Note that aliasing be rarely perceived in everyday life. Even when short-wavelength light tends to blur, aliasing hardly occurs. This is because chromatic aberrations blur short-wavelength light compared with cone sampling (D. R. Williams, Sekiguchi, et al. 1991). The aliasing of long- and medium-wavelength lights occurred only under particular conditions, such as varying the focus position. The human visual system seems to remove the aliasing of long- and medium-wavelength light strongly.

2.6.2 Small spot

Human vision can perceive color appearance even if it is difficult to resolve spatial details at the upper spatial resolution limit. Willmer reported that stimuli of chromatic pairs, light blue and green, orange-brown, and red-purple, were indistinguishable when the stimuli were 0.4° (Willmer

1944). This response was similar to the dichromat response to small stimuli reported by König at the end of the 19th century. Willmer subsequently performed a metameric color match to prove the dichromatic response to fine stimuli. This is a mixture of monochromatic light 460 and 650 nm matches the appearance of some visible lights (Willmer & Wright 1945). This result indicates that the fovea has a tritanopia that perceives all colors as cyanish or reddish because the tritanopia is less sensitive to blue-green due to the absence of the S cone. Small stimuli of 11 min appeared blue or green, with a frequency of approximately 80% (**Fig. 2.12A**, Weitzman & J. A. Kinney 1967). Since the S cone exists outside the parafovea, increasing the stimulus size recovers the trichromatic. The clinical test showed that the stimulus size, which appeared as tritanopia, was up to 18 min for 12 participants and up to 12 min for the other three participants (N. Davies & Morland 2003).

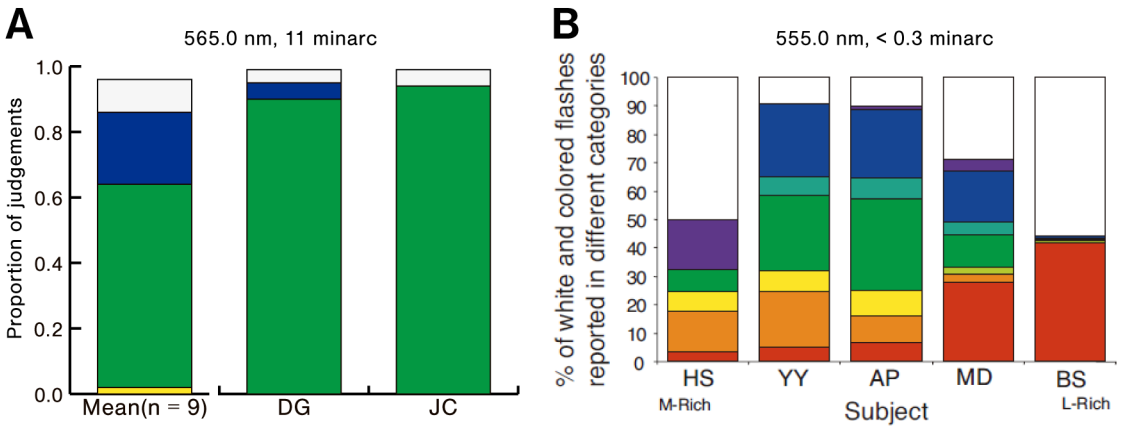

Figure 2.12 Proportion of color naming for fine stimuli

The stacked bars show the proportions of white and colored responses. The color names were red, yellow-green, green, blue-green, and blue. The common names for both panels are green, blue, red, yellow, and white. The details of the stimuli are shown in each panel. (**A**) These bars were replotted from the results with a 200 ms fixation of Weitzman & J. A. Kinney (1967). The left bar shows the average responses across the nine participants. The middle and right bars represent the two participants. (**B**) Response of each participant from Hofer, Singer, & D. R. Williams (2005). The horizontal positions of the bars are arranged in order of the bias of their cone ratio.

In the 1990s, adaptive optics (AO) obtained images of cone distribution in specific regions and presented stimuli to the retina while correcting aberrations. This development has led to a focus on research on fine color stimuli. Hofer et al. collected color names for fine stimuli of 0.3 min or less at approximately 1 deg retinal eccentricity while removing chromatic aberrations (**Fig. 2.12B**, Hofer, Singer, & D. R. Williams 2005). Their results showed that the color names to the 550 nm light were most common in white, and five to seven other names were required

(**Fig. 2.12B**). Number of the S cone was few at the retinal region, however, color names of blue and purple was also used. The L and M cone ratios biased the color-naming response. Further, participants who had many L cones tended to use reddish naming. Not removing the aberrations doubled achromatic naming. Comparing the results with the classical study, collecting chromatic aberrations reduce the tritanopia response and allow the perception of various colors.

Sabassen et al. again collected color names by presenting fine stimuli using an advanced AO system (Sabesan et al. 2016) and found that red and green responses were more common in the L and M cones, respectively. They also performed the same experiment using stimuli on a blue surrounding to collect color names at each cone and showed that the M cone yielded a blue response (Schmidt et al. 2018). This indicates that the color appearance of fine stimuli changes depending on the spatial context of their surroundings.

2.6.3 Spatial contexts

To the best of my knowledge, fine stimuli in chromatic backgrounds have rarely been investigated in the context of small spots. Instead, research on the color perception of fine stimuli has used stimuli of small color spots on an achromatic background. However, human vision perceives much more complicated contexts, and using these is essential for understanding the visual mechanism's strategy for fine color appearance. To understand the strategy, I focus on color illusions that depend on the spatial context, helping to understand the different aspects of fine color perceptions on chromatic backgrounds.

The mechanism of color illusion is a basic function for the visual system to achieve color constancy (Hurlbert & Wolf 2004; Lotto & Purves 2000) because color illusion causes a color shift with contrast and assimilation acting. Color assimilation represents the color appearance of a central area shifting to its surrounding color (**Fig. 2.13A**). The bars appear yellow and purple on yellow and purple backgrounds, respectively. The bar appearance was assimilated into the background. This phenomenon can remove fine spatial noise. The color contrast represents the color appearance shifting away from its surrounding color (**Fig. 2.13B**). The center squares appear cyanish and reddish on the red and cyan backgrounds, respectively. The square appearance was enhanced to its background. This phenomenon can be used to distinguish spatial patterns. Color assimilation and contrast occur even if the surroundings are composed of some colors and depend on spatial frequency and luminance contrast.

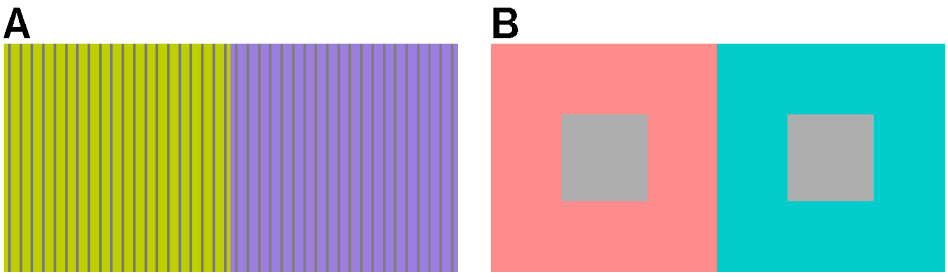

Figure 2.13 Demonstration of simultaneous color assimilation (**A**) and contrast (**B**)
The chromaticity of the bars and squares is identical between the left and right panels.

Color assimilation occurs at high spatial frequencies where the stimulus becomes finer. In contrast, color contrast occurs at low spatial frequencies, where the stimulus becomes coarser. Spatial frequency dependence represents the strategy of the human visual system; color assimilation reduces fine noise by averaging with the surroundings, and color contrast enhances subtle differences from the surroundings. The transition point from color assimilation to contrast was near 4 cpd (V. C. Smith, Jin, & Pokorny 2001), independent of the surrounding hue. The transition suggests that the difference in the opponent axes less affects the chromatic inductions, although the assimilation and contrast could derive from the single- and double-opponent cell activity (Shapley & Hawken 2011). However, neural spatial averaging for assimilation differed between the L/M and S pathways. The averaging field of the s axis in the MB space is larger than that of the L/M-cone color (Cao & Shevell 2005). In summary, there is less difference in the transition from assimilation to contrast, while there seems to be a difference in the neural averaging between the cardinal axes.

Optical factors such as aberrations also contribute to chromatic shifts in color illusions. The central area of a thin line mixes optically with its surroundings and causes assimilation. The color appearance above 9 cpd was explained by the spread of monochromatic light but not by chromatic aberrations (V. C. Smith, Jin, & Pokorny 2001). For the stimulus of 8 cpd on saturated surroundings, its color appearance shifted toward yellow, blue, and green; this shift seemed to be foveal tritanopia (Logvinenko & Hutchinson 2007). Although the difference in results using high spatial frequencies are still unknown, the cause of the assimilation contains the chromatic shift of the optical factors.

Color illusion depends on the luminance contrast of the stimuli. Lowering the luminance of the central area increases the magnitude of color assimilation. In contrast, increasing the luminance of the center increases the magnitude of color contrast. Kirschmann's third law states that the color contrast is maximum when the luminance of the center is the same as that of

the surrounding (Kirschmann 1891). This law has been examined in several studies (Bergström & Derefeldt 1975; Bergström, Derefeldt, & Holmgren 1978; Gordon & Shapley 2006; J. A. S. Kinney 1962; Xing et al. 2015). However, their results were inconsistent. Kinney reported that the magnitude of the color contrast increased with an increase in the luminance contrast between the center and the surrounding (J. A. S. Kinney 1962). Gordon and Shapley confirmed Kirschmann's third law when brightness or luminance contrast was minimal and demonstrated that the critical factor for the law is a change in the center luminance, but not the surrounding (Gordon & Shapley 2006). Kirschmann's third law may be a clue to elucidate the mechanism for the color perception of fine stimuli, as changes in the center luminance are the same as changes in fine details.

The surroundings, composed of some colors, cause a smaller or larger illusory effect than a uniform surrounding. For example, Shevell and Wei showed that the center area, which is placed around a red and green checkered pattern, caused a smaller shift than that of the uniform surrounding (Shevell & Wei 1998). They also found that the chromatic contrast of the surroundings affects color assimilation to the center area because the magnitude of color assimilation for the yellow surroundings became stronger than that for the checkered pattern.

Monnier and Shevell found that the magnitude of assimilation increased by alternating the surroundings, with two colors being the opponent colors (Monnier & Shevell 2003). This illusion causes strong color assimilation by summing the color assimilation from the first and color contrast from the second inducer (**Fig. 2.14A**, Monnier & Shevell 2003, 2004). The yellowish ring on the center appears purple when the purple ring flanks the center ring (**Fig. 2.14A**, top), whereas the center ring appears greenish when the green ring flanks (**Fig. 2.14A**, bottom). This thesis calls this illusion the Monnier–Shevell illusion. The Monnier–Shevell illusion represents color assimilation at high spatial frequencies and color contrast at low spatial frequencies occurring simultaneously (Otazu, Parraga, & Vanrell 2010). For example, by changing the first ring to achromatic, the center rings at the top and bottom still appeared purplish and greenish, although the shifts in color appearance were smaller (**Fig. 2.14B**). Furthermore, the ring width is almost thinner than typical color illusions; the optimal width was the inducer ring of 3.3 cpd (9.1 min), regardless of the test ring width (Shevell & Monnier 2005). Therefore, the Monnier–Shevell illusion helps investigate the mechanism of color perception of fine stimuli that depends on complex spatial contexts.

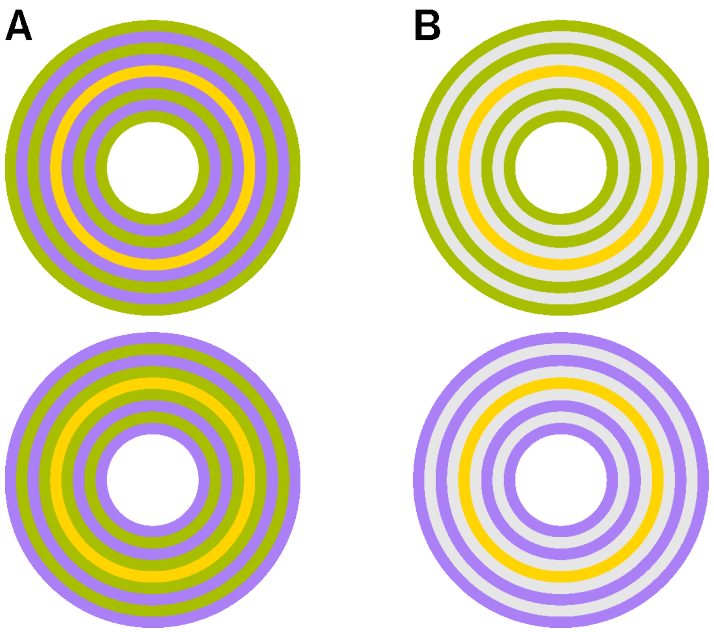

Figure 2.14 Demonstration of Monnierh–Shevell illusions
(**A**) The assimilation type of the Monnier–Shevell illusion of which the first inducing is chromatic. (**B**) The contrast type of the Monnier–Shevell illusion, wherein the first inducing is achromatic. All centered rings are identical.

The Monnier–Shevell illusion is a well-known illusion that shifts along the s axis because the illusion for the l axis requires more severe calibration than that of the s axis (Mély, Linsley, & Serre 2018). The result showed that the color shift of the illusion modulated along the s axis is larger than that modulated along the l axis (Cerda-Company et al. 2018). This difference could be attributed to the spatial resolution of the cardinal axes. To investigate the Monnier–Shevell illusion from the perspective of color perception of fine stimuli requires that its color shift occurs along the l axis because only the L and M cones exist at the fovea center.

The Monnier–Shevell illusion causes a shift in the color appearance only in the modulation direction of the inducer ring, even if the chromaticity of the test ring varies (Monnier & Shevell 2004). This result is correct given that the stimulus condition may not be optimal for l. The second question is whether a stimulus condition for the l causes a shift in color appearance along the l axis regardless of the chromaticity of the test area. In particular, the Monnier–Shevell illusion for the l might cause the shift along the cardinal axes. If the alternating pattern is effective for the l axis, changing the proximal chromaticity is severe for color shift of the test ring.

Luminance contrast also affects the spatial frequency dependence of color illusions; the transition point from assimilation to contrast changes depending on the luminance contrast (Cao & Shevell 2005). Moreover, the Monnier–Shevell illusion modulated along the s axis increased

the shift in color appearance with increasing luminance contrast (Cerda-Company et al. 2018). The question remains; how do changes in luminance affect the color appearance of the Monnier–Shevell illusion for the l axis? For the center-surround illusion, the magnitude of the color contrast changed depending on whether the luminance was varied in the center or the surrounding (Gordon & Shapley 2006; J. A. S. Kinney 1962). The Monnier–Shevell illusion may also be affected by the spatial position of luminance change. Neural models can predict the color shift of the Monnier–Shevell illusion of S-cone colors. Otazu et al. showed that the wavelet calculation based on the center-surround cell could predict the shift in both opponent axes ref. It has been suggested that the recurrent network model of the center-surround cell could cause color shifts from the alternating pattern (Mély, Linsley, & Serre 2018). Spitzer proposed the reducing function of chromatic shifts of optical artifacts using the difference between the L- and M-cone signals and showed the color shift of the Monnier–Shevell illusion. These models can predict the color shift along with S-cone modulation. However, they did not consider the dependence of the luminance contrast.

2.7 Summary

This chapter presents the background to studying the color perception of fine stimuli from the aspects of optics, physiology, and psychophysics. The eye has a great optics system for spatial vision; however, chromatic aberrations degrade the retinal image. Consequently, the color appearance can change with the receptive field of the center-surround cell. This cell leads to a color shift of the center area with chromatic surroundings, and this shift is commonly observed by the psychophysical method. The Monnier–Shevell illusion causes a large shift in the test area when the surrounding alternates with two opponent colors. The Monnier–Shevell illusion is evident for S-cone colors. However, whether the Monnier–Shevell illusion causes L/M-cone stimulation is still unknown. The illusion in the L/M-cone axis helps to understand the mechanism for the color perception of fine stimuli because the fovea packed the L and M cones serving as signals to the center-surround cell.

Chapter 3

Color illusion with complex spatial context

This chapter is published as a part of,
T. Kanematsu & K. Koida (2020). "Large enhancement of simultaneous color contrast by white flanking contours". In: *Sci. Rep.* 10.1, pp. 1–10. DOI: 10.1038/s41598-020-77241-5. URL: www.nature.com/scientificreports.

Part of this chapter is presented in this video,
T. Kanematsu & K. Koida (2018). *White + Gray = Red*. URL: http://illusionoftheyear.com/cat/top-10-finalists/2018/.

3.1 Introduction

Chapter 2 stated that investigations of fine color perception were limited to stimuli such as the spatial profile of the center-surround pattern. Complex spatial contexts are required to investigate the mechanism underlying fine color perception because human vision perceives fine colors depending on spatial contexts, the hue of surroundings (Gordon & Shapley 2006; J. A. S. Kinney 1962; V. C. Smith, Jin, & Pokorny 2001), luminance contrast (Bergström & Derefeldt 1975; Bergström, Derefeldt, & Holmgren 1978; Gordon & Shapley 2006; J. A. S. Kinney 1962; Xing et al. 2015), and spatial frequency (Cao & Shevell 2005; V. C. Smith, Jin, & Pokorny 2001). The Monnier–Shevell illusion is most suitable for examining the effect of complex spatial contexts because its surrounding alternates with two chromaticities, and the illusion requires a relatively thin line (Shevell & Monnier 2005) compared to the uniform surrounding. The Monnier–Shevell illusion causes color assimilation by alternating the s axis colors around the test ring (Monnier & Shevell 2003, 2004). The illusion was typically modulated along the s axis of the MB space and showed a large shift in color. Thus, the illusion of l, another cardinal axis, has not been fully investigated. This chapter reports a new spatial context for the Monnier–Shevell illusion modulated along with the red-green color and validates whether optical artifacts

explain the illusory effect. The results excluded the possibility of optical artifacts and concluded that the spatial context is a perceptual phenomenon.

3.1.1 Founding new spatial contexts

Fig. 3.1A shows a new spatial context of the Monnier–Shevell illusion using similar colors of the l axis. The thin lines in **Fig. 3.1A** appear reddish, whereas the lines in **Fig. 3.1B** appear slightly cyan-gray. However, these lines are identical in grey. The difference between **Fig. 3.1A** and **B** is the fine spatial contrast between the lines. The thin white lines flank the gray lines in **Fig. 3.1A** but not in **Fig. 3.1B** (**Fig. 3.1C** and **D** enlarged **A** and **B**). The lines must be thinner than the stimuli used in the previous studies. Here, I call the center gray line the *test line*, the white line the *contour*, and the chromatic surrounding the *inducer*. This illusion also occurs in other hues of the inducer (**Fig. 3.2**). The test lines with the contour appear yellowish or purplish-gray on violet and yellow inducers, respectively.

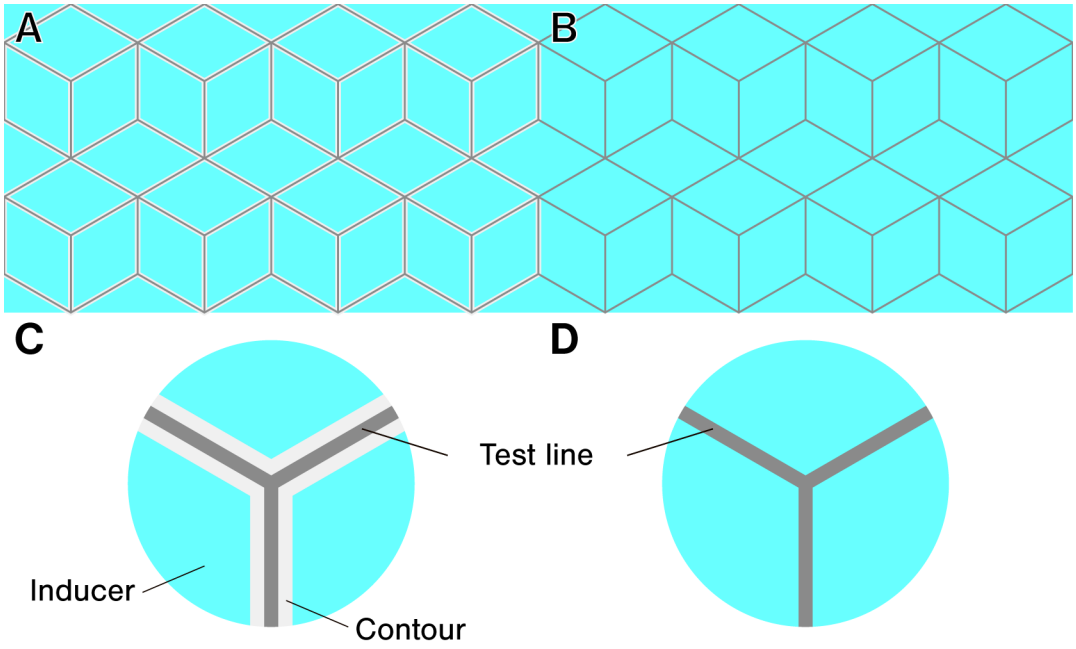

Figure 3.1 Monnier–Shevell illusion for red-green color
Thin gray lines appear reddish by flanking thin white lines (**A**), whereas gray lines without white lines appear as subtle cyan-gray lines (**B**). **C** and **D** are the enlarged part of **A** and **B**. The inducer and test lines are identical in **A** and **B**.

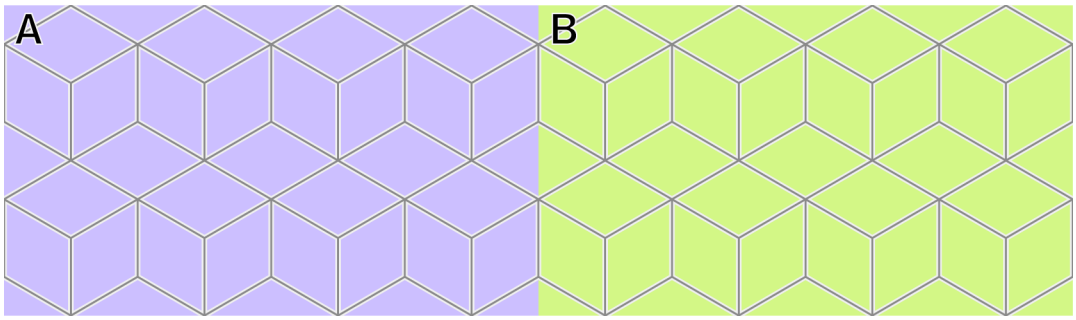

Figure 3.2 The spatial context we found for the other hues, violet (**A**) and yellow (**B**)
The test lines and contours are identical for **A** and **B**.

3.2 Validation chromatic aberrations

Although the thin lines are crucial to the new spatial context, chromatic aberrations could affect them, resulting in a chromatic shift. One of the aberrations, longitudinal chromatic aberrations, changes the focal plane along the optical axis depending on the wavelength of light (**Fig. 3.3A**). Then, the effect of the longitudinal chromatic aberration on the color appearance of the test line using a convex lens was investigated.

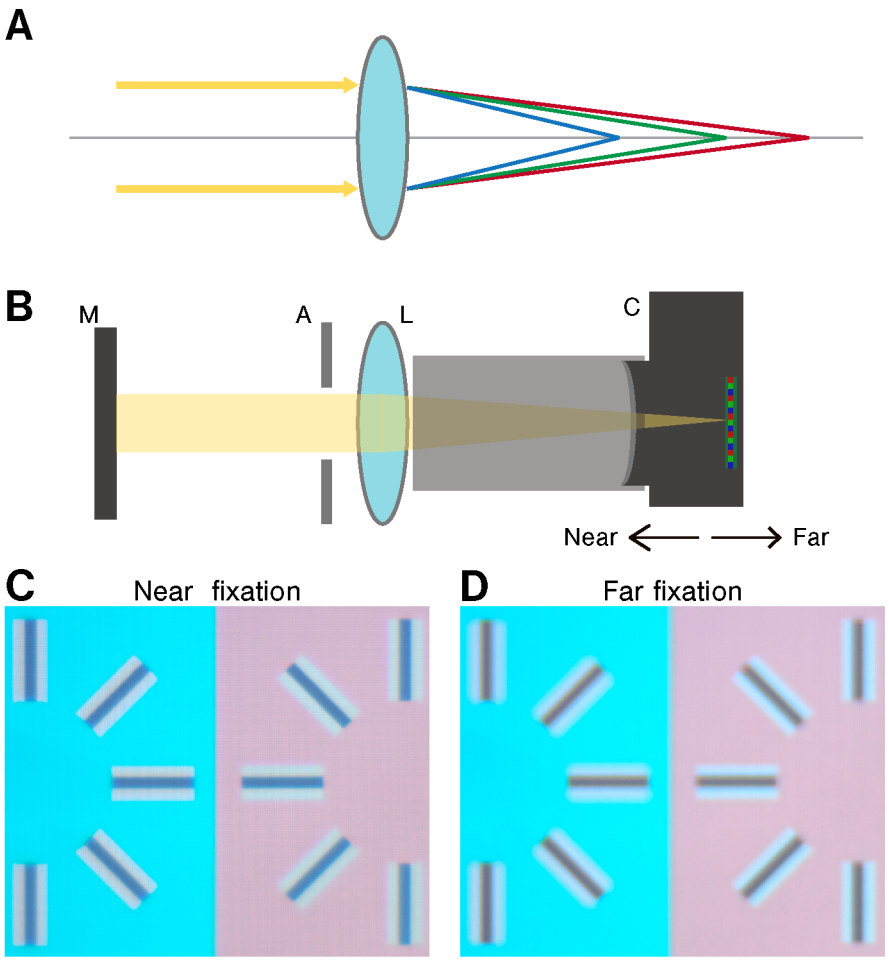

Figure 3.3 Chromatic shifts due to the longitudinal chromatic aberration (**A**) Schemas of longitudinal chromatic aberrations. (**B**) Apparatus for taking photographs when chromatic aberrations occur. The light of the monitor (M) was stopped by the aperture (A) and focused on the image sensor of the camera (C) using a convex lens (L). The camera removed its lens and was covered with a black paper tube to prevent stray light. **C** and **D** are the photographs with the longitudinal chromatic aberration was taken at the near and far camera positions.

Fig. 3.3B shows the top view of the apparatus to take photographs while occurring the chromatic aberrations in the new spatial context. First, the camera was positioned along the optical axis to reduce yellow blurring in the image shown on the monitor. Next, the camera was moved close to or away from the monitor, taking photographs at these points.

Positioning the camera near the lens to focus on the short-wavelength light resulted in blurred images of the long- and medium-wavelength lights. Thus, the gray line of the illusion changed in chromaticity to bluish (**Fig. 3.3C**). Contrastingly, positioning the camera far from the lens to focus on the long-wavelength light blurred images of the short- and medium-wavelength lights.

Thus, the gray line changed from chromaticity to red (**Fig. 3.3D**). These shifts were independent of the line orientation and inducer hue.

Another chromatic aberration, the transverse chromatic aberration, shifts the focal plane away from the optical axis depending on the wavelength (**Fig. 3.4A**). Thus, the transverse chromatic aberration magnifies the focal plane of the short-wavelength light and can cause chromatic fringes at the edge of the lines. Then, I confirmed how the transverse chromatic aberration explains the color appearance of the test using a convex lens.

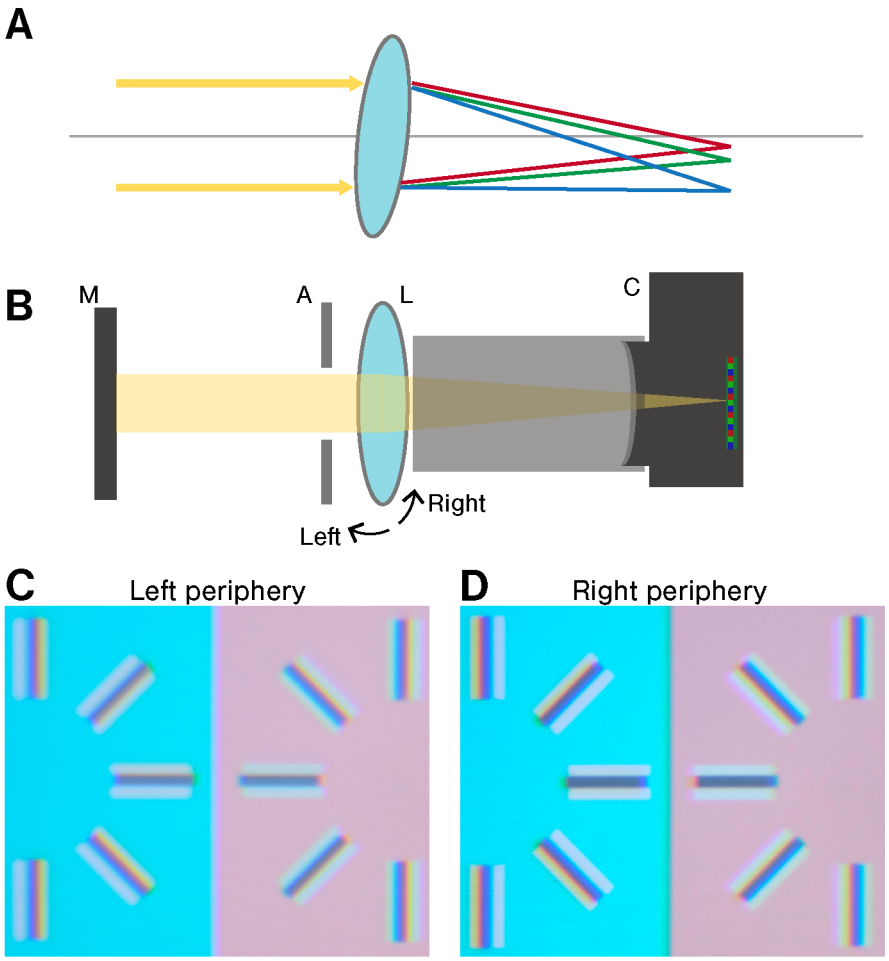

Figure 3.4 Chromatic shifts owing to transverse chromatic aberration
(**A**) Schemas of transverse chromatic aberrations. (**B**) Apparatus to take photographs while chromatic aberrations occur with the rotation of the lens. The apparatus is shown in the same format as **Fig. ??B**. **C** and **D** are the photographs with the longitudinal chromatic aberration taken at the near and far camera positions.

When the lens turned to the right or left, light from the monitor was formed on the focal plane away from the optical axis (**Fig. 3.4B**). The camera was then moved to the focal plane,

and a photograph was taken. **Fig. 3.4C** showed the photograph when the lens turned round to the left, which was chromatic fringes emerged at the left edge of the test lines. Contrastingly, when the lens turned round to the right, the photograph showed chromatic fringes that emerged at the right edge of the test lines (**Fig. 3.4D**). Here, the lens rotated along the orthogonal axis of the optical axis so that the fringes on the long sides of the vertical lines were prominent. However, the vertical lines were less affected by the inducer hue.

These photographs clarify how chromatic aberrations caused a shift in the chromaticity of the test lines. Considering that the human lens causes aberrations, possibly, the aberrations contribute to the color appearance of the gray test line, similar to photographs. Then, I performed two experiments to examine whether chromatic aberrations could explain the illusory effect.

3.2.1 Method

Participants

Five males and one female aged 22–44 years old participated in two experiments. All participants had the normal or corrected vision with glasses or contact lenses. Additionally, color vision was confirmed to be trichromatic using an Ishihara Plate.

Procedure for the longitudinal chromatic aberration test

In the longitudinal chromatic aberration test, a square annulus for the fixation and a computer monitor (UP2516D, Dell; 2560 × 1440 pixels, 59 Hz frame rate, Adobe RGB) were orthogonally arranged, and these two images were superimposed by a half-transparent mirror angled at 45°. The depth of the annulus was adjustable, whereas the depth of the monitor was kept constant. The annulus (29.5 cm x 21.0 cm, 30.0 deg × 21.6 deg at a visual distance of 55 cm) had a dark aperture (3.0 cm x 3.0 cm, 3.1 deg × 3.1 deg at a visual distance) in the center. The stimulus image on the monitor was presented at the aperture location. The participants were instructed to report the color appearance of the lines on the monitor while they gazed at the annulus. A fine texture was printed on the annulus surface to help the participants focus on the annulus. The focusing depth was either +1 (far), -1 (near), or 0 (zero) cm relative to the depth of the monitor. The stimulus (312 x 312 pixels, 7.0 deg) was the vertical gray line (*test line*, 1 pixel in width, 1.4 min, CIE $x = 0.313$, $y = 0.330$, $150\,\mathrm{cd/m^2}$) with the white contour on the chromatic background. The chromaticity of the background (*inducer*) was either cyan (CIE $x = 0.278$, $y = 0.330$, $189\,\mathrm{cd/m^2}$), red (CIE $x = 0.340$, $y = 0.330$, $190\,\mathrm{cd/m^2}$), or white (CIE $x = 0.312$, $y = 0.330$, $210\,\mathrm{cd/m^2}$).

Procedure for the transverse chromatic aberration test

In the lateral chromatic aberration test, participants gazed at a fixation point at the center of the monitor. Further, the stimulus image was presented to the right visual field and subtended

1.0 deg to 8.0 deg. Participants were instructed to report the color appearance of the lines. The stimuli (312 × 312 pixels, 7.0 deg) were a test line with a white contour on a chromatic background. The test lines were vertical or horizontal, and the inducer chromaticity was cyan, red, or white. The stimulus contained seven equally spaced test lines in this test instead of a single line. This repetition was intended to reduce the effect of eccentricity between the vertical and horizontal stimuli. The chromaticity and luminance of the stimuli were the same as those used for the longitudinal aberration test.

Analysis

Verbal responses to report color appearance were classified into three categories: reddish (terms including red, pink, orange, or yellow), bluish (terms including blue, water, or cyan), and achromatic (gray, black). When both chromatic and achromatic terms were used simultaneously (i.e., bluish-gray), the response was classified based on color (i.e., bluish). However, no response was observed when both the reddish and bluish terms were used simultaneously. This classification was valid for all responses, except one (green).

3.2.2 Result

Table 3.1 shows the results at the near fixation in the longitudinal chromatic aberration test. At near fixation, three out of six participants perceived the test line on the white inducer as blue, which is consistent with the photographs. The other three participants reported that the test line appeared achromatic. All six participants perceived the stimuli as red when the inducer color was switched to cyan. At the far depth, although no one perceived a red color on the white inducer, five out of six participants perceived a blue color when the inducer color was switched to red (**Table 3.2**). These results indicate that chromatic shifts due to longitudinal chromatic aberration could occur but not exceed the perceptual effect. Thus, the longitudinal chromatic aberration does not appear to be a major contributing factor to this effect.

Table 3.1 Responses at the near fixation.

	White	Cyan	Red
Achromatic	3	0	1
Reddish	0	6	0
Bluish	3	0	5
Others	0	0	0

Table 3.2 Responses at the far fixation.

	White	Cyan	Red
Achromatic	5	1	1
Reddish	0	5	0
Bluish	1	0	5
Others	0	0	0

Next, the color appearance of the test line in the right peripheral visual field was examined. Three participants perceived the vertical lines as reddish in the white surroundings (**Table 3.3**). When the inducer was switched to red, these three lines were perceived as bluish. Although three other participants perceived the white surroundings as achromatic or green, they perceived them

as reddish when the inducer was switched to cyan. Thus, shifts in color appearance due to transverse chromatic aberration could occur but not exceed the size of the perceptual effect. Thus, transverse chromatic aberration does not appear to be a major contributing factor to the illusion.

Table 3.3 Responses for the vertical lines.

	White	Cyan	Red
Achromatic	2	0	2
Reddish	3	6	0
Bluish	0	0	4
Others	1	0	0

Table 3.4 Responses for the horizontal lines.

	White	Cyan	Red
Achromatic	6	2	2
Reddish	0	3	1
Bluish	0	1	3
Others	0	0	0

3.3 Discussion

This chapter considered the Monnier–Shevell illusion as a tool to elucidate the mechanism underlying fine color perception and reported the founding of a new spatial context of the Monnier–Shevell illusion, which causes the chromatic contrast effect towards the red-green color similar to the l axis. The spatial context consisted of thin white lines flanking the thin gray lines on a cyan or red surrounding. The spatial context was independent of the inducer hue, and the complementary color of the inducer was induced in the gray test line. Two experiments showed that the chromatic shift of the chromatic aberrations did not exceed the illusory effect. This result indicates that the new spatial context induces a perceptual color shift.

The Monnier–Shevell illusion is served by summing the first inducer's assimilation effect and the second inducer's contrast effect. This summation indicates that the alternating pattern of inducers is not crucial and can be simplified. Mély already stated that and demonstrated that a spatial pattern composed of two inducers could sufficiently induce the assimilation effect (Mély, Linsley, & Serre 2018). However, they do not refer to the achromatic first ring of the Monnier-Shevell illusion.

If the chromatic ring of the first inducer replaces the achromatic ring, the chromatic assimilation effect from the first inducer vanishes (Monnier & Shevell 2004). Subsequently, the chromatic contrast effect from the second inducer remained. The replacement could also be applied to the spatial pattern of the two inducers, so the white contour is the same as the first inducer of the alternating pattern. The chapter demonstrated that the simple pattern could also be applied by the Monnier–Shevell illusion of the achromatic first inducer. **Fig. 3.1A** and **B** shows the shift in the color appearance of the gray lines without the white contour was smaller than that with the white contour.

The spatial context can easily estimate the chromatic shift due to chromatic aberrations because the spectral component of the white contour is equal irrespective of the inducer hue.

Estimating the chromatic shift is more difficult for the chromatic first inducer of the alternating pattern. The achromatic line of the first inducer has an advantage in that the optical artifact from the first inducer is almost constant across the hues of the second inducer.

The experiment used stimuli composed of thin lines of 1.4 min. Classical illusions commonly use widths ranging from 3.3 to 96 min (Gordon & Shapley 2006; V. C. Smith, Jin, & Pokorny 2001) or up to 4 min for examination of the artifact contributing to the assimilation (Cao & Shevell 2005). The width I used was smaller than the widths. The degree of the thin width is almost similar and small to that of the Monnier–Shevell illusion, which occurs at the maximum effect using alternating surrounding of 3.3 cpd (9.1 min) and a test ring of 6.0 min (Shevell & Monnier 2005). However, how width affects the illusory effect in the achromatic ring of the Monnier–Shevell illusion is unknown. Validation to quantify the optimal width for the spatial context is required to elucidate the mechanism for fine color perception.

3.4 Summary

The chapter took up the Monnier–Shevell illusion as a tool to elucidate the mechanism underlying fine color perception and showed that a new spatial context is valid to cause the Monnier–Shevell illusion for red-green color, similar to L/M-cone colors. The spatial context consisted of thin white lines flanking the thin gray lines on a cyan or red surrounding. The gray lines appeared the complementary color of the surroundings. Thus, the appearance was considered a simultaneous chromatic contrast. To conclude that appearance is a perceptual effect, I performed two experiments in which participants reported that the appearance forced chromatic aberrations to occur. Furthermore, the experiments demonstrated that the chromatic shift of the chromatic aberrations did not exceed the illusory effect. Thus, the spatial context of the white contour is valid for elucidating the mechanisms of fine color perception.

Chapter 4

Additivity of chromatic induction

4.1 Introduction

Spatial patterns modulate the surface appearance. Modulation also occurs in chromatic patterns and chromatic induction. The chromatic contrast enhances the difference in color appearance between a center and its surrounding area. That chromatic induction achieves to average the surface signals to reduce some noise and to enhance the signal contrast to detect spatial changes. If the surroundings are composed of a single chromaticity and the center area is a neutral color, then the complementary color of the surroundings is induced. However, if the center area is not a neutral color, chromatic induction occurs along a vector between the chromaticity of the center and surrounding area (Ekroll & Faul 2012; V. C. Smith, Jin, & Pokorny 2001). Thus, chromatic induction with a uniform surrounding depends on the spatial contrast of the center area.

The Monnier-Shevell illusion causes a large shift in the color appearance by a patterned surrounding with two chromaticities (Monnier & Shevell 2003). This induction is the summation of both the assimilation from the proximal area and the contrast effect of the distant area of the center area (Monnier & Shevell 2004). For example, the surrounding alternating S-cone colors induced a color shift in the S-cone modulation to the test area. Previous studies reported that the shift was large in S-cone modulation, even though the test chromaticity had an L-cone contrast relative to the distant and proximal areas (Monnier & Shevell 2003, 2004; Shevell & Monnier 2006). This is inconsistent with previous results using stimuli with the center-surround pattern.

Chapter 3 shows that the thin gray line flanked by the white contour appears reddish in the cyan inducer. However, it is still unknown how modulation along only the L/M-cone axis affects the color shift in the test area with varying chromaticity. Therefore, it is important to discuss whether the alternating pattern is valid for the L/M-cone opponent and chromatic induction from the alternating pattern of S-cone colors.

This chapter shows that the surrounding pattern alternating the L/M-cone colors induces a large shift along with the L/M-cone modulation. Induction was independent of test chromaticity.

A color shift occurs in the S-cone axis when the test chromaticity has an S-cone contrast with the surroundings.

4.2 Method

4.2.1 Participants

Seven participants (five male and two female, ages 23–47 years) with normal or corrected-to-normal visual acuity participated in the experiments. Normal trichromacy was assessed using Ishihara color plates. The Committee for Human Research at the Toyohashi University of Technology approved the experimental procedure per the ethical guidelines outlined in the Declaration of Helsinki. The experiment was conducted following the approved protocol. Each participant provided informed consent after receiving the procedural details.

4.2.2 Apparatus

Stimuli were presented on a liquid crystal monitor (UP2516D, Dell; 2560 × 1440 pixels, 59 Hz frame rate, Adobe RGB). The monitor was connected via an HDMI cable to the graphics card (GeForce RTX 3070, NVIDIA, 10 bits) of a PC running Ubuntu 20.04.3 LTS (64 bits). The color and luminance were calibrated with spectroradiometer specbos 1211-2 (JETI, Germany) under the same illumination conditions as the experiment. The experiment was controlled using custom software developed in MATLAB 2020b (Mathworks) and Psychtoolbox 3.0.17 (D. H. Brainard 1997). All analyses were performed using the Statistics and Machine Learning Toolbox 12.0, MATLAB R2020b, MathWorks).

4.2.3 Stimuli

The color chromaticity of the stimuli was defined by the MacLeod–Boynton (MB) chromaticity coordinates MacLeod & Boynton (1979) using the Smith and Pokorny cone fundamentals (V. C. Smith & Pokorny 1975). The spectral intensity of the monitor was measured using a spectroradiometer specbos 1211-2 (JETI, Germany) to obtain the cone excitation. Two axes l and s, the relative activation of the L- and M-cones [$l = \mathrm{L}/(\mathrm{L} + \mathrm{M})$], and the activation of the S-cone [$s = \mathrm{S}/(\mathrm{L} + \mathrm{M})$] in an equiluminant plane were considered. The unit of s is arbitrary and was normalized in this study to 1.0 for equal-energy white.

The sample and comparison were presented on a gray background (CIE $x = 0.313$, $y = 0.329$, 50 cd/m^2, $l = 0.635$, $s = 0.864$) side-by-side at 1.2 deg apart, and their positions on the left or right were randomized. A vertical line (1 pixel in width, 1.9 min, *test line*) was placed at the center of the colored square (101 × 101 pixels in width 3.1 deg, inducer area). There were three conditions for the sample stimuli: white-contour condition with a white contour (**Fig. 4.1A**), chromatic-contour condition with an opponent color contour of the inducer (**Fig. 4.1B**), and no-contour condition without any flanking contours (**Fig. 4.1C**).

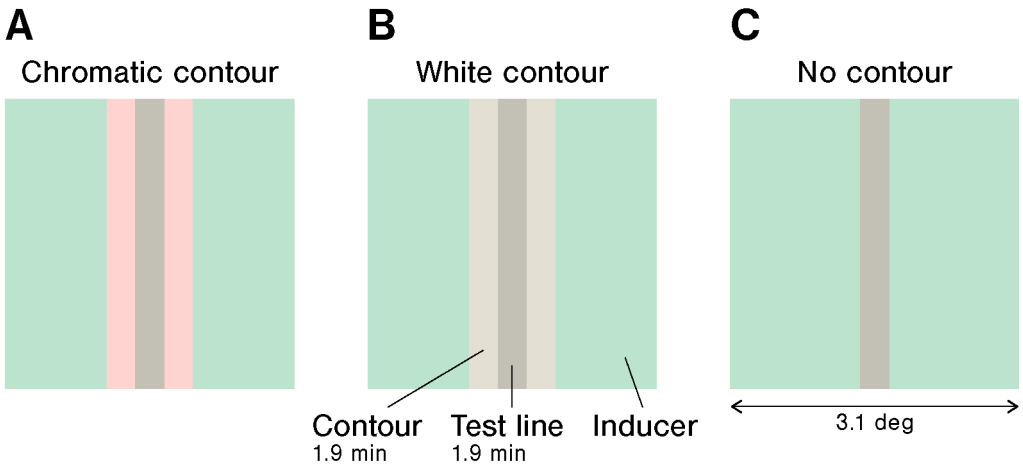

Figure 4.1 Stimuli for the experiment

Lines were placed at the center of the chromatic background. The chromatic and white contours flank the test line for the chromatic- (**A**) and white-contour conditions (**B**). The no-contour condition (**C**) was the test line without contours. These displays are the enlargement of actual stimuli.

Fig. 4.2 shows the chromaticities for the stimuli. The contours (1 pixel in width, 1.9 min, 210 cd/m^2) were placed adjacent to the left and right edges of the test line. The colors of the contour were white (CIE $x = 0.313$, $y = 0.329$, $l = 0.635$, $s = 0.864$), cyan (CIE $x = 0.277$, $y = 0.340$, $l = 0.618$, $s = 0.864$) and red (CIE $x = 0.344$, $y = 0.319$, $l = 0.652$, $s = 0.864$). The chromaticity of the test line was three: violet (CIE $x = 0.362$, $y = 0.441$, $l = 0.635$, $s = 1.364$), yellow (CIE $x = 0.284$, $y = 0.264$, $l = 0.635$, $s = 0.364$) and gray (CIE $x = 0.313$, $y = 0.329$, $l = 0.635$, $s = 0.864$). The luminance of the test line was 150 cd/m^2. The inducer area was either cyan (CIE $x = 0.277$, $y = 0.340$, $l = 0.612$, $s = 0.864$) or red (CIE $x = 0.344$, $y = 0.319$, $l = 0.652$, $s = 0.864$).

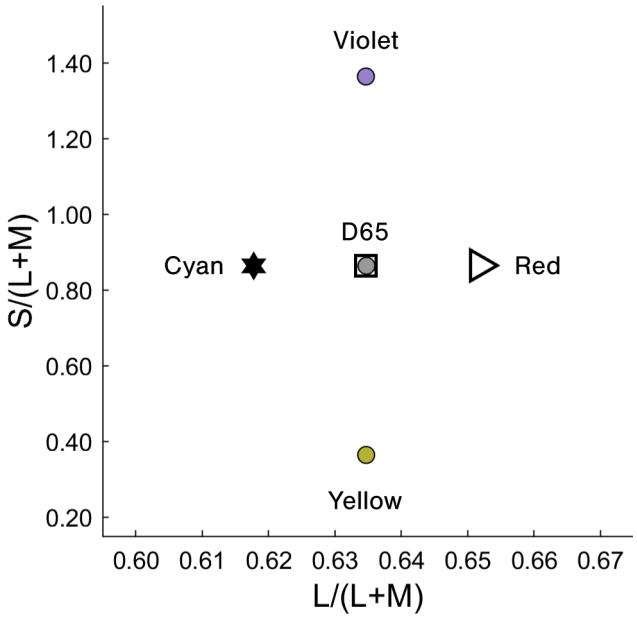

Figure 4.2 Stimuli chromaticities in the MacLeod-Boynton coordinates for the cyan inducer

Edged circles indicate the chromaticity of the test line. The filled stars indicate the chromaticity of the inducer. Open squares and triangles indicate contour chromaticity. Stimuli for the red inducer switched the chromaticity between the cyan inducer and chromatic contour.

Stimuli also contained a baseline stimulus, which was the test line on the gray inducer (190 cd/m^2, CIE $x = 0.313$, $y = 0.329$, $l = 0.635$, $s = 0.864$) to evaluate the quality of participant matching. The comparison stimulus had a white square (101 $\times$ 101 pixels, 3.12 deg), which had the same color and luminance as the white contour, and one vertical line (1-pixel width, 1.9 min) located at the center.

4.2.4 Procedure

Participants' heads were secured on a chin rest at a viewing distance of 40 cm from the monitor. The participants were asked to adjust the color and luminance of the line of comparison to match the appearance of the sample line using a gamepad. Vertical manipulation of one stick changed the luminance of the line of comparison. Another stick manipulated the chromaticity of the comparison line in MB space. Fixation was not required. After the participants were satisfied with the matching, they pressed the button to complete the trial and proceeded to the next trial with a 500 ms blank screen (D65, 50 cd/m^2).

Before the experiment, the participants were trained on the apparatus, and symmetric color matching was performed while adapting to the illuminated room. The training stimuli were composed of a sample and comparison; both had a thin line (1px in width 1.9 min) on a white

background. The stimuli for training were the same as those for the baseline stimuli.

In the experiment, 21 sample stimuli were presented in random order. A short break of at least 2 min was interleaved with completing the matching of the seven stimuli. Each participant repeated the matching three times with at least a 5-minute break between the sessions. The time required for one session was approximately 20–45 min.

4.3 Result

The shift in color appearance of the test lines was measured under three conditions: in the contour condition (squares), the white contour flanked the test line; in the chromatic contour (triangles), the chromatic contour flanked the test line; in the no-contour condition (filled circles), no contour flanked. Finally, the baseline testing (diamonds) the test line with a uniform gray surrounding.

Fig. 4.3 shows the result of the cyan inducer. The baseline matching did not significantly shift in the l axis from the test chromaticity ($p > 0.05$, t-test, **Fig. A.2A**). The matchings show the quality of participants' matching. Matching to the chromatic-contour condition caused the large l to shift away from the inducer chromaticity (**Fig. A.2A**) and passed over the red contour chromaticity. This shift corresponds to the assimilation effect from the contour and the contrast effect from the inducer. Matching to the white-contour condition shifted away from the inducer chromaticity along the l axis (**Fig. A.2A**). The no-contour condition also shifted slightly away from the inducer chromaticity (**Fig. A.2A**). These shifts indicate the contrast effect to that of the inducer. The shift magnitude in the l axis differed across the conditions ($p < 0.05$, $F(2, 180) = 98.10$; contour, $p > 0.05$, $F(2, 180) = 0.22$; test, 2-way ANOVA, **Table 4.1)**. The magnitudes under the chromatic-contour condition were larger than those under the white-contour condition (**Fig. A.2A**). All the conditions showed a significant shift in the l axis, irrespective of the test chromaticity.

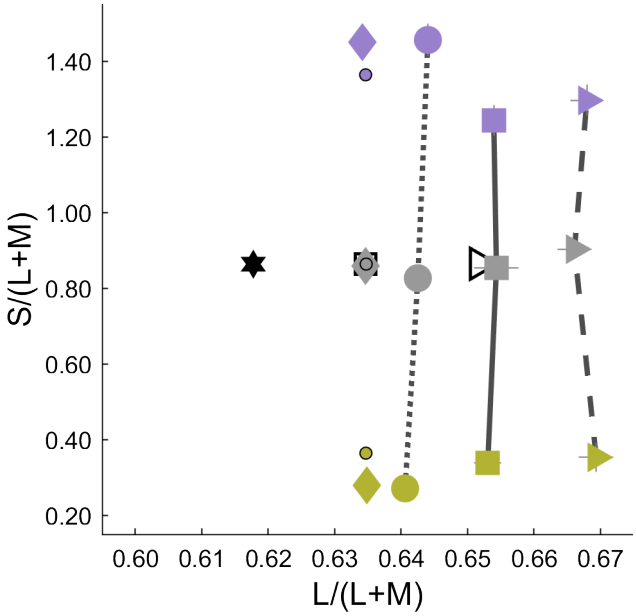

Figure 4.3 Matching the appearance of the test lines (edged circles) on the cyan inducer (filled star) plotted in MB chromaticity space

The filled square, triangle, and circle markers represent matching to the test line of the white-, chromatic- no-contour conditions, respectively. The filled diamonds represent matchings to the test line of the baseline stimuli. The colors of these markers correspond to the three chromaticities of the test lines. The open square and triangle represent the contour chromaticity. Matchings were averaged across all participants (n = 7). Error bars represent the standard error of the mean.

Table 4.1 Two-way ANOVA of the l shift in the contour conditions of cyan inducer

Source	SS	df	MS	F	p
Contour	0.02	2	0.01	98.10	0.00
Test	0.00	2	0.00	0.22	0.80
Contour*Test	0.00	4	0.00	0.52	0.72
Error	0.02	180	0.00		
Total	0.04	188			

SS: Sum of squares, df : degrees of freedom, MS: Mean squares

Fig. 4.4 shows the result of the red inducer. The shift in the l axis of the red inducer was opposite to that of the cyan inducer. Matchings of the baseline condition were close to the physical chromaticity of the test lines (**Fig. A.2B**). The chromatic-contour condition caused a large shift in the l axis towards contour chromaticity (**Fig. A.2B**). The white- and no-contour matchings shifted to a lower l (**Fig. A.2B**). This shift is the contrast effect to the red inducer. The shift magnitude in the l axis differed across the conditions ($p < 0.05$, $F(2, 180) =$

107.02; contour, p >0.05, F(2, 180) = 0.18; test, 2-way ANOVA, **Table 4.2)**. The shifts in the chromatic-contour condition were larger than those in the white-contour condition (**Fig. A.2B**).

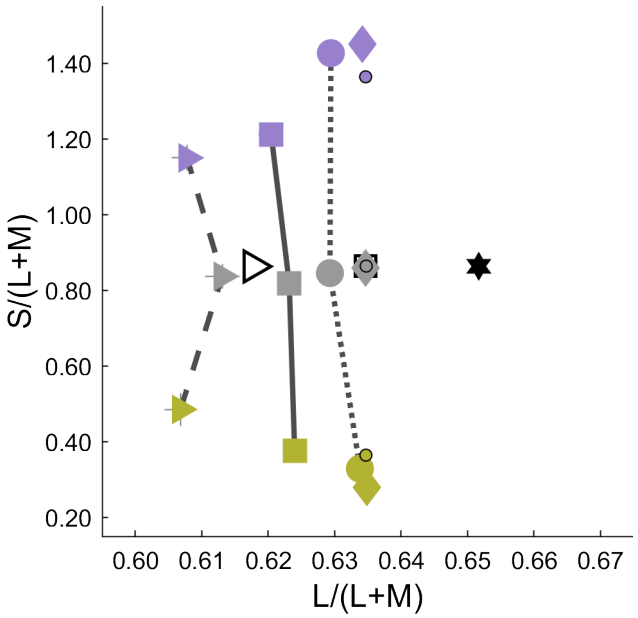

Figure 4.4 Matching the appearance of the test lines (edged circles) on the red inducer (filled star) plotted in MB chromaticity space
The format is the same as in **Fig. 4.3.**

Table 4.2 Two-way ANOVA of l shift in the contour conditions of the red inducer

Source	SS	df	MS	F	p
Contour	0.01	2	0.01	107.02	0.00
Test	0.00	2	0.00	1.75	0.18
Contour*Test	0.00	4	0.00	2.29	0.06
Error	0.01	180	0.00		
Total	0.03	188			

SS: Sum of squares, df : degrees of freedom, MS: Mean squares

Fig. 4.5 shows the shifts in the s axis from the test chromaticity. The shifts in the l axis had the same trend between inducers, whereas the shifts in the s axis did not. The matchings of the violet test line with the contours shifted to lower s for both the inducers. The violet line of the baseline and no-contour conditions matched the higher s axis. Further, the s shifts of the contour conditions in the yellow test line were not consistent between the inducers. The gray test matched to close to zero in the s axis of both the inducers.

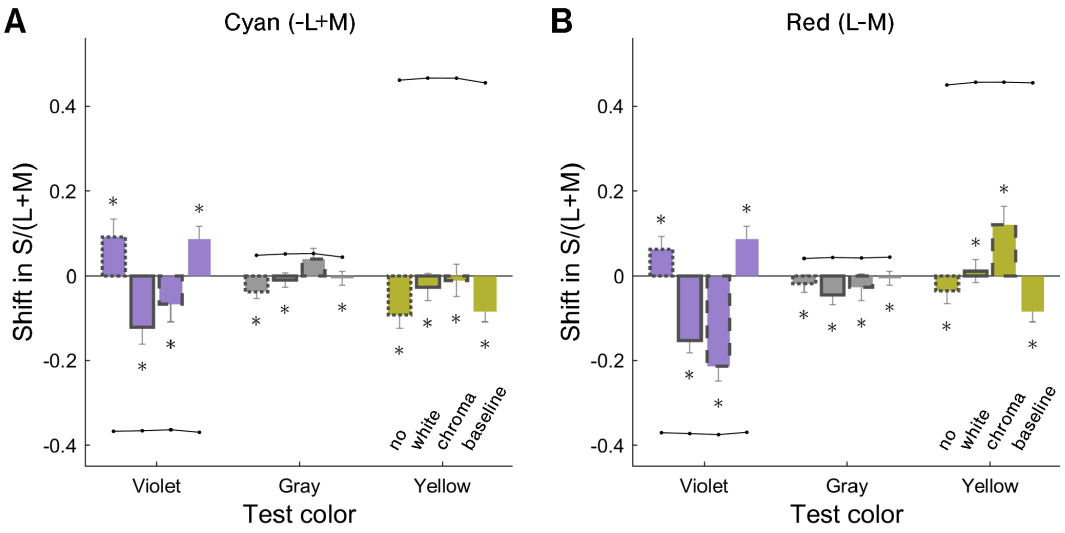

Figure 4.5 Shifts in the *s* axis from the test chromaticity

Bars surrounded by dotted, bold, dashed, and no lines indicate the color shifts of the no-, white-, chromatic-contour, and baseline, respectively. The bar colors correspond to the test colors, as shown on the horizontal axis. The error bars are the same as those in **Fig. 4.3** and **Fig. 4.4.** The dotted line represents the chromatic shift of the simulated artifact (see details for Analysis). Asterisks represent the significant difference between matching and artifact chromaticity ($p < 0.05$, t-test). (**A**) cyan, (**B**) red inducer.

4.3.1 Optical artifacts

The shifts in the violet test were larger than those in the yellow and gray tests. Therefore, the optical artifacts might be the cause of the *s* shift. The shift was attributed to the chromatic shift of optical artifacts because the violet light contained much short-wavelength light. The cornea and lens focus images of the retina. Several artifacts emerge in the retinal image due to human ocular optics imperfections. Wavelength-independent aberrations, referred to as monochromatic aberrations, blur an image. Wavelength-dependent aberrations, referred to as chromatic aberrations, arise from a difference in the refractive index, where short-wavelength light is further refracted. There are two types of chromatic aberrations: longitudinal and transverse aberrations. Longitudinal aberrations cause a difference in the focus points along an optical axis; thus, short-wavelength light is blurred on the image plane, while long-wavelength light is focused. Transverse aberrations occur when long-wavelength light is focused on a peripheral position farther than that of short-wavelength light, thus causing a chromatic fringe at an edge. These artifacts degrade the quality of retinal images, particularly the color and spatial details. We used extremely thin stimuli. Thus, artifacts significantly influenced the image. A chromatic shift similar to the assimilation is observed if the monochromatic aberration causes the light to

spread from the inducer to the test line. If the longitudinal chromatic aberration causes light to spread from the inducer and contour to the test line, blue chromaticity is induced. To determine whether the color shift observed in the experiment originated from optical or neural factors, it was necessary to quantitatively predict these optical artifacts and compare them with the results of color matching.

Marimont & Wandell (1994) proposed a model for calculating retinal images using human ocular optics. The model integrates a formula representing the wavelength-dependent defocus (Thibos, Ye, et al. 1992) and the optical transfer function (OTF), including longitudinal chromatic aberrations (D. R. Williams, D. H. Brainard, et al. 1994), into the OTF of Hopkin's eye model (Hopkins 1955). We applied this model to the stimuli and examined whether optical artifacts accounted for the color shift observed in the experiment.

The model calculates a retinal image from an input image using ocular optics. The input image was the same as that used in the experiment, with a resolution of 0.48 min per pixel. The region of the test line of the output image was averaged the MB space. Although aberrations change significantly in chromaticity and intensity, we determined the artifacts in the MB space to focus on color shift. The pupil diameter used in the calculation was 3.05 mm. This value is appropriate for a background luminance of 50 cd/m^2 and a screen with a width of 79.2 deg and a height of 45.0 deg (Atchison et al. 2011; Stanley & A. K. Davies 1995; Watson & Yellott 2012). All parameters in the model were set to focus on the wavelength of 580 nm (Marimont & Wandell 1994).

The dotted lines represent the chromatic artifact shift from the test chromaticity as shown in **Fig. 4.5A**. For the cyan inducer, the artifact of the violet test caused a shift to a lower s. This was irrespective of the conditions. The artifact of the violet test caused a shift to a lower s, irrespective of the conditions. The artifact of the yellow test caused a shift to a higher s, irrespective of the conditions. Further, the artifacts in the gray test hardly shifted. Except for the gray test of the chromatic condition, the chromatic shifts of the artifact were significantly different from the matching ($p < 0.05$, t-test).

The simulated artifacts in the red inducer produced the same trend as those in the cyan inducer (**Fig. 4.5B**). The violet and yellow tests artifact caused a shift to lower and higher s, irrespective of the conditions. The chromaticity of the grey test shifted slightly to higher s. All matches were significantly different from the simulated artifact ($p < 0.05$, t-test).

4.4 Discussion

The matching experiment quantified the shift in the color appearance of the test line with chromatic surroundings. All the test lines on the uniform achromatic surroundings matched the physical chromaticity. The test line of the no-contour condition on the uniform cyan or red surrounding, differing from the L/M-cone stimulation, shifted away from the surrounding

chromaticity along the l axis. This was irrespective of the test chromaticity. When the test line flanked the white contour, the color shift became larger than the no-contour condition. The contour was changed to a complementary color, resulting in the largest shift away from the inducer. The induced color of the test chromaticity, which had the s contrast to the inducer, slightly shifted along the s axis (These shifts could be attributed to the assimilation effect from the white contour). The matchings of the red inducer showed the same trend as those of the cyan inducer. The contour conditions of the red inducer resulted in a color shift away from the inducer along the l axis.

The large shift along the MB axis was consistent with the results of a previous study. Monnier and Shevell examined the color shift of the test ring with the surroundings alternating with the S-cone colors. Moreover, they showed that its shift was along the s axis irrespective of the test chromaticity (Monnier & Shevell 2003, 2004). This shift in the s axis can be represented by the center-surround cell that receives inputs from the S cone. The center-surround cell could sum up the assimilation from the proximal ring and the contrast effect from the distant ring. When the test and proximal ring are exposed to the center-receptive field, the proximal ring's light is mixed with the test ring's light. Further, it is inhibited by the surrounding lights, irrespective of the test chromaticity. Additionally, the center-surround cell exists in the L/M cone channel. Thus, it could be predicted that the shift in the l axis occurs irrespective of the test chromaticity. These results align with the predictions.

A color shift also occurred in the s axis for the contour conditions, irrespective of the inducer color. Because the test line was thin, there was a possibility that the optical artifacts contributed to the color shift. Thus, the proposed model simulated the chromatic shift of the artifact to compare it with the matching shift. However, this artifact failed to explain the color shift in the s axis.

The s shift tended to be larger in the purple and yellow tests but not in the gray test. This difference could reflect the chromatic contrast between the test and contour in s. The spatial patterns of the purple and yellow tests correspond to the no-contour condition along with s. The fine spatial pattern modulated along s is affected by perceptual induction (Cao & Shevell 2005; V. C. Smith, Jin, & Pokorny 2001).

Previous studies using S-cone alternating were inconsistent with the shift along the other axis in this chapter (Monnier & Shevell 2003, 2004; Shevell & Monnier 2006). This discrepancy could be due to the difference in the spatial extent of each cardinal axis. The red-green axis from the L/M-cone modulation can have a high spatial frequency of the spatial pattern because the L and M cones are densely packed in the retina. Thus, chromatic induction in L/M-cone modulation might occur in a higher spatial pattern. Previous studies used stimuli with 9 min-width lines. This width is approximately five times greater than that of the stimuli in this chapter. Otazu, Parraga, & Vanrell (2010) have shown the chromatic induction in the l and s axis varied with changing the spatial frequency of stimuli alternating both cardinal axes colors. To discuss this

discrepancy, it is necessary to independently investigate the spatial extent of the alternating pattern that causes chromatic induction.

4.5 Summary

The patterned surroundings shifted the color appearance of the fine test area. If the surroundings are alternated with two chromaticities of the S-cone colors, a shift occurs along with the S-cone stimulation. This is irrespective of the test chromaticity. However, it was unknown how the patterned surroundings of the L/M-cone colors affect the color shift of the test area. An experiment was performed to quantify the shift in the appearance of the test area on a chromatic inducer by varying the test chromaticity. The results showed that the appearance of the test area with or without the contour shifted away from the inducer chromaticity along the l axis of the MB space. The color shifts were larger under the chromatic, white, and no-contour conditions. These results support the receptive field model of the center-surround cell, which is a basic function that produces a color shift. The violet (higher s) and yellow (lower s) tests with the contour matched the sight lower s and higher s, respectively. Moreover, the slight shifts in the s axis suggest that the spatial extent of the receptive field.

Chapter 5

Line width dependency

This chapter is published as the paper,
T. Kanematsu & K. Koida (2022). "Influence of Stimulus Size on Simultaneous Chromatic Induction". In: *Front. Psychol.* 13.818149, pp. 1–12. DOI: 10.3389/FPSYG.2022.818149.

5.1 Introduction

Human visual perception is influenced by spatial contexts such as chromatic surroundings, luminance, and size. The influence of the surrounding chromaticity (chromatic induction) on the centered area can be classified as assimilation and contrast depending on the direction of changes in the color appearance. The assimilation is a type of spatial averaging that contributes to reliable chromatic signal detection. The chromatic contrast process facilitates the detection of low-contrast objects and contributes to color constancy (Hurlbert & Wolf 2004; Lotto & Purves 2000). To fully understand these chromatic inductions, it is necessary to assess the contributions of optical and neural factors to various stimulus sizes and luminance contrasts, given that both factors generally lead to similar shifts in color appearance.

Monnier & Shevell (2003) reported that surrounding rings alternating between two chromaticities produces a strong shift in the color appearance of the centered ring. This chromatic induction was interpreted as an additive integration from the chromatic assimilation effect of the proximal rings and the chromatic contrast effect of the distant rings (Mély, Linsley, & Serre 2018; Monnier & Shevell 2003, 2004). For example, when the proximal and distant rings were violet and lime-yellow, respectively, the color of the centered ring was strongly perceived as bluish (**Fig. 2.14A** top). Switching the chromaticity between the proximal and distant rings induced a greenish color to the test ring (**Fig. 2.14A** bottom). Similar color shifts were observed even when the proximal ring was achromatic, which was due to the contrast effect of the distant rings (**Fig. 2.14B**; Monnier & Shevell 2004). Chapter 3 reported a new spatial context for the Monnier-Shevell illusion that causes the color shift along with red-green colors. The new spatial context is a thin white contour (*contour*) flanks a thin gray line (*test line*), which

is perceived as the complementary color of the chromatic background (*inducer*). This contour and the chromatic inducer are thought to correspond to the proximal and distant surrounds of the Monnier-Shevell illusion. These results suggest that color induction from the chromatic modulation is effective irrespective of hues.

Similar to ordinary chromatic induction (Bergström & Derefeldt 1975; Bergström, Derefeldt, & Holmgren 1978; Cao & Shevell 2005; De Weert & Spillmann 1995; Fach & Sharpe 1986; Gordon & Shapley 2006; J. A. S. Kinney 1962; Kirschmann 1891; Pinna, Brelstaff, & Spillmann 2001; V. C. Smith, Jin, & Pokorny 2001), the Monnier–Shevell illusion is dependent on the ring width (Shevell & Monnier 2005) and luminance contrast (Cerda-Company et al. 2018). The width dependency of the Monnier–Shevell illusion was investigated for the S-cone chromaticity, given that the illusory effect was prominent for S-cone chromaticity, although the effect was observed for the L/M-cone chromaticities (Cerda-Company et al. 2018; Lin, C.-C. Chen, & Chien 2010; McCamy 2003). The neural mechanism of the Monnier–Shevell illusion is based on the excitatory-center and the inhibitory-surrounding organization receiving inputs from the S cone (Mély, Linsley, & Serre 2018; Monnier & Shevell 2004). It was conjectured that the significant effect does not occur only for the S-cone chromaticity, given that the center-surround organization in V1 occurred for the L/M-cone chromaticity (Brouwer & Heeger 2009; Chatterjee & Callaway 2003; Conway & Livingstone 2006; E. N. Johnson, Hawken, & Shapley 2001; E. N. Johnson, Hawken, & Shapley 2008; Lennie, Krauskopf, & Sclar 1990). This physiological evidence questions whether previous reports of weak illusional effects for L/M-cone chromaticities (Cerda-Company et al. 2018) could be due to the non-optimal, large width of the stimuli.

Three points remain quantitatively unknown: (1) the optimal width for the illusion modulated along the L/M-cone, (2) the difference in the optimal width when compared with the S-cone, and (3) the influence of optical artifacts on the width and luminance dependency. In this study, we performed a psychophysical experiment by varying the width of a center line, the width of a flanking contour, and the luminance levels of the center line to quantitatively evaluate the following: whether the color appearance changes with respect to the width, and whether the optimal width changes with respect to the surrounding chromaticity. Moreover, we estimated artificial chromatic shifts due to the human ocular optics, and participants were asked to comment on the influence of the optical artifacts on the perceptual color shifts. This enabled us to isolate the optical factors from neural factors.

In this manuscript, we report that the color shift is evident for thin lines when the surrounding has an L/M-cone chromaticity. On a cyan background (-L + M), the thinnest ring on the center appeared reddish, and the thicker rings appeared gray (**Fig. 5.1A**). On the red background (L - M), the thinnest ring on the center appeared cyan (**Fig. 5.1B**). On the violet background [S - (L + M)], all the rings appeared yellowish (**Fig. 5.1C**). Finally, on the yellow background [-S + (L + M)], all the rings appeared bluish (**Fig. 5.1D**). All the rings were initially and gray, and the flanking contours were white.

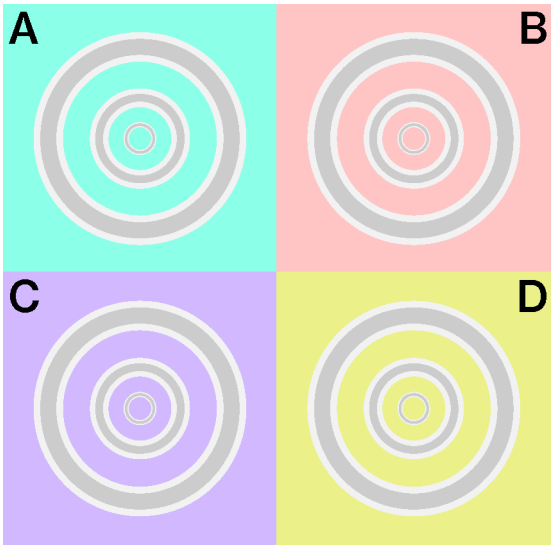

Figure 5.1 Chromatic induction demos

The color appearance of gray rings differed among the chromaticities of the backgrounds although the physical chromaticity of the rings was the same. Concentric gray rings were flanked by white contours. The innermost ring appeared reddish on the cyan background (**A**), and cyan on the red background (**B**). Moreover, all the rings appeared yellowish on the violet background (**C**) and bluish on the yellow background (**D**). Note: please adjust the viewing distance for the effective illusion, and maintain a distance from the figure to maximize effectiveness.

5.2 Method

5.2.1 Perticipants

Seven participants (6 males, 1 female; ages 23 to 44) with normal or corrected-to-normal visual acuity participated in the experiments. Normal trichromacy was assessed using the Ishihara color plates. The experimental procedure was approved by the Committee for Human Research at Toyohashi University of Technology in accordance with the ethical guidelines outlined in the Declaration of Helsinki. The experiment was conducted in accordance with the approved protocol. Each participant provided informed consent after receiving the procedural details.

5.2.2 Apparatus

This experiment was performed using the monitor (UP2516D, Dell; 2560 x 1440 pixels, Adobe RGB color monitor), equipment, script environment (Psychtoolbox 3.0.15, D. H. Brainard (1997) on Matlab R2018a, Mathworks), and calibration with a chroma meter (CS-200, Konica Minolta, Japan), which were the same as those employed in a previous study (Kanematsu & Koida 2020).

5.2.3 Stimuli

The color chromaticity of the stimuli was defined by the MacLeod–Boynton (MB) chromaticity coordinates (MacLeod & Boynton 1979) using the Smith and Pokorny cone fundamentals (V. C. Smith & Pokorny 1975). The spectral intensity of the monitor was measured using an illuminance spectrophotometer (CL-500A, Konica Minolta, Japan) to obtain the cone excitation. Two axes l and s, the relative activation of the L- and M-cones [l = L/(L + M)], and the activation of the S-cone [s = S/(L + M)] in an equiluminant plane were considered. The unit of s is arbitrary, which was normalized in this study to 1.0 for equal-energy white.

The sample stimulus was a vertical straight line (test line) tinted in pale or dark gray (D65, $l = 0.66$, $s = 0.87$, CIE $x = 0.313$, $y = 0.329$, luminance = 25, 150 cd/m^2; **Fig. 5.2)**. It is known that a straight line induces a similar illusory effect as the Monnier–Shevell illusion (McCamy 2003). A straight line is convenient for displaying stimuli with an exact width per pixel. The widths of the test lines were 0.9, 1.9, 3.7, 7.4, 14.9, and 29.7 min (1, 2, 4, 8, 16, and 32 pixels; **Fig. 5.3)**. The test line was placed at the center of an inducer area (4.8 deg = 312 or 311 pixels square; **Fig. 5.2B**). The inducer chromaticity was selected along the cardinal axis of the MB chromaticity coordinates (**Fig. 5.2A**). Chromaticities of the inducers were cyan ($l = 0.64$, $s = 0.87$, CIE $x = 0.278$, $y = 0.329$), red ($l = 0.68$, $s = 0.87$, CIE $x = 0.340$, $y = 0.330$), violet ($l = 0.66$, $s = 1.12$, CIE $x = 0.297$, $y = 0.291$), and yellow ($l = 0.66$, $s = 0.61$, CIE $x = 0.334$, $y = 0.380$). The luminance of the inducer area was 190 cd/m^2. Two stimuli conditions were used (**Fig. 5.3)**: a white-contour condition with a flanking white contour (D65, 210 cd/m^2) and a no-contour condition without a flanking contour. The widths of the contours were 0.9, 1.9, 3.7, and 7.4 min (1, 2, 4, and 8 pixels, respectively; **Fig. 5.3)**.

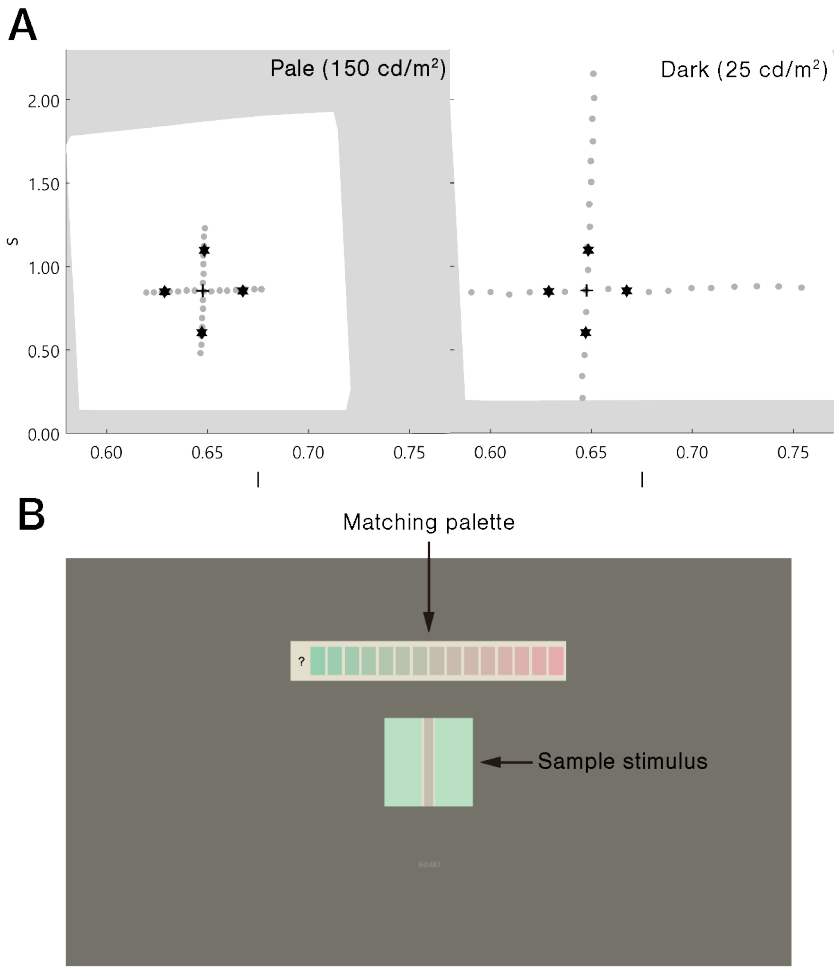

Figure 5.2 Chromaticity of the stimuli and the screen design

(**A**) The stimulus was defined in the MacLeod–Boynton (MB) chromaticity space. The stars, cross, and gray dots indicate the inducer, D65 of the neutral gray, and the matching palettes, respectively. The white background indicates the gamut of the monitor. The upper and lower panels correspond to the pale (150 cd/m^2) and dark (25 cd/m^2) test line conditions, respectively. Note: the luminance of the inducer was maintained at 190 cd/m^2. (**B**) The screen. The stimulus was placed at the center of the screen. The matching palette was placed above the stimulus.

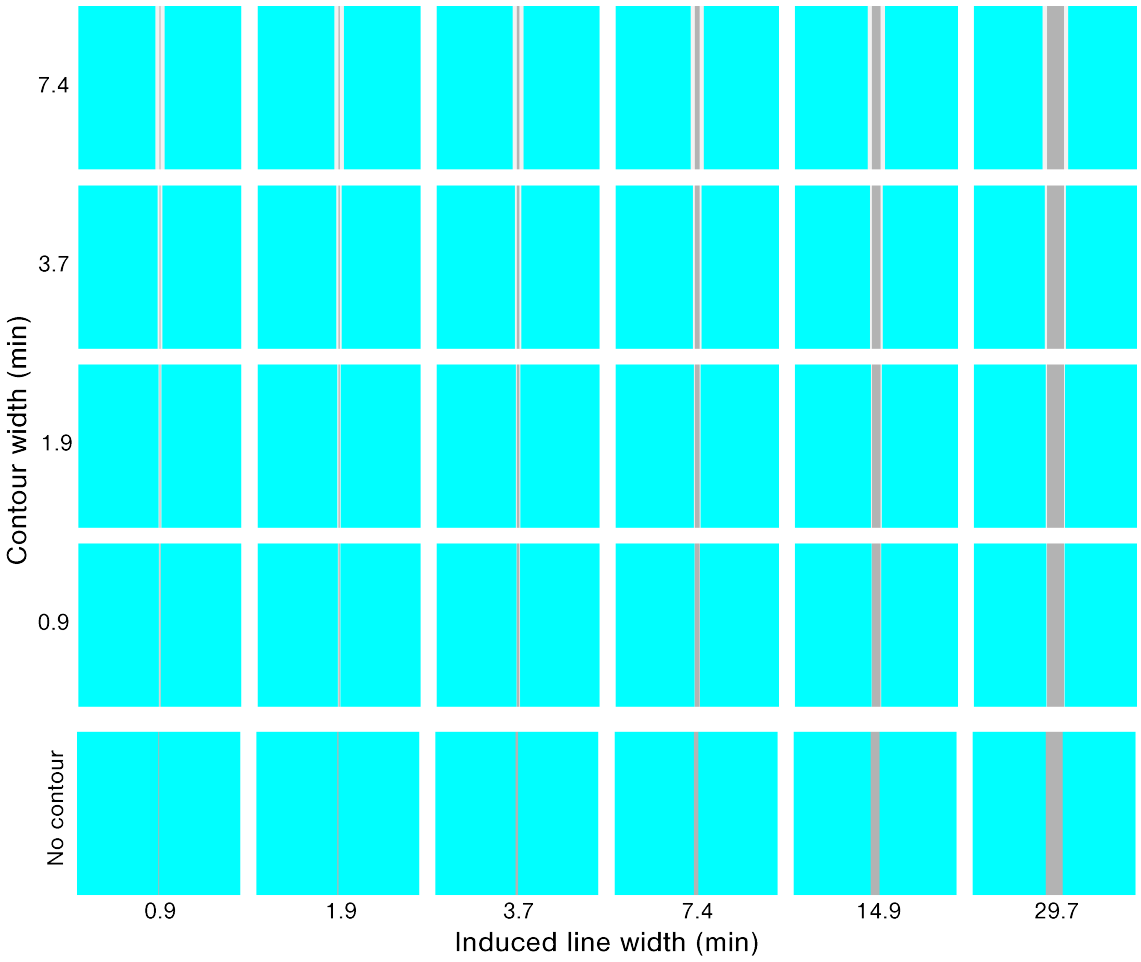

Figure 5.3 Stimulus example of the cyan inducer

The test line increased in thickness toward the right, and the white contour increased in thickness toward the top. The no-contour condition is shown at the bottom. The color and brightness were optimized for presentation.

A matching palette made of horizontally aligned chromatic rectangles (0.8 deg x 1.6 deg) with a gap of 0.2 deg was used. This palette was placed above the stimulus with a gap of 2.0 deg (130 pixels). The luminance of the rectangles and the test line was the same. The chromaticity of the palette was evenly spaced along the cardinal axes of the MB chromaticity space, including the neutral gray D65 (Figure 2A). The number of rectangles was 15–17 depending on the chromaticity of the inducer. The density of the palette on the MB chromaticity was higher for the pale condition and lower for the dark condition. These ranges and densities were determined based on the participant responses in the preliminary experiment. The rectangles were placed on a white background (D65, 210 cd/m^2) to maintain the same luminance contrast as that of the test line of the white-contour condition. The screen outside the stimulus and matching palette was painted gray (D65, $l = 0.66$, $s = 0.87$, CIE $x = 0.313$, $y = 0.329$, 50 cd/m^2, 39.6 deg x 22.3

deg).

5.2.4 Procedure

After the participants adapted to a dimly illuminated room for 5 min, the experiment was initiated. The head of each participant was fixed on a chin rest at a viewing distance of 80 cm from the monitor. The participants were then instructed to select the rectangle from the matching palette that matched the color appearance of the test line **Fig. 5.2B**) using the mouse. Fixation was not required. Thereafter, the participants pressed the button to proceed to the subsequent trial. A 300-ms blank screen (D65, 50 cd/m^2) was shown between each trial. The total number of presented stimuli was 240, including four inducers, two luminance levels, six widths of the test lines, four widths of the white contour, and the no-contour condition. The 240 stimuli were presented in random order. Participants were provided with a break of approximately 4 min after every 80 matchings, and all the matchings were completed after approximately 40 min (including breaks). This experiment was conducted three times for each participant, with a minimum break of 10 min between sets.

5.2.5 Analysis

The participants were permitted to select the question mark on the left of the palette if no suitable chromaticity was present on the palette or if they were unable to distinguish the test line. Even in the most frequent case, the percentage was less than 10% for each stimulus (**Fig. B.1)**. Therefore, we concluded that the responses to the question had a low impact, and such responses were considered as missing data.

To compare the matching across different chromaticities of the inducers, the matched chromaticity was normalized by the inducer chromaticity based on the metrics of the MB chromaticity. Hereafter, we refer to the contrast effect, similar to the metric in a previous study (Cerda-Company et al. 2018), as $\Delta E_m/\Delta E_i$, where ΔE_m is the distance of the matching from D65, and ΔE_i is the distance of the inducer from D65. The contrast effects of the cyan and red inducers are defined by the l axis. The matching of the violet and yellow inducers is defined by the s axis. A positive contrast effect indicates a color shift away from the inducer, a negative contrast effect indicates a color shift toward the inducer, and zero indicates no color shift.

All analyses were performed using the fitrm and ranova functions (Statistics and Machine Learning Toolbox 12.0, MATLAB R2020b, MathWorks) for N-way analysis of variance (ANOVA) with repeated measures.

To examine the difference in the optimal width, which was distributed in two dimensions between the two groups, we performed a bootstrap test. The optimal width presented in the main analyses was obtained after averaging, smoothing, and then determining the maxima. Here, the optimal width was obtained individually instead, and 21 optimal widths were obtained (seven participants repeated three times). The distance between the two groups was determined by

the Euclidean distance between the mean of each group in the metrics of log (min). The null hypothesis was that the optimal widths of the L/M- (including both cyan and red inducers) and S-cone chromaticities (including both violet and yellow inducers) were the same. Based on the null hypothesis, the optimal widths were randomly shuffled across the two groups, and the mean distance was obtained. This re-sampling was performed 2,000 times to obtain the distribution of the mean distance. Subsequently, the distance inducing 95% of the distribution was calculated and compared with the original distance in the experiment. Moreover, the bootstrap test of the luminance levels for each cardinal axis was performed.

5.3 Result

5.3.1 Optimal line width

The color appearance of the pale test line is shown in **Fig. 5.4.** For the cyan inducer, the largest shift toward red was observed at 0.9 min of the test line and 1.9 min of the contour. The observed contrast effect was 0.59, which significantly deviated from zero (**Fig. 5.4,** $p < 0.05$, sign test). This contrast effect was significantly larger than that of the no-contour condition for the same width of the test line (**Fig. B.2,** $p < 0.05$, sign test), thus indicating that the white contour induced a strong simultaneous chromatic contrast. The contrast effect gradually faded when the width deviated from the optimal level [$p < 0.05$, $F(5, 95) = 6.87$; width of test line, $p < 0.05$, $F(3, 57) = 34.44$; contour width, 2-way repeated measures ANOVA; see **Table B.1** for complete statistics]. The no-contour condition induced a similar contrast effect for all the widths [$p > 0.05$, $F(5, 100) = 1.80$; width of test line, one-way ANOVA with repeated measures; see **Table B.2** for complete statistics]. Similar trends were observed for the red inducer. For the violet and yellow inducers, significant chromatic contrast effects and width dependencies were observed, although relatively thicker lines resulted in the most significant effects.

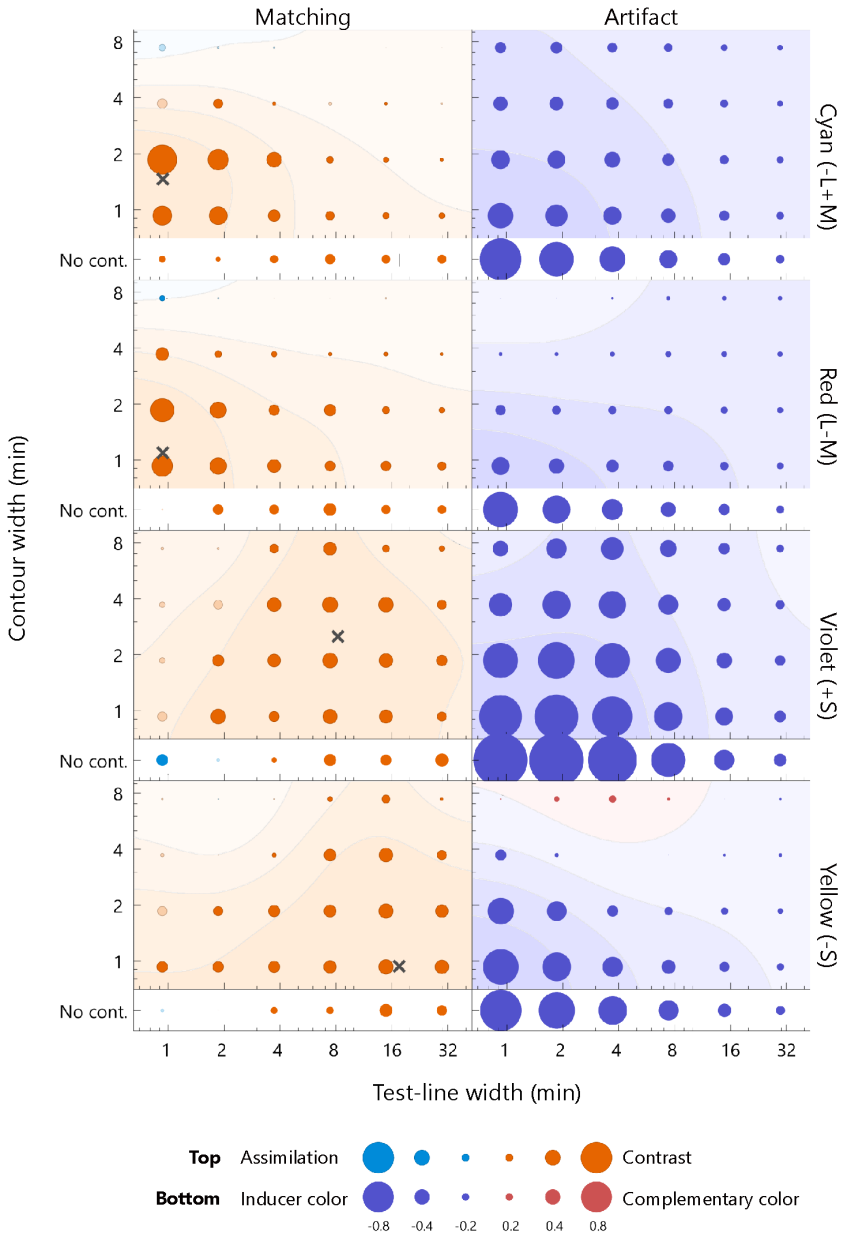

Figure 5.4 The averaged matching across all the participants (top row) and the estimated artifacts (bottom row) for the pale test line

The chromaticities of the inducers from left to right was cyan, red, violet, and yellow. The horizontal axis indicates the width of the test line, and the vertical axis indicates the width of the contour. The diameter of each bubble indicates the magnitude of the color shift. The actual values for the diameters are below the axis label. The warm colored bubbles indicate the shift away from the inducer, and the cool colored bubbles indicate the shift toward the inducer. The filled bubbles represent a significant difference from zero ($p < 0.05$, sign test). The color shift was calculated on the l-axis for the cyan and red inducer, s-axis for the violet and yellow inducer, and normalized by the inducer chromaticity (see section 5.2.5). A contour map represents smoothed data based on a two-dimensional Gaussian filter [sigma = log(1.5) for both the horizontal and vertical axes]. The contour map was normalized with the largest positive value and visualized with 25% increments. The red and blue surfaces indicate a shift away from the inducer and toward the inducer, respectively. The points of the widths inducing the largest color shift were estimated from smoothed data, as indicated by the cross marks. The actual values of the matching and artifact were shown in **Fig. B.2.**

To quantitatively estimate the width resulting in the maximum effect of chromatic contrast (hereafter optimal width), the matching was interpolated by smoothing (Gaussian SD = 1.5 log unit; see **Fig. 5.4** caption). The optimal width was determined to maximize the smoothed surface (the cross markers in **Fig. 5.4a**nd **Fig. 5.5)**. The optimal widths of the pale test line for cyan, red, violet, and yellow were 0.9, 0.9, 8.2, and 0.9 min, respectively, and those of the contour for the colors were 1.5, 1.1, 2.5, and 0.9 min, respectively (**Fig. 5.4)**. To compare the optimal widths of the inducers, we calculated the Euclidean distance of the optimal widths of between a pair of the inducers in the two-dimensional stimulus space instead of calculating the differences in the width of the test line and those of the contour separately. The observed optimal widths were significantly different between L/M-cone (the data of the cyan and red inducers were integrated) and S-cone inducers (the data of violet and yellow inducers were integrated) ($p < 0.05$, bootstrap test). Similar conclusion was obtained if significance was tested separately; the optimal width of the test line was different ($p < 0.01$, t-test) and the optimal width of the contour was different ($p < 0.01$, t-test). The ratios of the optimal width of the S-cone to L/M-cone ranged from 9.1 to 19.4 for the test line and 0.6–2.3 for the contour. Thus, the S-cone had a larger optimal width than the L/M-cone.

The color appearance of the dark test line is shown in **Fig. 5.5.** For the cyan inducer, the largest shift was observed at 0.9 min for the test line and at 1.9 min for the contour. The observed contrast effect was 1.48, which significantly deviated from zero ($p < 0.05$, sign test). For the same width of the test line, this contrast effect was significantly larger than that in the no-contour condition (**Fig. B.3;** $p < 0.05$, sign test), thus indicating that the white contour induced a strong simultaneous chromatic contrast. The contrast effect gradually faded when the width deviated from the optimal level [**Table B.3;** $p < 0.05$, $F(5, 100) = 17.16$; width of test line, $p < 0.05$, $F(3, 60) = 11.02$; contour width, two-way ANOVA with repeated measures]. Similar width dependencies were observed for the red inducer, although the magnitudes were smaller than those for the pale test line. Consistent chromatic assimilation was observed for the violet inducer. Additionally, the yellow inducer demonstrated a strong simultaneous chromatic contrast.

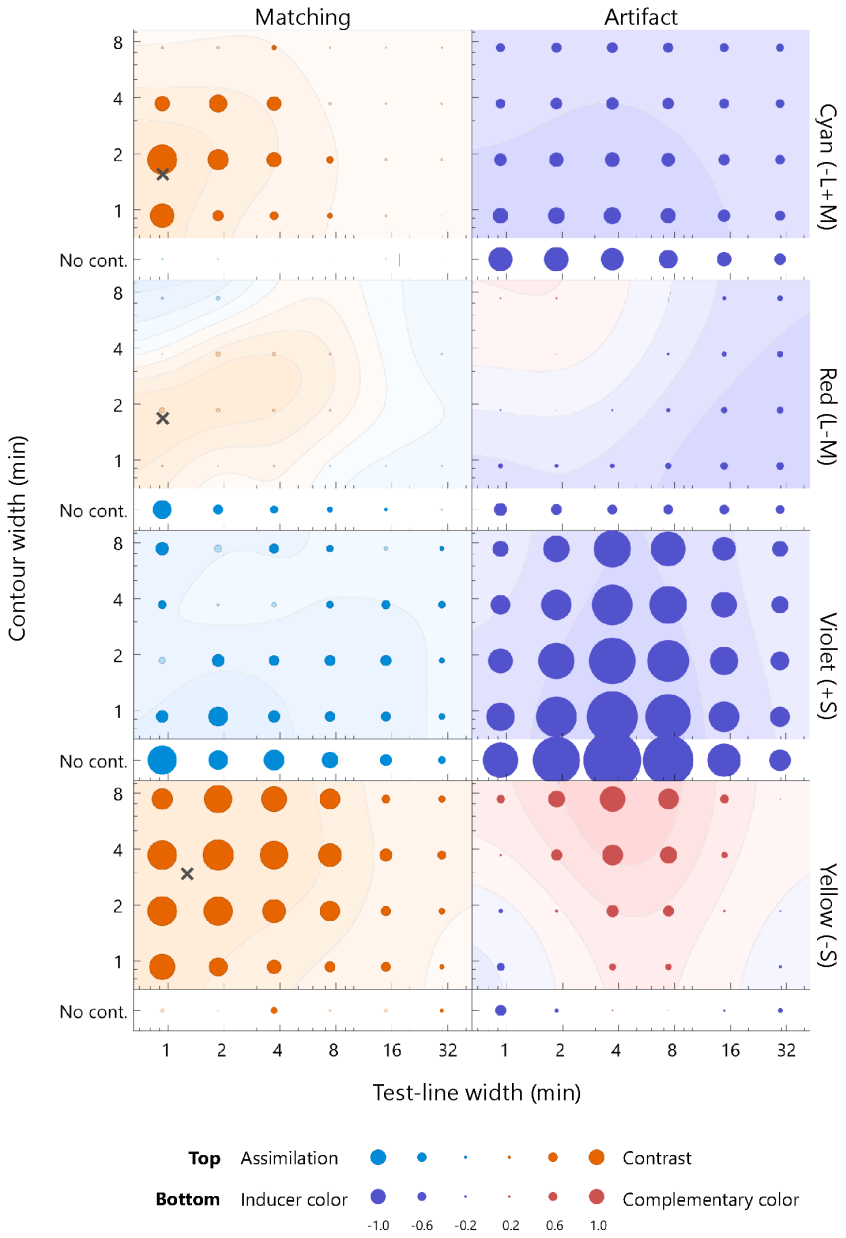

Figure 5.5 The averaged matching across all participants (top row) and the estimated artifacts (bottom row) for the dark test line

The format is the same as in **Fig. 5.4.** Note: the scale of the bubble size is different, as shown in the key below. The points inducing the largest color shift are indicated by cross marks, with the exception of the violet inducer, given that the positive contrast effect was not observed. The actual values of the matching and artifact were shown in **Fig. B.3.**

The optimal widths of the dark test line were 0.9, 0.9, and 1.3 min for the cyan, red, and yellow inducers, respectively, and the those of the contour were 1.6, 1.7, and 2.9 min, respectively (**Fig. B.3**). The optimal width for the violet inducer could not be defined because no chromatic-

contrast effect was induced. The ratios of the optimal width of the S-cone to L/M-cone were 1.4 for the test line and 1.7–1.8 for the contour. Thus, the optimal width for the S-cone was larger than that for the L/M cone.

We compared the dark and pale conditions. However, the optimal widths for the L/M-cone were not significantly different (for both red and cyan inducers, $p > 0.05$, bootstrap test). It was difficult to compare the results of the violet inducer, given that the sign of the color shift changed. For the yellow inducer, the optimal widths were significantly different ($p < 0.05$, bootstrap test). Moreover, the ratios of the optimal width of the pale to dark test line condition were 13.5 for the test line and 0.3 for the contour.

5.3.2 Optical artifacts

Optical artifacts, such as blurring and chromatic aberrations, degrade the retina image. The experiment used thinner lines than lines in Chapter 3 and 4, so the optical artifacts could become more severe to the color shift. In this chapter, the proposed simulation (Marimont & Wandell 1994) obtained the chromatic shift due to the optical artifacts through the same method in Chapter 4 and compared to the matching. The input image was the same as that used in the experiment with a resolution of 0.46 min per pixel. The region of the test line of the output image was averaged in the MB space and then normalized to calculate the contrast effect, similar to the matching experiment. Although aberrations change significantly in both chromaticity and intensity, we determined the artifacts in the MB space to focus on the color shift. The color shift was defined along one of the cardinal axes: the l axis for the cyan and red inducers and the s axis for the violet and yellow inducer. The pupil diameter used in the calculation was 3.63 mm. This value is appropriate for a background luminance of 50 cd/m^2 and a screen with a width of 39.6° and height of 22.3° (Atchison et al. 2011; Stanley & A. K. Davies 1995; Watson & Yellott 2012). All parameters in the model were set to focus on a wavelength of 580 nm (Marimont & Wandell 1994).

The bottom panels of **Fig. 5.4** present the estimated artifacts for the pale test line. The chromaticity of the test line generally shifted toward the inducer chromaticity. This shift was significant for the thin lines. For the yellow inducer, small chromatic shifts away from the inducer chromaticity were observed at the thick contour (7.4 min). For the no-contour condition, consistent shifts toward the inducer chromaticity were observed. The artifact ranged from -0.84 to -0.12, -0.71 to -0.02, -1.09 to -0.17, and -0.83 to 0.16 for the cyan, red, violet, and yellow inducers, respectively, including both the contour and no-contour conditions.

The optical artifacts caused a shift similar to the chromatic assimilation and had an opposite effect compared to that of the matching experiment. We calculated the correlation coefficient between the artifacts and the matching to evaluate similarities in the dependences of the line widths. The correlation coefficients were negative for all the inducers (cyan: $r = -0.78$, $p < 0.05$; red: $r = -0.83$, $p < 0.05$; violet: $r = -0.19$, $p > 0.05$; yellow: $r = -0.48$, $p < 0.05$). Therefore, the

optical artifact did not account for the illusory effect, particularly for the cyan and red inducers.

The bottom panels of **Fig. 5.5** present the estimated artifacts for the dark test line. The chromaticity of the test line shifted toward the inducer chromaticity for the cyan and violet inducers, and the chromatic shift was maximum at the test line of 3.7 min for both. The chromatic shift for the red inducer was weak; however, it was sufficient, and a shift toward the inducer chromaticity was observed for the thick lines. For the yellow inducer, the chromaticity of the test line generally shifted away from the inducer chromaticity and exhibited a maximum shift at the 3.8-min test line with a thick contour. The artifacts ranged from -1.25 to -0.42, -0.68 to 0.14, -2.90 to -0.81, and -0.58 to 1.29 for the cyan, red, violet, and yellow inducers, respectively, including both the contour and no-contour condition. It should be noted that the bubble scaling differed from that in **Fig. 5.4.**

The directions of the artificial shifts for the cyan and red inducers were opposite to those of the color shift observed in the matching. On the other hand, for the violet and yellow inducers, the directions of the artificial shifts were similar to those of the matching. Correlation coefficients between the matching and artifacts were significantly negative for the cyan inducer (r = -0.51, p $<$ 0.05); however, there was no correlation for the red inducer (r = 0.14, p $>$ 0.05). Therefore, the artifacts did not account for the illusory effect along the L/M-cone chromaticities. The correlation coefficients for the violet and yellow inducers were positive and non-significant (violet: r = 0.40, p $>$ 0.05; yellow: r = 0.37, p $>$ 0.05). Thus, we could not exclude the contribution of artifacts to the illusory effect along the S-cone chromaticities.

5.4 Discussion

5.4.1 Optimal width and extent of inhibitory surroundings

We found optimal line widths for the color shift. The observed optimal widths from the S-cone inducers were moderate, and those from the L/M-cone inducers were thin. The observed optimal widths and the magnitudes of the color shift were compared with those observed in previous studies, as follows.

Shevell & Monnier (2005) measured the magnitude of the color shift from S-cone-patterned surroundings by independently changing the width of the centered ring and surrounding stripes. The magnitude of the color shift was maximum when the test line was the thinnest (however, tests were conducted for widths of up to 6 min) and the surrounding stripe was 3.3 cpd (the medium frequency they used, Shevell & Monnier 2005). To compare the abovementioned results with those from this study, the pale test line (-21% luminance) was considered instead of the dark test line (-87% luminance), given that the previous study used a +33% brighter test line stimuli on the patterned background. The results of the present study revealed that the color shift for the violet and yellow inducers was the strongest when the width of the test line was 8.2–7.5 min and that of the contour was 0.9–2.5 min. This optimal width of the test line was

slightly wider; however, it was similar to that obtained by Shevell and Monnier. In contrast, the optimal contour width (0.9–2.5 min) was 3.6–10.1 times less than that in the study conducted by Shevell and Monnier (3.3 cpd; 9 min for each stripe).

It should be noted that the optimal width was lower than in previous studies. One possible explanation is the difference in the surrounding patterns. Shevell and Monnier used stripes of rings with alternating S+ (violet) and S- (lime) chromaticities. This alternating surrounding was made of the first proximal (say S+), second proximal (S-), third proximal (S+), and other higher-order proximal. Due to the spatially antagonistic center-surround receptive field, as the neural substrate mediating the color shifts, the extent of the surrounding suppression determines the contrast effect (Mély, Linsley, & Serre 2018). If the extent of suppression is larger than that of the second ring, the suppression region is exposed to both the second (S-) and third (S+) chromaticities. The amplitude of the surrounding suppression is consequently weakened because of the elimination of the second and third inducers. To maximize the contrast effect using an alternating stimulus, the second ring should be sufficiently thick to cover the extent of the suppressive surrounding. Given that Shevell and Monnier modulated the stimulus width of the first, second, and third rings simultaneously, the low spatial frequency and thicker second ring was effective for the color shift. In contrast, the stimulus in our study had a uniformly chromatic surrounding, with the exception of the contour; thus, the colors did not cancel each other in the suppressive region. Therefore, the optimal width was less than those obtained in previous studies wherein alternating stimuli were used.

We observed a strong color shift for the L/M-cone when the fine test line and contour were used. Although previous studies revealed that the Monnier–Shevell illusion emerged along the L/M-cone (Cerda-Company et al. 2018; Lin, C.-C. Chen, & Chien 2010; McCamy 2003), the optimal width of the illusion for the L/M-cone was not investigated. The line widths used in those previous studies were 9 min (Lin, C.-C. Chen, & Chien 2010) or 15.5 min Cerda-Company et al. 2018 and were sufficient for the S-cone. However, it was unclear whether the widths were appropriate for the L/M-cone. The results revealed that the optimal width was 1.7 min for the test line and 1.6–1.7 min for the contour with respect to the L/M-cone. In this study, the optimal widths were 5–9 times smaller than the widths used in previous studies. Thus, the Monnier–Shevell illusion for the L/M-cone could be more significant if a thinner patterned surrounding is used. Cerda-Company et al. (2018) revealed that the magnitude of the effect for the L/M-cone was smaller than that for the S-cone. However, in our current study, the results revealed comparable effects for the L/M-cone and S-cone when the optimal width was used. Given that the stimuli were different in spatial configuration from those used in the study conducted by Shevell and Monnier, further research is required to examine the appearance of a thinner L/M-cone patterned background in the Monnier–Shevell illusion.

The illusory effect of the L/M-cone chromaticities was evident for the contours and test lines with small widths, and the optimal widths for the L/M-cone were smaller than those for

the S-cone. To reconcile this discrepancy, we proposed that different spatial resolutions for each cardinal axis led to different optimal widths. It is known that the two cardinal axes originate from different types of cones in the retina. The density of each cone type is not uniform. In particular, the S-cone only accounts for 5% of the population (Calkins 2001; Hofer, Carroll, et al. 2005; Roorda & D. R. Williams 1999). The densities of the L- and M-cone are 67 and 28%, respectively, on average, although there are large individual differences Hofer, Carroll, et al. 2005; A. Neitz et al. 2020; Roorda & D. R. Williams 1999. The midget ganglion cell at the fovea receives the input from a single L or M cone to its central receptive field (Wool, Packer, et al. 2019) and conveys the fine details of the L/M-cone information. In contrast, the bistratified ganglion cell receives inputs from several S cones; thus, the spatial details of individual S-cone information are lost (Wool, Packer, et al. 2019). These retinal properties are preserved in the lateral geniculate nucleus (LGN). Thus, the parvo cells of the LGN, which receive inputs from the midget cell, convey the fine details of the L/M-cone information. The konio cells, which receive inputs from the bistratified cell, convey the relatively coarse S-cone information (Irvin, Casagrande, & Norton 1993; Tailby et al. 2008; Xu, Bonds, & Casagrande 2002). Reflecting this early visual processing, the cells in the cortex respond to higher spatial frequencies of the L/M-modulating stimuli than those in the S-cone (E. N. Johnson, Van Hooser, & Fitzpatrick 2010; Solomon, Peirce, & Lennie 2004; Wandell & Silverstein 2003). Psychophysical experiments revealed that observers can detect higher spatial stimuli that modulate the L/M-cone chromaticity than those that modulate the S-cone chromaticity (Barboni et al. 2013; McKeefry, Murray, & Kulikowski 2001; Mullen 1985; Mullen & Kingdom 2002; Webster, Switkes, & De Valois 1990). This suggests that the spatial resolution of color vision is higher for the L/M-cone chromaticities than for the S-cone chromaticities. Assuming that the center-surround organization is the neural basis of the Monnier–Shevell illusion (Mély, Linsley, & Serre 2018; Monnier & Shevell 2004), the fact that the optimal width for the L/M-cone is smaller than that for the S-cone chromaticity is in accordance with the property of color vision from the retina to perception.

5.4.2 Integration of chromatic and luminance signals

The optimal width for the L/M-cone chromaticities was 0.9 min (33.3 cpd) for the test line, and it was equivalent to a resolution level of one cone photoreceptor (approximately 1 min at fovea, D. R. Williams & Coletta 1987. This width is nearly equal to the resolution limit for the luminance grating (the critical fusion frequency of 32–36 cpd, which corresponds to 0.9–0.8 min sampling, Mullen 1985). The stimuli could be detected by the luminance channel. However, the critical fusion frequency of the L/M-cone chromatic stimuli is 11–12 cpd (Mullen 1985); hence, the test line and the contour were hardly detectable solely by the chromatic channel. Given that the test line and contour had the same chromaticity, we could assume that these lines were the same for the chromatic channel. Upon the addition of the optimal contour width to the test line, the total width became 3.1–4.3 min (9.7–7.0 cpd). This line width could be detected

by the chromatic channel. Despite this assumed integration of the test line and contour, color appearance of the test line and contour was reddish and white for cyan inducer. This appearance was confirmed by all six participants (including three naïve) in an additional query. The illusional perception of the colored test line contained coarse chromatic information with line widths of 3.1–4.3 min and detailed luminance information with test line widths of 0.9 min. This process may be a type of color capture by luminance signals.

5.4.3 Optical artifacts

To evaluate the influence of optical artifacts, we compared the matching data to the estimated artifacts using the proposed model (Marimont & Wandell 1994). The estimated artifacts were as follows.

(1) Large artifacts on the dark test line: The aberration leaked a constant amount of visible light from the inducer and from the contour toward the test line, regardless of the luminance levels of the test line. Thus, the chromatic shift due to the artifacts on the dark test line was larger than that on the pale test line. The maximum artifact on the dark test line was 1.49, 0.96, 2.66, and 1.55 times larger than that of the pale test line for the cyan, red, violet, and yellow inducer, respectively. The artifacts increased as the luminance of the test line decreased, with the exception of the red inducer. The similar artifacts of the red inducer can be attributed to the longitudinal chromatic aberration, which induces a bluish color and cancels red light from the inducer [see (3) below].

(2) Large artifacts on thin lines: The artifacts were significant in the vicinity of the inducer and contour; thus, the chromatic shift due to the artifacts was large on the thin lines. This was confirmed for all the chromaticities of the inducer with respect to the pale test line. However, for the dark test line, the maximum artifact was the test line with a width of 3.7 min for the violet and yellow inducers. This can be attributed to the balance between the monochromatic aberration and longitudinal chromatic aberration.

(3) Bluish chromatic shifts: The chromaticity of the test line shifted toward the inducer chromaticity for the cyan and violet inducers but shifted away from the inducer chromaticity for the red and yellow inducers. The longitudinal chromatic aberration led to the selective dispersion of short-wavelength light from the inducer and the contour to the test line. The short-wavelength light corresponds to a shift in chromaticity toward cyan and violet. Thus, the chromatic aberration caused a chromatic shift toward the inducer chromaticity for the cyan and violet inducers and a shift away from the inducers for the red and yellow inducers. It should be noted that the magnitude of the chromatic shift was calculated by the shift along the corresponding cardinal axis and ignored the shift along the other axes, although the shift occurred in the three-dimensional cone excitation space. In contrast, monochromatic aberrations involve the simple scattering of the inducer chromaticity and usually cause a shift similar to that of chromatic assimilation. By integrating monochromatic and chromatic aberrations, the

chromatic shifts would be large for the cyan and violet inducers, and the chromatic shifts would be small for the red and yellow inducers. The simulation revealed that the estimated artifacts for the cyan and violet inducers were large and shifted toward the inducer chromaticity for both luminance levels. For the red and yellow inducers, the estimated artifacts generally shifted toward the inducer chromaticity and away from the inducer chromaticity for several lines with thick contours. The thick contours prevented spreading from the inducers; thus, the artificial chromatic shift primarily reflected the longitudinal chromatic aberration from the contour, which corresponded to a chromatic shift away from the chromaticity of the red and yellow inducers.

It is unclear whether the parameters used in the simulations were consistent with those of the participants in the experiment. There were large individual differences in the opacity of the ocular optics and pupil diameters, and these differences influenced the balance between blurring and chromatic aberrations. The simulation results serve as estimations of the average chromatic shift across observers. Thus, future work is required to examine the relationship between individual differences in ocular optics and color matching.

In summary, the artifacts were found to be dependent on the line widths, luminance of the test line, and inducer chromaticity. The artifacts robustly shifted toward or away from the inducer chromaticity, depending on the inducer chromaticity. The direction of the artifacts was determined by the balance between monochromatic and longitudinal chromatic aberrations. The artifact of the pale test line was adequately large and shifted toward the inducer chromaticity for all the inducers; this shift was opposite to the perceptual color shifts. This indicates that the magnitude of the illusory effect exceeded that of the artifact, and the neural mechanisms predominate the illusory effect. For the dark-test line, the artifact was more significant, and it occasionally exceeded the magnitude of the illusory effect, given that less light of the test line was susceptible to the artifact.

5.4.4 Luminance dependency with respect to artifacts

Cerda-Company et al. (2018) found that luminance dependency switched depending on the chromaticity of the proximal surroundings of the Monnier–Shevell illusion. The color shift was large when the test ring was dark and when the proximal chromaticity was violet (S+). Conversely, the color shift was large when the test ring was bright and when the proximal chromaticity was yellow (S-). The effect of optical artifacts was not investigated experimentally using artificial pupil (Monnier & Shevell 2003) or theoretically by simulations. The luminance dependency was qualitatively consistent with the effect of optical artifacts. We found that the estimated artifact was similar to the illusional effect when the line was dark and when the distant surroundings were yellow (corresponding to S+ proximal).

3.2 show that the illusory effect cannot be sufficiently explained by chromatic aberrations, as observers consistently perceived the illusory color, irrespective of its fixation near or far from the stimuli that induced different chromatic fringes by chromatic aberrations. However,

in the previous study, we did not quantitatively examine the effect of optical artifacts. Thus, the influence of the artifacts on the color shift for different luminance levels of the test line is uncertain.

The results of this study revealed that the optimal widths and direction of the color shift were the same for the pale and dark test lines with respect to the cyan and red inducers, whereas they varied significantly for the yellow and violet inducers. The simulation results revealed that the artifacts led to a larger chromatic shift for the dark test line than the pale test line; thus, the observed change in the optimal width of the illusion between luminance levels may be due to the artifacts. To evaluate the influence of artifacts on the optimal widths, the following analysis was performed. In this analysis, we assumed that the observed matching was the result of a linear summation of the artifacts and neural shift. If this assumption is true, the neural shift could be plotted by subtracting the artifacts from the matching. The subtraction is shown in **Fig. 5.6.** Generally, the contrast effect was observed for all chromaticities, and the color shift between the luminance levels was more consistent than that shown in **Fig. 5.4** and **Fig. 5.5.** To compare the color shifts quantitatively, correlation coefficients were calculated for the pale and dark test lines ($r = 0.93$, $p < 0.05$, cyan; $r = 0.63$, $p < 0.05$, red; $r = 0.63$, $p < 0.05$, violet; $r = 0.57$, $p < 0.05$, yellow). They were all significantly and positively correlated; thus, the neural spatial properties were consistent across luminance levels. We therefore concluded that the changes in the optimal widths between the luminance levels for the S-cone chromaticities were mainly due to the artifacts and that the underlying neural mechanisms were the same, regardless of the luminance levels.

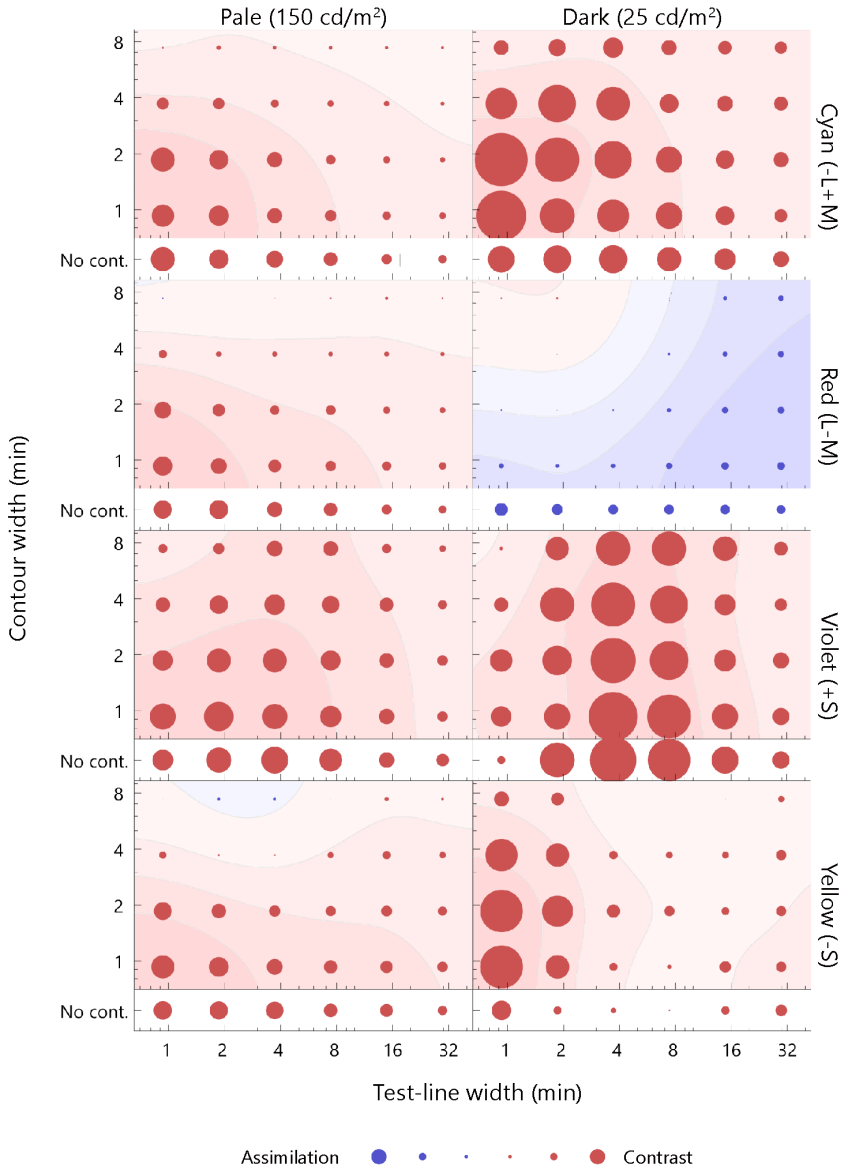

Figure 5.6 The difference between the matching and artifact

The difference was estimated by subtracting the artifact from the matching on the MB chromaticity, and considered as the neural factor of the chromatic induction. The upper row presents the pale test line, and the lower row presents the dark test line. The smoothed contour plots were plotted using the same calculation as that employed for **Fig. 5.4.** The format is the same as that of **Fig. 5.4.**

5.5 Summary

The optimal width for the simultaneous chromatic contrast effect of the patterned surroundings differed between the cardinal axes. The optimal widths of the center line and contour for the L/M-cone chromaticities were 0.9 min and 1.1–1.7 min (as small as one cone photoreceptor), respectively, and those for the S-cone chromaticities were 8.2–17.5 min and 0.9–2.5 min, respectively. There is a high probability that these differences reflect the spatial resolution limit between the L/M-cone and S-cone chromatic modulations. The optical artifact influenced the chromatic shift, particularly for the darker test line; however, the chromatic contrast effect for the L/M-cone chromaticities (especially cyan) exceeded that of the artifact. Thus, it was concluded that the dominant factor of the color shift is neural rather than optical. The optimal line width for the L/M-cone chromaticities was finer than the resolution limit of the chromatic channel, thus indicating that the color appearance of the thin line is inferred by integrating broader chromatic contrast information and detailed luminance contrast information. This visual inference of color is particularly important for recognizing the color of distant and fine objects.

Chapter 6

Luminance dependency

This chapter is published as a part of,
T. Kanematsu & K. Koida (2020). "Large enhancement of simultaneous color contrast by white flanking contours". In: *Sci. Rep.* 10.1, pp. 1–10. DOI: 10.1038/s41598-020-77241-5. URL: www.nature.com/scientificreports.

6.1 Introcudtion

Simultaneous color assimilation and contrast depend on the spatial configuration of luminance variations in an image. Color assimilation becomes larger when the luminance contrast between the center and the surround area is high (Cao & Shevell 2005; Cerda-Company et al. 2018; Devinck, Delahunt, et al. 2005; Devinck, Spillmann, & Werner 2006). However, the magnitude of the simultaneous color contrast is optimized when the luminance contrast between the surrounds and the center is absent, and this effect is greatly attenuated by the luminance contrast, known as Kirschmann's third law (Kirschmann 1891). The law has been examined repeatedly by various methods of scaling (Gordon & Shapley 2006), naming (Bimler, Paramei, & Izmailov 2009), rating (Bergström & Derefeldt 1975; Xing et al. 2015), matching (J. A. S. Kinney 1962; Otazu, Parraga, & Vanrell 2010), and canceling (Bergström, Derefeldt, & Holmgren 1978) to measure the perceived change in color, with the majority of findings from these studies supporting the law. The variation in color appearance depending on the stimulus luminance has long been investigated in the context of color constancy (Bäuml 2001; D. H. Brainard 1998; Chichilnisky & Wandell 1996; Helson 1938; Helson; & Michels 1948; Judd 1940; Kuriki 2006, 2015; Werner & Walraven 1982). Color constancy is a feature that assigns constant colors to objects under varying illumination conditions. However, under colored illumination, a discrepancy remains between Kirschmann's law and the dependence of color appearance on luminance. A darker target is susceptible to the surrounds; this is known as the Helson–Judd effect (Bäuml 2001; D. H. Brainard 1998; Chichilnisky & Wandell 1996; Helson 1938; Helson; & Michels 1948; Judd 1940; Kuriki 2006, 2015; Werner & Walraven 1982).

Using the alternating color of proximal and distal surrounds, Monnier and Shevell reported an illusion inducing a large color shift by the synergy of simultaneous color assimilation and contrast. The magnitude of the color shift is large even when the proximal surrounds have a neutral color compared to the color shift of uniformly colored surrounds. These color shifts were explained by receptive field organization in which an additive effect arising from a proximal surround and a subtractive effect arising from a distal surround (Monnier & Shevell 2004; Shevell & Monnier 2006). This illusion reflects not only the synergistic effect, but also the luminance contrast of the center (Cerda-Company et al. 2018). The greater the luminance contrast of the center, the larger color shifts that occur.

Although a synergistic effect along the S cone axis and its dependence on luminance contrast is already known to exist, it is unknown whether this synergistic effect persists along red-cyan color axis and whether it is influenced by luminance contrast. In this study, we examined whether color appearance varies depending on the existence of a contour. Below, we compared the magnitude of the color shifts between different contrasts of the contour to test whether the spatial explanation of the color induction from proximal and distal surrounds is valid or not, irrespective of the luminance contrast of the proximal surround. We finally measured the effect of the luminance level of the gray line. If the luminance dependency is similar to that observed for the S cone axis, then high contrast stimuli would induce larger color shifts.

6.2 Method

6.2.1 Perticipants

Five participants aged 22-44 years old, three males and two females, participated in a color-matching experiment. All participants had normal vision or corrected normal vision with glasses or contact lenses. The color vision was confirmed to be trichromatic by the Ishihara Plate.

6.2.2 Apparatus

Stimuli were presented on a liquid crystal monitor (UP2516D, Dell; 2560 $\times$ 1440 pixels, 59Hz frame rate, Adobe RGB). The monitor was connected via a HDMI cable to the onboard graphics card (Intel HD Graphics 620, 8 bits) of a PC running Microsoft Windows 10 Home Edition (64 bits). Color and luminance were calibrated with the chroma meter CS-200 (Konica Minolta, Japan) under the same illumination condition as the experiment. Pixel intensity was measured in sub-pixel resolution using a microscope (Dinolite basic, Dinolite), and the confirmed gray lines were the same across stimuli. The experiment was controlled using custom software developed using MATLAB 2018a (Mathworks) and Psychtoolbox 3.0.15 (D. H. Brainard 1997). The apparatuses were the same as those employed in Chapter 5.

6.2.3 Stimuli

Stimuli were defined by CIE 1931 color space. For the purpose of comparison with previous studies, we calculated corresponding color in MacLeod-Boynton (MB) chromaticity coordinates (MacLeod & Boynton 1979; V. C. Smith & Pokorny 1975). The MB chromaticity was normalized by the same metric in Chapter 5.

The sample and comparison were presented on a gray background (CIE $x = 0.312$, $y = 0.329$, 51.5 cd/m^2, $l = 0.65$, $s = 0.85$) side-by-side at 1.24 deg apart as showed in **Fig. 6.1A**, and their position on the left or right were randomized. A gray vertical line (1 pixel in width, 0.03 deg, test line) was placed in the center of the colored square (101 $\times$ 101 pixel in width 3.12 deg, inducer area). There were three conditions of the sample stimuli: white-contour condition with a white contour (**Fig. 6.1B**), black-contour condition with a black contour (**Fig. 6.1C**), and no-contour condition without any flanking contours (**Fig. 6.1D**). A white contour (1 pixel in width, 0.03 deg, CIE $x = 0.312$, $y = 0.330$, 210.2 cd/m^2, $l = 0.65$, $s = 0.85$) or a black contour (1 pixel in width, 0.03 deg, CIE $x = 0.312$, $y = 0.330$, 8.5 cd/m^2, $l = 0.65$, $s = 0.85$) was placed adjacent to the left and right edge of the test line. The test line was gray (CIE $x = 0.313$, $y = 0.330$, $l = 0.65$, $s = 0.85$) and had three levels of luminance (50.0, 75.0, 150.0 cd/m^2). The inducer area was either cyan (CIE $x = 0.278$, $y = 0.330$, 189.0 cd/m^2, $l = 0.63$, $s = 0.92$) or red (CIE $x = 0.340$, $y = 0.330$, 190.1 cd/m^2, $l = 0.66$, $s = 0.79$). These two colors differed only in the luminance of the red and cyan (i.e., green + blue) pixels of the display. The comparison stimulus had a white square (101 $\times$ 101 pixel, 3.12 deg), which was the same color and luminance as the white contour, and one vertical line (1 pixel in width, 0.03 deg) located at the center.

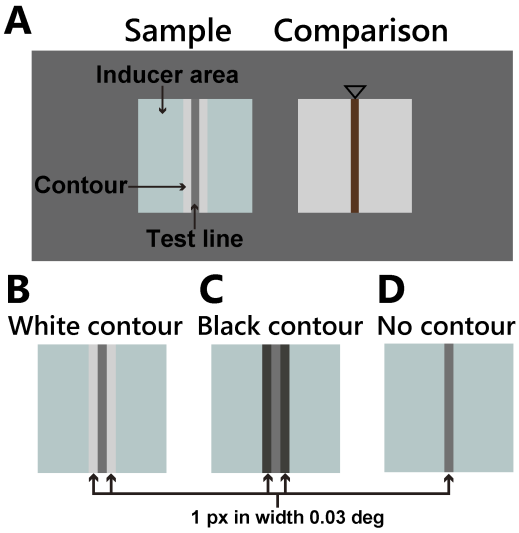

Figure 6.1 Stimuli used in the appearance matching experiment
(**A**) The sample and comparison stimuli sized at 3.12 deg arranged horizontally and separated by 1.24 deg on a uniform gray screen. (**B**) Sample stimuli of the white-contour condition. A gray vertical line (test line) was placed on a uniform colored background (inducer area). White lines (white contour) were located adjacent to both sides of the test line. (**C**) Sample stimuli of the black-contour condition. Black lines (black contour) were located adjacent to both sides of the test line. (**D**) Sample stimuli of the no-contour condition. The test line was placed on the inducer area without any contour. The width of both the contour and the test line was 1 px (0.03 deg).

6.2.4 Procedure

The head of the participants was secured on a chin rest with a viewing distance of 40 cm from the monitor. The participants were asked to adjust the color and luminance of the line of the comparison to match the appearance of the line of the sample, using a trackball. Vertical and horizontal manipulations of the trackball induced luminance and color changes, respectively. The initial color and luminance of the comparison's vertical line were randomized. Fixation was not required. After the participants were satisfied with the matching, they pressed the button to complete the trial and proceed to the next trial with a 300 ms blank screen (D65, 50 cd/m^2). Before the experiment, the participants were trained on the apparatus and performing symmetric color matching while adapting to the illuminated room. The training stimuli were composed of a sample and a comparison, both had a thin line (1px in width 0.03 deg) on a white background. The thin line of the sample was either dark gray (CIE $x = 0.313$, $y = 0.330$, 50.0 cd/m^2, $l = 0.65$, $s = 0.85$), red (CIE $x = 0.340$, $y = 0.330$, 190.1 cd/m^2, $l = 0.66$, $s = 0.79$), or cyan (CIE $x = 0.278$, $y = 0.330$, 189.0 cd/m^2, $l = 0.63$, $s = 0.92$). Each participant repeated the training 2 to 3 times until they became competent on the trackball's operation. In the experiment, there

were 18 sample stimuli, including two colors of the inducer, three luminance levels of the test line, and the white-contour, black-contour, and no-contour conditions. The sample stimuli were presented in random order. The time required for the matching of all presentation stimuli was about 15 minutes. Each participant repeated the matching three times with at least a 7-minute break between sessions.

6.3 Result

For the white-contour condition of the cyan inducer, the matched color significantly shifted toward the opposite direction from the inducer color irrespective of the luminance of the test line (square markers in **Fig. 6.2A**, sign test; $p < 0.05$ for three luminance conditions). These shifts indicate simultaneous color contrast. For the black-contour condition, the matched colors did not significantly shift from neutral (triangle markers in **Fig. 6.2A**, sign test; $p > 0.05$). These trends were replicated for the red inducer (**Fig. 6.2B**). The white-contour condition induced a contrast effect (sign test; $p < 0.05$ for all three luminance conditions).

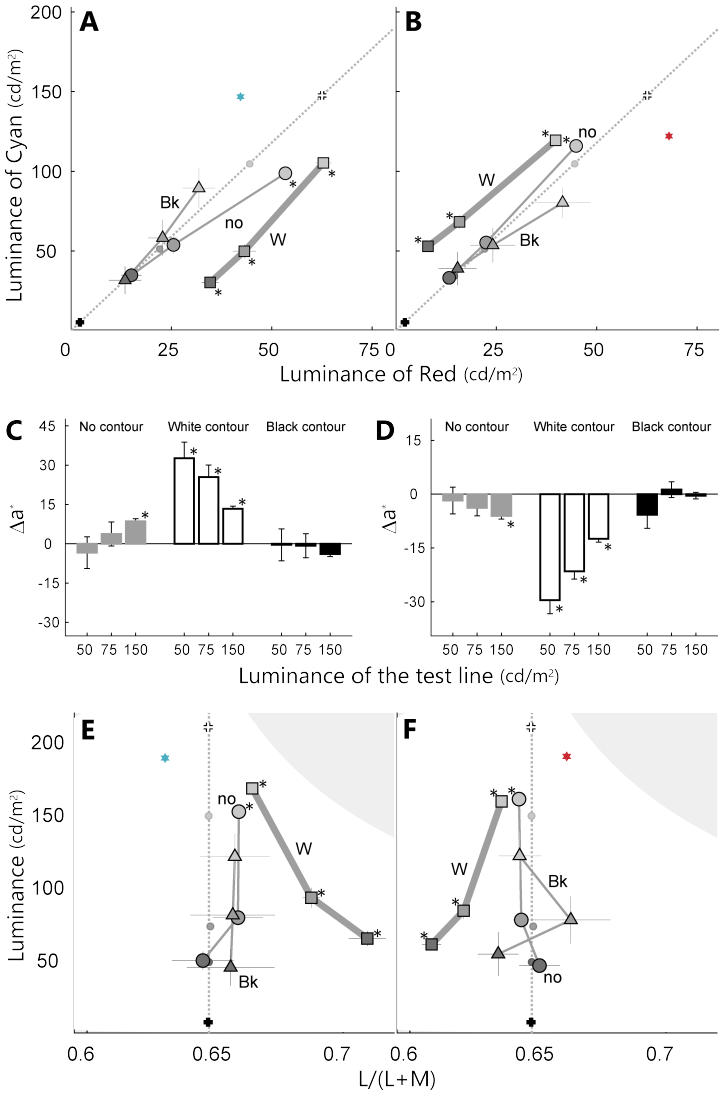

Figure 6.2 Results of the appearance matching averaged across all participants (n = 5).

The panels show the results of the cyan (**A**, **C** and **E**) and red inducers (**B**, **D** and **F**). **A** and **B** are scatterplots describing the color and luminance of the stimuli. One axis is the luminance of the red phosphor and the other axis is the luminance of the cyan (green + blue) phosphor. The diagonal line represents neutral conditions (D65). Small dots on the diagonal line represent the three levels of the test lines. The colored star represents the inducer of the sample. Circles, squares, and triangles represent the matched color of the no-contour, the white-contour, and the black-contour conditions, respectively. White and black crosses represent the color of the white and black contours of the sample stimuli, respectively. (**C**) and (**D**) summarize the color shift quantified by Δa^* of the CIELAB color space. A positive value on the vertical axis indicates a reddish, a negative value indicates a cyanic, and zero indicates no color shift. The horizontal axis shows the luminance of the test line. Gray, white, and black bars show the results of the no-, white-, and black-contour conditions, respectively. (**E**) and (**F**) summarize the color shift quantified by cone excitation space. The horizontal axis is relative cone excitation of L-cone divided by sum of L- and M-cone, and the vertical axis is luminance. The markers are same as in A. Gray area denotes outside of the display gamut. The error bar is the standard error of the mean. An asterisk indicates a significant difference between each matching and a neutral gray color ($p < 0.05$, sign test in **A**, **B**, **E**, **F**, t-test in **C**, **D**).

The observed color shifts were transformed into the CIELAB color space, which is an approximate uniform color scale describing perceptual color differences (**Fig. 6.2C**, **D**). Because the distance on the luminance axes in **Fig. 6.2A** and **B** are not indicative of perceptual color differences, the uniform color scale was used to compare the perceived color shifts between stimuli of different luminance levels. One of the color axes, Δa^*, of the CIELAB space corresponded to the color difference along the red to cyan axis for our stimuli.

Again, the no-contour condition induced a moderate color contrast effect. A significant shift was observed only for the pale test (t-test; $p < 0.05$). This effect may support Kirschmann's third law, but the effect of luminance for the test line was not significant (cyan; $p > 0.05$, $F(2, 42) = 1.85$, red; $p > 0.05$, $F(2, 42) = 0.70$, 1-way repeated measures ANOVA). The white-contour condition induced a significant color contrast effect for all luminance levels (t-test; $p < 0.05$), and its magnitude was significantly larger than that for the no-contour condition ($p < 0.05$, t-test between the white-contour and the no-contour condition for each luminance level). Their magnitudes decreased as the luminance of the test line increased (cyan; $p < 0.01$, $F(2, 42) = 27.18$, red; $p < 0.05$, $F(2, 42) = 15.87$, 1-way repeated measures ANOVA), contrary to the prediction based on Kirschmann's law. The black-contour condition induced no significant color shifts (t-test; $p > 0.05$).

The observed color shifts were again transformed into the luminance and cone excitation chromaticity (L/(L+M)) space (**Fig. 6.2E** and **F**), which is widely used in color research. The white-contour condition again induced significant color shifts (sign-test; $p < 0.05$ for three luminance conditions). Significant color shifts of the no-contour condition were observed only for the pale test (sign test; $p < 0.05$). The black-contour condition induced no significant color shifts (sign test; $p > 0.05$). The result of the black contour may not appear similar to the result in CIELAB space, because some observers matched to low luminance appeared black, irrespective of color and sometimes resulted in very large values for L/(L+M). Thus, results showed a large deviation in color settings (see the Supplemental **Fig. C.1** and **Fig. C.1** for individual data).

6.4 Discussion

We provide evidence for a new color illusion that induces large enhancements of simultaneous color contrast using white flanking contours. We quantified the appearance of the thin gray line which was flanked by the white or black contours on a colored background. The white-flanking contour condition induced a large and significant simultaneous color contrast effect, irrespective of the luminance of a centrally flanked gray line. The magnitude of color shift was quantified on CIELAB-Δa^*, where we show that the shifts in perceived color decreased as the luminance of the central gray line increased. The color shift for the no-contour condition was significant only for the pale gray line. The black-contour condition induced no significant color shift.

Color shifts also occur due to wavelength-independent factors such as blurring. Luminance

contrasts may change for very thin lines due to the optical blur or neural summation. If image blurring reduces luminance contrast, a strong color contrast effect should be induced as per Kirschmann's law. To test this, we blurred the luminance by averaging the contour and test line. The luminance of the test lines of pale (50 cd/m^2), middle (75 cd/m^2), and dark (150 cd/m^2) then change to be 157, 165, 190 cd/m^2 for the white contour, 22, 31, 56 cd/m^2 for the black contour, and 143, 152, 177 cd/m^2 for no contour, respectively. Thus, the blurred contrast of the center to background will be -17.5, -13.2, 0.0% for the white contour, -88.6, -84.2, -71.1% for the black contour, and -24.6%, -20.2%, -7.0% for no-contour condition, respectively. Thus, the lowest contrast is the pale test with white contour. According to Kirschmann's law, there are two possible predictions. First, the pale test with the white contour (0.0%) should generate the strongest color shift. Second, conditions having similar luminance contrast—i.e., the dark test with the white contour (-17.5%) and the mid test with the no contour (-20.2%)—should lead to similar color shifts. These predictions were, however, inconsistent with the results. The magnitude of color shift for the pale test in the white contour condition was not larger than the other two tests in the white contour condition (**Fig. 6.2)**. The magnitude of the color shift for the dark test with the white contour induced significant color shift, but the mid test with no contour did not. In sum, simple blurring of the test line with Kirschmann's law failed to explain the results.

For the white-contour condition, we observed when the luminance contrast of the test line was higher (darker test line), the color shifts were larger. This trend was similar to recent results. Cerda-company et. al. showed that color shifts of the Monnier–Shevell illusion for S-cone stimuli were larger when the luminance contrast of the test was higher (Cerda-Company et al. 2018). Color shifts along L-M cone stimuli in their study, however, were smaller at all luminance levels, suggesting that a luminance dependency along L-M cone was not observed. This inconsistency could be attributed to the difference in line width between the stimuli as shown in Chapter 5.

Either synergistically or antagonistically, the effect of proximal and distal surrounds appears to have a simple spatial explanation. This explanation is applicable to our stimuli, but were limited to the white-contour condition. Observed color shifts were small for the black contour condition, indicating the distant contrast effect did not occur. This result of the black-contour condition is consistent with those of previous studies, which reporting that outlining a black line reduced the effect of both assimilation and contrast color (Faul, Ekroll, & Wendt 2008; Hurlbert 1996; Xing et al. 2015). Thus, the black contour overrides and diminishes both the assimilation and contrast effects and thus, diminishes the synergistic effect.

Observed color shifts of the white-contour condition could be explained by an augmented synergy theory based on intensity space, rather than chromaticity. For the cyan inducer with the white-contour condition, the observed color shifts were almost constant for all three gray levels in luminance space: the shift from the dark test (20.1, -3.9 cd/m^2, red and cyan luminance axes respectively), the mid (21.1, -1.4 cd/m^2, red and cyan luminance axes respectively) and the pale

(18.3, 0.6 cd/m^2, red and cyan luminance axes respectively). These shifts closely matched the difference between the inducer and the white contour (-20.3, -0.8 cd/m^2, red and cyan luminance axes respectively), except the sign was opposite. For the red inducer, the observed color shifts of the white contour were almost the same among the three gray levels (-6.6, 18.8 cd/m^2, -6.3, 17.0 cd/m^2 , -4.8, 14.8 cd/m^2 for the dark, mid and pale line), and the shifts closely matched the difference between the red inducer and the white contour (5.4, -25.5 cd/m^2). Thus, contrast effects from distant surrounds based on synergy theory could be regarded as invariant with the changes in luminance of the gray line.

The invariant contrast effect for luminance of the gray line and the applicability of the synergy theory apart from the S cone color are important for explaining the color appearance of our stimuli. Suppose the invariant contrast effect from distal surrounds can be adapted for the no-contour condition, then the synergy theory predicts the observed difference between the white-contour and the no-contour conditions, which is attributed to the proximal assimilation effect. Since the observed difference increased monotonically as the luminance of the gray line was decreased, the color assimilation effect from the proximal surround varied depending on the luminance of the gray line. This dependency is consistent with the former findings. The no-contour condition was equivalent to a uniform surround that was widely used in the literature examining the luminance-dependency of simultaneous color contrast effects (Kirschmann's third law). The luminance dependency could be explained by the augmented synergy theory involving the invariant contrast effect arising from a distal surround and the variable assimilation effect arising from the proximal area.

However, in chromaticity space, the white-contour condition showed that the darker the gray line, the larger the color contrast effect. This trend is similar to the Helson–Judd effect (Helson 1938; Judd 1940), where the color appearance of a light of fixed chromaticity varies with the intensity under the colored illuminant, and this effect was repeatedly investigated in the context of color constancy (Bäuml 2001; D. H. Brainard 1998; Chichilnisky & Wandell 1996; Helson; & Michels 1948; Kuriki 2006, 2015; Werner & Walraven 1982). The effect was interpreted as the fact that the surrounding color has a large impact on dark targets compared with bright targets (Chichilnisky & Wandell 1996).

There is discrepancy between the Helson–Judd effect and Kirschmann's law. Which effect represents the color contrast effect? They could be reconciled by considering the relative amount of contrast effect to the assimilation effect. Previous studies that investigated the Helson–Judd effect fully adapted to the colored surrounds (Bäuml 2001; D. H. Brainard 1998; Chichilnisky & Wandell 1996; Helson 1938; Helson; & Michels 1948; Judd 1940; Kuriki 2006, 2015; Werner & Walraven 1982), thus both spatial and temporal factors enhanced the color contrast effects. The relatively large amount of the contrast effect dominates the color appearance and diminishes the color assimilation effect from the proximal surrounds if it exists. For our white-contour condition, the color assimilation effect from the proximal surround became weak because of the white

contour. Thus, a relatively large amount of contrast effect dominated the color appearance. As a consequence, the white-contour condition induced an effect similar to the Helson–Judd effect. We conclude that a consistent feature of the contrast effects is that dark targets are affected more than bright targets, similar to the Helson–Judd effect.

6.5 Summary

Simultaneous color contrast and assimilation are mutually opposing effects on color appearance, and their magnitude depends on spatial context. The Monnier–Shevell illusion induces a large color shift by a synergy of simultaneous assimilation and contrast using the alternating color of proximal and distant surrounds. The illusion induces a prominent effect along the blue-yellow color axis, but a subtle effect along the orthogonal color axis. In this study, we report an illusion generated by an extremely thin gray line on a cyan background that appears reddish when the line is flanked by thin white contours. We quantified the color appearance of the gray line in a color matching experiment and found that the color shift of the gray line with white contours induced large color shifts. It is also known that luminance contrast between a center and its surrounds affects the magnitude of simultaneous color contrast. However, our color contrast effects were larger for a dark line rather than for a pale line. In contrast, the perceived color shift of the line without the contours increased as the luminance of the gray line increased, supporting the known effect of Kirschmann's third law. Observed color shifts could be explained by an augmented synergy theory based on intensity space, rather than chromaticity.

Chapter 7

General discussion

7.1 Spatial inhibition in the L/M-cone modulation

This thesis showed the following results: (1) the color appearance of the test area shifted by the L/M-cone patterned surroundings; (2) the optimal width of the shift depended on the cardinal axes of the surrounding modulation; and (3) contour luminance was critical for the shift, although the test luminance had a negligible effect. This section discusses the mechanism to induce the color shift by patterned surroundings, per the study of S-cone-patterned surroundings. Although the mechanism could explain the color shift by the surroundings defined in the chromatic signal, it is not complete to the results of the achromatic-contour conditions.

The first point is the spatial extent of spatial inhibition for L/M-cone modulation. The spatial extent is the center-surround organization, modeled by a difference of Gaussian (DoG). The DoG adds signals around the test area and subtracts the signals of the test and second inducer. Thus, the DoG function can enhance the contrast of the chromatic signal and provide the perception of the Monnier–Shevell illusion. The surroundings modulated along the L/M-cone colors induced the large shift in the test appearance along the L/M-cone axis. When the contour was chromatic, the appearance of the test area shifted toward the chromaticity of the contour (**Fig. 4.3** and **Fig. 4.4)** and away from the chromaticity of the second inducer. This shift can be represented by the spatial inhibition received from the inputs of the L/M cone (**Fig. 7.1A**). The appearance shifted away from the second inducer when the contour was achromatic. The chromatic-contour condition causes the outputs from the center Gaussian to become zero because both the test and contour were neutral in the chromatic space. Therefore, the total output of the induction reflects the surrounding Gaussian distribution (**Fig. 7.1B**). The no-contour condition cancels the outputs from the center and surrounding Gaussian (**Fig. 7.1C**). The DoG function supports color induction in the L/M-cone modulation and S-cone.

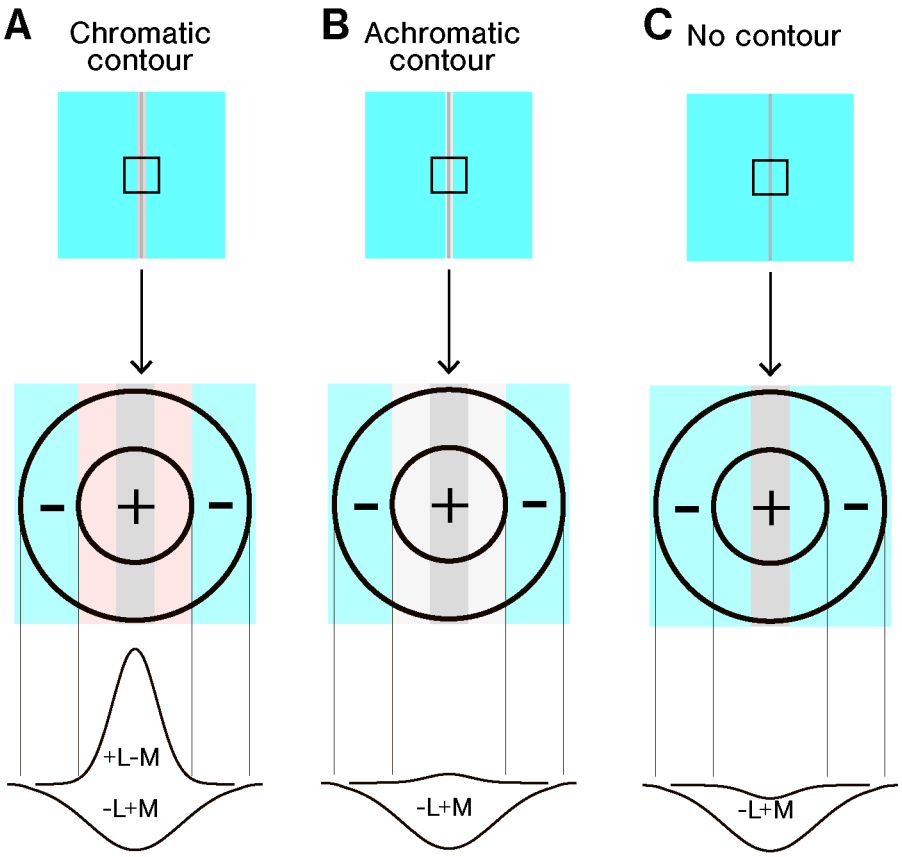

Figure 7.1 Spatial inhibition causes color induction

Spatial inhibition of L/M cones also causes color induction. The center Gaussian adds the signals of the test and contour, and the surrounding Gaussian subtracts the test area signals from the inducer signals. When the inducer and contour chromaticities were opposite to each other (**A**), the test appearance largely shifted to the contour chromaticity. When the contour is achromatic (**B**), the color shift reflects the surrounding Gaussian. When the contour and inducer color is opposite pair, the gaussian outputs are canceled.

7.1.1 Limitation

I also observed the dependency on luminance polarity in the achromatic-contour condition. The result showed that the white contour, which was brighter than the inducer luminance, significantly caused color shifts (**Fig. 6.2**). However, darker than the inducer luminance, the black contour hardly caused color induction. A summary of the luminance dependence is shown in **Fig. 7.2.** The test lines with brighter contours are perceived as reddish, whereas those with darker contours are slight. The equiluminant conditions induced a color shift on the contour, in addition to the test line. Contrastingly, the brighter contours still appeared achromatic and were reported by the participants (see the discussion in Chapter 5). Changing the luminance profile does not affect color induction if the DoG is constantly effective. Moreover, DoG predicts a color

shift in the achromatic contour. However, this result contradicts the prediction. Therefore, the color inductions of the DoG can be gated using luminance signals.

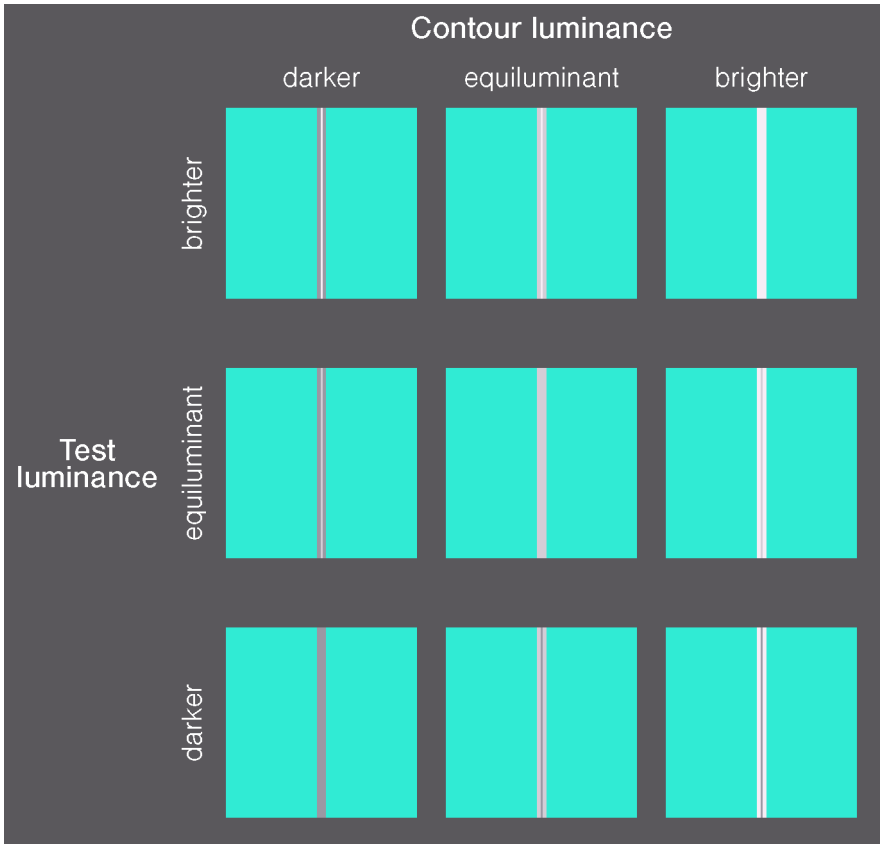

Figure 7.2 Demonstrations of luminance dependency on achromatic contours
The gray test line is placed on all cyan backgrounds, and the achromatic contour flanked some. The contour brightness increased from left to right. The test brightness increased from the bottom to the top. Equiluminant indicates no luminance contrast to the cyan background, resulting in the no-contour condition for the diagonal stimuli. The chromaticities of the lines were identical. The colors were calibrated using a monitor.

7.1.2 Luminance dependency on the DoG

The white-contour condition can be described by both the physical profiles for the color and luminance signals (**Fig. 7.3A**). Optical artifacts blur the profiles, resulting in a decrease in their contrast (**Fig. 7.3B**); therefore, the contour and test line might be interpreted as representing a cyanic hue. Thus, the visual system must solve the task of picking up an achromatic point from chromatic signals contaminated by artifacts. Defining a point representing an achromatic surface is critical to solving this task. White points tend to be brighter and more unsaturated than the surroundings. Thus, I propose a peak with a contrast in the luminance and chromatic

profiles as a reference point.

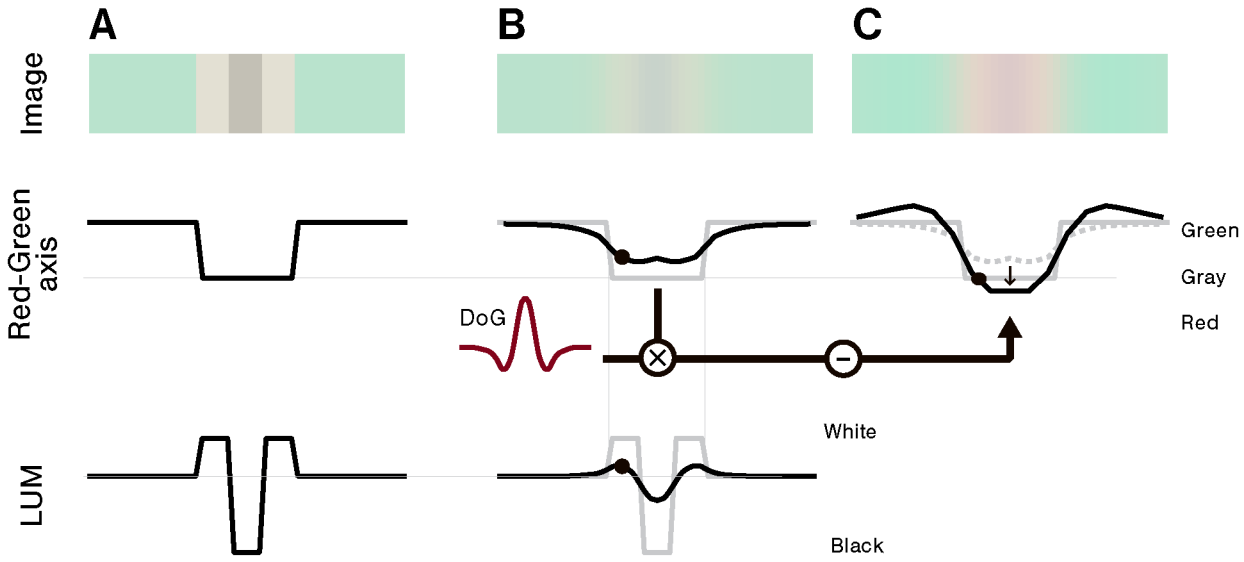

Figure 7.3 Explanation of the proposed correction

The top, middle, and bottom rows represent the stimulus image and its chromatic and luminance profiles, respectively. The physical stimulus (**A**) is affected by optical artifacts, resulting in a blurred image (**B**). The proposed correction moves the reference point to the null of the chromatic axis and produces output (**C**). The moving subtracts the DoG output from the artifact profile. The filled circles indicate the reference points. These images and profiles are obtained from the results of Chapter 4.

The chromatic profile must be shifted or enhanced to correct the reference point to neutral gray. Herein, I consider this enhancement. The enhancement is performed by subtracting the DoG profile from the blurred chromatic profile because the correction needs to remove the blur of the optical artifacts (**Fig. 7.3B**). Additionally, the reference point on the artifact profile is more saturated than the test area. Thus, the correction results in a shift in the test area over the neutral point to the red direction (**Fig. 7.3C**). Therefore, the chromatic signal in the test area became reddish.

The correction also predicts that the magnitude of the matching varies with decreasing test luminance. The prediction was performed using the following steps: The correction was first performed using the Gaussian filter (3 min sigma), blurred the l profile, and then performed down-sampling (3 min step). These calculations correspond to the cut-off for chromatic signal sampling in the retina. Then, the DoG filter (1 min of the center sigma and 2 min of the surround sigma, center-surround weighting 1:1) was adapted to the filtered $l$profile to obtain the spatial chromatic change. Next, the reference point was defined by the maximum DoG (1 min of the center sigma and 2 min of the surround sigma, center-surround weighting 1:1) signal

from the luminance profile. Finally, the DoG profile was subtracted from the filtered l profile to ensure that the reference point moved to null in the l axis to correct the artifact stain.

Fig. 7.4A shows the predicted shift of both the cyan and red inducer. The correction indicates that the color shift varied with decreasing test luminance. Additionally, the correction predicted the contrast effect for both the inducers. The color shift increased with a decrease in the test luminance. When the test luminance was decreased, the contrast at the reference point decreased relative to the brighter test. This correction indicates that the reference point shifts to the achromatic null. Thus, the shift is more significant in the darker test. The predicted shift agrees with the luminance dependence of the white-contour condition (**Fig. 7.4B**).

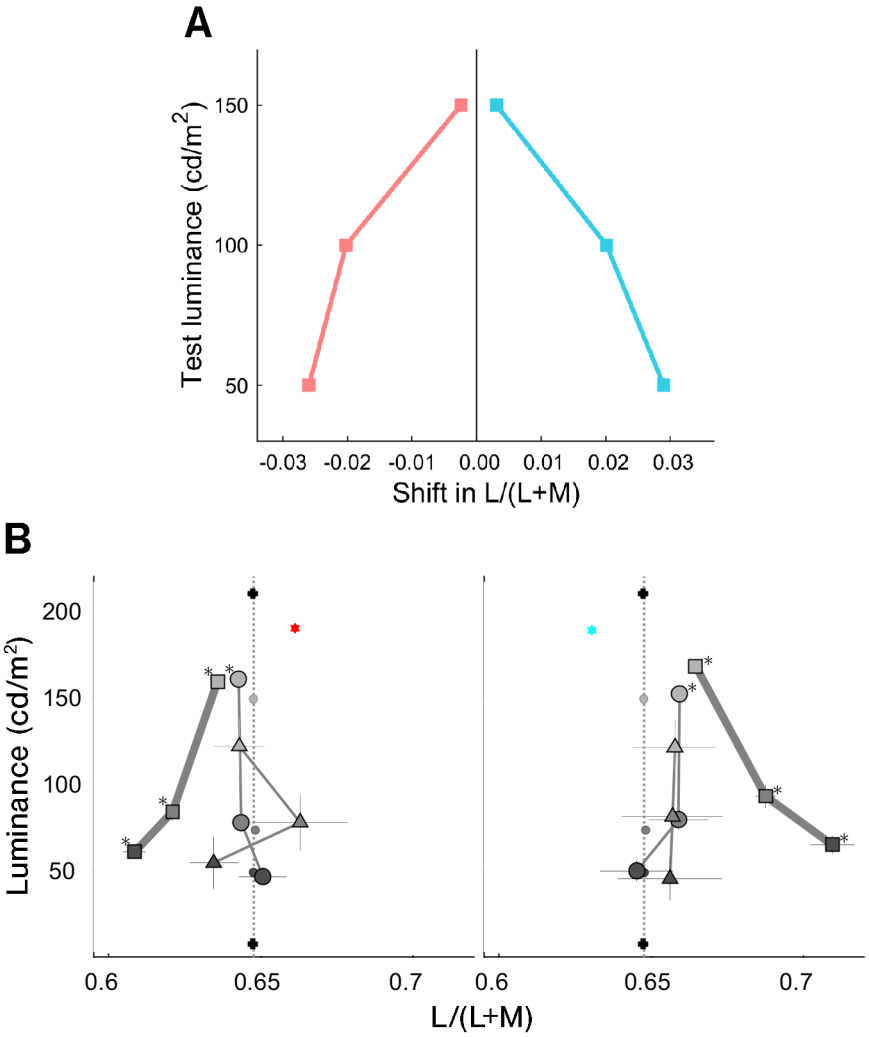

Figure 7.4 Predicted shifts and matching results

(**A**) The vertical and horizontal axis indicates the test luminance and the predicted shift in the test area from the actual value. The blue and red markers represent the predicted shifts of cyan and red inducers, respectively. The artifact calculation was the same as that used in the analysis in Chapter 4. The stimuli had the same chromaticity as the gray test and spatial pattern of the white-contour condition, as in Chapter 4. (**B**) Results of luminance dependency in Chapter 6. The square and dot markers represent the matching of the white-contour condition and the test luminance. The left and right panels show the results for the cyan and red inducers, respectively. The other format is the same as in **Fig. 6.2E** and **F**.

7.1.3 Another explanation

Because the luminance contrast between the center and the surroundings commonly affects chromatic inductions (Bergström & Derefeldt 1975; Bergström, Derefeldt, & Holmgren 1978; Gordon & Shapley 2006; J. A. S. Kinney 1962; Xing et al. 2015), it is necessary to focus on studies

to investigate brightness induction. Edge integration theory can explain brightness induction in stimuli with alternating white and black (Rudd & Zemach 2004, 2005, 2007; Vladusich, Lucassen, & Cornelissen 2006). This theory assumes that the local edge contrast between the test and first inducer modulates the induction from the remote edge between the first and second inducers. Is this assumption valid for the achromatic-contour condition of the chromatic inducer? Here, the local contrast in the achromatic-contour condition is on edge between the test and contour. The remote contrast is on edge between the contour and inducer. Considering this result, the inductions defined in the chromaticity space were consistent with this assumption, while the inductions defined in the luminance space were not (**Fig. 6.2)**. Because the edge integration can be represented in the excitation space, I concluded that the achromatic-contour condition hardly shows this assumption.

7.2 Color induction in the cardinal axes

The direction of chromatic induction is consistent with the modulation direction of the surroundings in both cardinal axes. In particular, previous studies have reported that the shift occurs only in the modulation direction of the surroundings, even though the test chromaticity had a chromatic contrast orthogonal to the modulation axis of the surrounding (Monnier & Shevell 2003, 2004; Shevell & Monnier 2006). The shift in one direction is inconsistent with evidence that the center-surround pattern causes chromatic induction.

In Chapter 4, the shift in the s axis occurred in the purple and yellow test lines under achromatic- and chromatic-contour conditions. The test line had a constant contrast in the S-cone axis to the contour and inducer. Thus, the stimuli were described as the no-contour condition in the s space. According to the results of the line-width dependency in this thesis, 1.9 min-width of the no-contour condition for the S-cone color resulted in slight chromatic induction (the violet inducer in **Fig. 5.4)**. Thus, a shift similar to the no-contour condition was observed in the purple and yellow test lines. Although varying the line width isolates effectively the shift from each cardinal axis, it is necessary to take care of the broad extent of spatial inhibition in the S-cone axis.

7.3 Future prediction

This thesis discovered the optimal widths using a high-resolution monitor. The optimal width for L/M-cone color was approximately 1 min. This width corresponds to a viewing angle of 1 pixel for 218 PPI if the viewing distance is 40 cm with a 16:9 resolution. Thus, it is not surprising that the Monnier–Shevell illusion for the L/M-cone colors is found, as high-resolution monitors are now available. This also indicated that the advanced monitor obtained a new finding. Improvements in devices help validate scientific questions, such as perceiving fine colors.

Chapter 8

Conclusion

This chapter summarized the thesis contents as follows.

- Reported a new spatial context of the Monnier-Shevell illusion. The spatial context is the thin gray line and thin white lines on the chromatic surroundings (*inducer*). The gray line (*test line*) appears as the complementary color of the inducer by flanking the white lines (*contour*), regardless of the inducer chromaticity. The influence of chromatic aberrations could not fully explain the appearance of the test line.

- The surrounding modulated along with the L/M-cone axis causes a significant shift in the L/M-cone axis. The shift can be represented by the receptive field of the center-surround cell, similar to the surrounding alternating S-cone colors.

- The spatial extent of the chromatic induction in the spatial context is different between the cardinal axes. The width inducing the maximum shift was approximately 1 min for L/M-cone color. The optimal width for the S-cone colors was approximately eight times greater than that for the L/M-cone colors. The difference between the cardinal axes reflects the difference in the upper limit of spatial resolution between the cardinal axes. The simulated shift due to optical artifacts could explain the shift in the S-cone colors.

- The luminance of the achromatic contour is critical to the color shift, while the test luminance is independent. This was not explained by the center-surround cell. I propose a mechanism to remove chromatic shifts due to optical artifacts. This mechanism may help recover the actual color appearance in detail.

References

Atchison, D. A. et al. (2011). "Influence of field size on pupil diameter under photopic and mesopic light levels". In: *Clin. Exp. Optom.* 94.6, pp. 545–548. DOI: 10.1111/j.1444-0938.2011.00636.x. URL: http://www.ncbi.nlm.nih.gov/pubmed/21929524.

Barboni, M. T. et al. (2013). "Chromatic spatial contrast sensitivity estimated by visual evoked cortical potential and psychophysics". In: *Brazilian J. Med. Biol. Res.* 46.2, pp. 154–163. DOI: 10.1590/1414-431X20122428. URL: http://dx.doi.org/10.1590/1414-431X20122428%20http://www.ncbi.nlm.nih.gov/pubmed/23369980%20http://www.pubmedcentral.nih.gov/articlerender.fcgi?artid=PMC4899949.

Bäuml, K. H. (2001). "Increments and decrements in color constancy". In: *J. Opt. Soc. Am. A* 18.10, pp. 2419–2429. DOI: 10.1364/josaa.18.002419.

Bergström, S. S. & G. Derefeldt (1975). "Effects of surround/test field luminance ratio on induced colour". In: *Scand. J. Psychol.* 16.1, pp. 311–318. DOI: 10.1111/j.1467-9450.1975.tb00198.x.

Bergström, S. S., G. Derefeldt, & S. Holmgren (1978). "Chromatic induction as a function of luminance relations". In: *Scand. J. Psychol.* 19.1, pp. 265–276. DOI: 10.1111/j.1467-9450.1978.tb00330.x. URL: http://doi.wiley.com/10.1111/j.1467-9450.1978.tb00330.x%20https://onlinelibrary.wiley.com/doi/10.1111/j.1467-9450.1978.tb00330.x.

Bimler, D. L., G. V. Paramei, & C. A. Izmailov (2009). "Hue and saturation shifts from spatially induced blackness". In: *J. Opt. Soc. Am. A* 26.1, p. 163. DOI: 10.1364/josaa.26.000163. URL: http://www.ncbi.nlm.nih.gov/pubmed/19109613.

Brainard, D. H. (1997). "The Psychophysics Toolbox". In: *Spat. Vis.* 10.4, pp. 433–436. DOI: 10.1163/156856897X00357. URL: http://www.ncbi.nlm.nih.gov/pubmed/9176952.

— (1998). "Color constancy in the nearly natural image 2 Achromatic loci". In: *J. Opt. Soc. Am. A* 15.2, pp. 307–325. DOI: 10.1364/josaa.15.000307.

Brainard, D. H. & D. R. Williams (1993). "Spatial reconstruction of signals from short-wavelength cones". In: *Vision Res.* 33.1, pp. 105–116. DOI: 10.1016/0042-6989(93)90063-3.

Brouwer, G. J. & D. J. Heeger (2009). "Decoding and Reconstructing Color from Responses in Human Visual Cortex". In: *J. Neurosci.* 29.44, pp. 13992–14003. DOI: 10.1523/JNEUROSCI.3577-09.2009. URL: www.jneurosci.org%20https://www.jneurosci.org/lookup/doi/10.1523/JNEUROSCI.3577-09.2009.

Calkins, D. J. (2001). "Seeing with S cones". In: *Prog. Retin. Eye Res.* 20.3, pp. 255–287. DOI: 10.1016/S1350-9462(00)00026-4. URL: CSF;.

Calkins, D. J., S. J. Schein, et al. (1994). "M and L cones in macaque fovea connect to midget ganglion cells by different numbers of excitatory synapses". In: *Nature* 371.6492, pp. 70–72. DOI: 10.1038/371070a0. URL: https://www.nature.com/articles/371070a0.

Calkins, D. J., Y. Tsukamoto, & P. Sterling (1998). "Microcircuitry and mosaic of a blue-yellow ganglion cell in the primate retina". In: *J. Neurosci.* 18.9, pp. 3373–3385. DOI: 10.1523/jneurosci.18-09-03373.1998. URL: https://www.jneurosci.org/content/18/9/3373%20https://www.jneurosci.org/content/18/9/3373.abstract.

Callaway, E. M. (2005). "Structure and function of parallel pathways in the primate early visual system". In: *J. Physiol.* 566.1, pp. 13–19. DOI: 10.1113/jphysiol.2005.088047.

Campbell, F. W. & D. G. Green (1965). "Optical and retinal factors affecting visual resolution." In: *J. Physiol.* 181.3, pp. 576–593. DOI: 10.1113/jphysiol.1965.sp007784.

Campbell, F. W. & R. W. Gubisch (1966). "Optical quality of the human eye". In: *J. Physiol.* 186.3, pp. 558–578. DOI: 10.1113/jphysiol.1966.sp008056. URL: https://onlinelibrary.wiley.com/doi/full/10.1113/jphysiol.1966.sp008056%20https://onlinelibrary.wiley.com/doi/abs/10.1113/jphysiol.1966.sp008056%20https://physoc.onlinelibrary.wiley.com/doi/10.1113/jphysiol.1966.sp008056.

Cao, D. & S. K. Shevell (2005). "Chromatic assimilation: Spread light or neural mechanism?" In: *Vision Res.* 45.8, pp. 1031–1045. DOI: 10.1016/j.visres.2004.10.016.

Caves, E. M., N. C. Brandley, & S. Johnsen (2018). "Visual Acuity and the Evolution of Signals". In: *Trends Ecol. Evol.* 33.5, pp. 358–372. DOI: 10.1016/j.tree.2018.03.001.

Cerda-Company, X. et al. (2018). "The effect of luminance differences on color assimilation". In: *J. Vis.* 18.11, pp. 1–23. DOI: 10.1167/18.11.10. URL: http://jov.arvojournals.org/article.aspx?doi=10.1167/18.11.10%20http://www.ncbi.nlm.nih.gov/pubmed/30347096.

Chatterjee, S. & E. M. Callaway (2003). "Parallel colour-opponent pathways to primary visual cortex". In: *Nature* 426.6967, pp. 668–671. DOI: 10.1038/nature02167. URL: https://www.nature.com/articles/nature02167.

Chen, T. L. & C. Y. Yu (1996). "The relationship between visual acuity and color contrast in the OSA uniform color space". In: *Color Res. Appl.* 21.1, pp. 18–25. DOI: 10.1002/(SICI)1520-6378(199602)21:1<18::AID-COL2>3.0.CO;2-8.

Chevreul, E. (1839). *De la loi du contraste simultané des couleurs et de l'assortiment des objets colorés*. Imprimerie Nationale. URL: https://books.google.nl/books?hl=en%7B%5C&%7Dlr=%7B%5C&%7Did=WBBZDyRspUAC%7B%5C&%7Doi=fnd%7B%5C&%7Dpg=PA12%7B%5C&%7Ddq=De+la+loi+du+contraste+simultan%7B%5C'%7Be%7D%7D+des+couleurs%7B%5C&%7Dots=b95VjTZ9n3%7B%5C&%7Dsig=kZ%7B%5C_%7DCp6LwAhgU%7B%5C_%7DA0lgHK4mEzZwZk%7B%5C%7D5Cnhttps://books.google.nl/books?hl=en%7B%

5C&%7Dlr=%7B%5C&%7Did=WBBZDyRspUAC%7B%5C&%7Doi=fnd%7B%5C&%7Dpg=PA12%7B%5C&%7Ddq=De+la+loi.

Chichilnisky, E. J. & B. A. Wandell (1996). *Seeing gray through the ON and OFF pathways.* DOI: 10.1017/s0952523800008270.

Conway, B. R. & M. S. Livingstone (2006). "Spatial and temporal properties of cone signals in alert macaque primary visual cortex". In: *J. Neurosci.* 26.42, pp. 10826–10846. DOI: 10.1523/JNEUROSCI.2091-06.2006. URL: www.jneurosci.org.

Crook, J. D., C. M. Davenport, et al. (2009). "Parallel ON and OFF cone bipolar inputs establish spatially coextensive receptive field structure of blue-yellow ganglion cells in primate retina". In: *J. Neurosci.* 29.26, pp. 8372–8387. DOI: 10.1523/JNEUROSCI.1218-09.2009. URL: https://www.jneurosci.org/content/29/26/8372%20https://www.jneurosci.org/content/29/26/8372.abstract.

Crook, J. D., M. B. Manookin, et al. (2011). "Horizontal cell feedback without cone type-selective inhibition mediates "red-green" color opponency in midget ganglion cells of the primate retina". In: *J. Neurosci.* 31.5, pp. 1762–1772. DOI: 10.1523/JNEUROSCI.4385-10.2011. URL: https://www.jneurosci.org/content/31/5/1762%20https://www.jneurosci.org/content/31/5/1762.abstract.

Cuenca, N., I. Ortuño-Lizarán, & I. Pinilla (2018). "Cellular Characterization of OCT and Outer Retinal Bands Using Specific Immunohistochemistry Markers and Clinical Implications". In: *Ophthalmology* 125.3, pp. 407–422. DOI: 10.1016/j.ophtha.2017.09.016.

Curcio, C. A., K. A. Allen, et al. (1991). "Distribution and morphology of human cone photoreceptors stained with anti-blue opsin". In: *J. Comp. Neurol.* 312.4, pp. 610–624. DOI: 10.1002/cne.903120411.

Curcio, C. A., K. R. Sloan, et al. (1990). "Human photoreceptor topography". In: *J. Comp. Neurol.* 292.4, pp. 497–523. DOI: 10.1002/cne.902920402.

Dacey, D. M. & B. B. Lee (1994). "The 'blue-on' opponent pathway in primate retina originates from a distinct bistratified ganglion cell type". In: *Nature* 367.6465, pp. 731–735. DOI: 10.1038/367731a0.

Davies, N. & A. Morland (2003). "Extent of foveal tritanopia in diabetes mellitus". In: *Br. J. Ophthalmol.* 87.6, pp. 742–746. DOI: 10.1136/bjo.87.6.742. URL: https://bjo.bmj.com/content/87/6/742%20https://bjo.bmj.com/content/87/6/742.abstract.

De Weert, C. M. & L. Spillmann (1995). "Assimilation: Asymmetry between brightness and darkness?" In: *Vision Res.* 35.10, pp. 1413–1419. DOI: 10.1016/0042-6989(95)98721-K.

Devinck, F., P. B. Delahunt, et al. (2005). "The watercolor effect: Quantitative evidence for luminance-dependent mechanisms of long-range color assimilation". In: *Vision Res.* 45.11, pp. 1413–1424. DOI: 10.1016/j.visres.2004.11.024.

Devinck, F., L. Spillmann, & J. S. Werner (2006). "Spatial profile of contours inducing long-range color assimilation". In: *Vis. Neurosci.* 23.3-4, pp. 573–577. DOI: 10.1017/S0952523806233224.

Ekroll, V. & F. Faul (2012). "New laws of simultaneous contrast ?" In: 25.2, pp. 107–141.

Fach, C. & L. T. Sharpe (1986). "Assimilative hue shifts in color gratings depend on bar width." In: *Percept. Psychophys.* 40.6, pp. 412–418. DOI: 10.3758/BF03208201. URL: http://www.ncbi.nlm.nih.gov/pubmed/3808908.

Faul, F., V. Ekroll, & G. Wendt (2008). "Color appearance: The limited role of chromatic surround variance in the "gamut expansion effect"". In: *J. Vis.* 8.3, pp. 1–20. DOI: 10.1167/8.3.30.

Geisler, W. S. (1989). "Sequential Ideal-Observer Analysis of Visual Discriminations". In: *Psychol. Rev.* 96.2, pp. 267–314. DOI: 10.1037/0033-295X.96.2.267. URL: /record/1989-24741-001.

Gordon, J. & R. Shapley (2006). "Brightness contrast inhibits color induction: Evidence for a new kind of color theory". In: *Spat. Vis.* 19.2-4, pp. 133–146. DOI: 10.1163/156856806776923498.

Grünert, U. & P. R. Martin (2020). "Cell types and cell circuits in human and non-human primate retina". In: *Prog. Retin. Eye Res.* 78, p. 100844. DOI: 10.1016/j.preteyeres.2020.100844.

Helson, H. (1938). "Fundamental problems in color vision. I. The principle governing changes in hue, saturation, and lightness of non-selective samples in chromatic illumination". In: *J. Exp. Psychol.* 23.5, pp. 439–476. DOI: 10.1037/h0060971. URL: http://content.apa.org/journals/xge/23/5/439.

Helson; H. & W. C. Michels (1948). "The Effect of Chromatic Adaptation on Achromaticity". In: *J. Opt. Soc. Am.* 38.12, pp. 1025–1032. DOI: 10.1364/JOSA.38.001025. URL: https://www.osapublishing.org/abstract.cfm?URI=josa-38-12-1025.

Hofer, H., J. Carroll, et al. (2005). "Organization of the human trichromatic cone mosaic". In: *J. Neurosci.* 25.42, pp. 9669–9679. DOI: 10.1523/JNEUROSCI.2414-05.2005. URL: http://www.jneurosci.org/cgi/doi/10.1523/JNEUROSCI.2414-05.2005%20http://www.ncbi.nlm.nih.gov/pubmed/16237171%20http://www.pubmedcentral.nih.gov/articlerender.fcgi?artid=PMC6725723.

Hofer, H., B. Singer, & D. R. Williams (2005). "Different sensations from cones with the same photopigment". In: *J. Vis.* 5.5, pp. 444–454. DOI: 10.1167/5.5.5. URL: http://journalofvision.org/5/5/5/444.

Hopkins, H. H. (1955). "The frequency response of a defocused optical system". In: *Proc. R. Soc. London. Ser. A. Math. Phys. Sci.* 231.1184, pp. 91–103. DOI: 10.1098/rspa.1955.0158. URL: https://royalsocietypublishing.org/doi/10.1098/rspa.1955.0158.

Hurlbert, A. (1996). "Colour vision: Putting it in context". In: *Curr. Biol.* 6.11, pp. 1381–1384. DOI: 10.1016/s0960-9822(96)00736-1.

Hurlbert, A. & K. Wolf (2004). "Color contrast: a contributory mechanism to color constancy." In: *Prog. Brain Res.* 144, pp. 145–160. DOI: 10.1016/s0079-6123(03)14410-x. URL: https://linkinghub.elsevier.com/retrieve/pii/S007961230314410X%20http://www.ncbi.nlm.nih.gov/pubmed/14650846.

Irvin, G. E., V. A. Casagrande, & T. T. Norton (1993). "Center/surround relationships of magnocellular, parvocellular, and koniocellular relay cells in primate lateral geniculate nucleus". In: *Vis. Neurosci.* 10.2, pp. 363–373. DOI: 10.1017/S0952523800003758.

Johnson, C. A. & E. J. Casson (1995). "Effects of luminance, contrast, and blur on visual acuity". In: *Optom. Vis. Sci.* 72.12, pp. 864–869. DOI: 10.1097/00006324-199512000-00004. URL: https://europepmc.org/article/med/8749333.

Johnson, E. N., M. J. Hawken, & R. Shapley (2001). "The spatial transformation of color in the primary visual cortex of the macaque monkey". In: *Nat. Neurosci.* 4.4, pp. 409–416. DOI: 10.1038/86061. URL: http://neurosci.nature.com.

Johnson, E. N., M. J. Hawken, & R. Shapley (2008). "The orientation selectivity of color-responsive neurons in macaque V1". In: *J. Neurosci.* 28.32, pp. 8096–8106. DOI: 10.1523/JNEUROSCI.1404-08.2008. URL: http://www.jneurosci.org/cgi/doi/10.1523/JNEUROSCI.1404-08.2008%20http://www.ncbi.nlm.nih.gov/pubmed/18685034%20http://www.pubmedcentral.nih.gov/articlerender.fcgi?artid=PMC2896204.

Johnson, E. N., S. D. Van Hooser, & D. Fitzpatrick (2010). "The representation of S-cone signals in primary visual cortex". In: *J. Neurosci.* 30.31, pp. 10337–10350. DOI: 10.1523/JNEUROSCI.1428-10.2010. URL: www.jneurosci.org.

Judd, D. B. (1940). "Hue Saturation and Lightness of Surface Colors with Chromatic Illumination". In: *J. Opt. Soc. Am.* 30.1, pp. 2–32. DOI: 10.1364/JOSA.30.000002. URL: https://www.osapublishing.org/abstract.cfm?URI=josa-30-1-2.

Kanematsu, T. & K. Koida (2018). *White + Gray = Red*. URL: http://illusionoftheyear.com/cat/top-10-finalists/2018/.

— (2020). "Large enhancement of simultaneous color contrast by white flanking contours". In: *Sci. Rep.* 10.1, pp. 1–10. DOI: 10.1038/s41598-020-77241-5. URL: www.nature.com/scientificreports.

— (2022). "Influence of Stimulus Size on Simultaneous Chromatic Induction". In: *Front. Psychol.* 13.818149, pp. 1–12. DOI: 10.3389/FPSYG.2022.818149.

Kinney, J. A. S. (1962). "Factors affecting induced color". In: *Vision Res.* 2.12, pp. 503–525. DOI: 10.1016/0042-6989(62)90052-4.

Kirschmann, A. (1891). "Über die quantitativen Verhältnisse des simultanen Helligkeits- und Farbkontrastes". In: *Psychol. Stud.* 6, pp. 417–463.

Kolb, H. et al. (1995). "The Architecture of the Human Fovea". In: *Webvision Organ. Retin. Vis. Syst.* URL: http://www.ncbi.nlm.nih.gov/pubmed/32129967.

Kuriki, I. (2006). "The loci of achromatic points in a real environment under various illuminant chromaticities". In: *Vision Res.* 46.19, pp. 3055–3066. DOI: 10.1016/j.visres.2006.03.012.

— (2015). "Lightness dependence of achromatic loci in color-appearance coordinates". In: *Front. Psychol.* 6.67, pp. 1–10. DOI: 10.3389/fpsyg.2015.00067.

Lennie, P., J. Krauskopf, & G. Sclar (1990). "Chromatic mechanisms in striate cortex of macaque". In: *J. Neurosci.* 10.2, pp. 649–669. DOI: 10.1523/jneurosci.10-02-00649.1990. URL: http://www.ncbi.nlm.nih.gov/pubmed/2303866.

Lin, Y.-j., C.-C. Chen, & S. H.-l. Chien (2010). "The Munker–White effect and chromatic induction share similar nonlinear response properties". In: *Seeing Perceiving* 23.3, pp. 223–240. DOI: 10.1163/187847510X516395. URL: http://booksandjournals.brillonline.com/content/journals/10.1163/187847510x516395.

Logvinenko, A. D. & S. J. Hutchinson (2007). "Evidence for the existence of colour mechanisms producing unique hues as derived from a colour illusion based on spatio-chromatic interactions". In: *Vision Res.* 47.10, pp. 1315–1334. DOI: 10.1016/j.visres.2006.10.025.

Lotto, R. B. & D. Purves (2000). "An empirical explanation of color contrast." In: *Proc. Natl. Acad. Sci. U. S. A.* 97.23, pp. 12834–12839. DOI: 10.1073/pnas.210369597.

MacLeod, D. I. & R. M. Boynton (1979). "Chromaticity diagram showing cone excitation by stimuli of equal luminance." In: *J. Opt. Soc. Am.* 69.8, pp. 1183–1186. DOI: 10.1364/JOSA.69.001183. URL: https://www.osapublishing.org/abstract.cfm?URI=josa-69-8-1183%20http://www.ncbi.nlm.nih.gov/pubmed/490231.

Marimont, D. H. & B. A. Wandell (1994). "Matching color images: the effects of axial chromatic aberration". In: *J. Opt. Soc. Am. A* 11.12, p. 3113. DOI: 10.1364/josaa.11.003113. URL: https://www.researchgate.net/publication/246773955%20https://www.osapublishing.org/abstract.cfm?URI=josaa-11-12-3113.

McCamy, C. S. (2003). "Colors of some small figures on colored grounds". In: *Color Res. Appl.* 28.4, pp. 242–250. DOI: 10.1002/col.10159. URL: https://onlinelibrary.wiley.com/doi/full/10.1002/col.10159%20https://onlinelibrary.wiley.com/doi/abs/10.1002/col.10159%20https://onlinelibrary.wiley.com/doi/10.1002/col.10159.

McKeefry, D. J., I. J. Murray, & J. J. Kulikowski (2001). "Red-green and blue-yellow mechanisms are matched in sensitivity for temporal and spatial modulation". In: *Vision Res.* 41.2, pp. 245–255. DOI: 10.1016/S0042-6989(00)00247-9.

Mély, D. A., D. Linsley, & T. Serre (2018). "Complementary surrounds explain diverse contextual phenomena across visual modalities". In: *Psychol. Rev.* 125.5, pp. 769–784. DOI: 10.1037/rev0000109. URL: http://dx.doi.org/10.1037/rev0000109%20http://doi.apa.org/getdoi.cfm?doi=10.1037/rev0000109%20http://www.ncbi.nlm.nih.gov/pubmed/30234321.

Monnier, P. & S. K. Shevell (2003). "Large shifts in color appearance from patterned chromatic backgrounds". In: *Nat. Neurosci.* 6.8, pp. 801–802. DOI: 10.1038/nn1099.

— (2004). "Chromatic induction from S-cone patterns". In: *Vision Res.* 44.9, pp. 849–856. DOI: 10.1016/j.visres.2003.11.004.

Mullen, K. T. (1985). "The contrast sensitivity of human colour vision to red-green and blue-yellow chromatic gratings". In: *J. Physiol.* 359.1, pp. 381–400. DOI: 10.1113/jphysiol.1985.sp015591.

Mullen, K. T. & F. A. Kingdom (2002). "Differential distributions of red-green and blue-yellow cone opponency across the visual field". In: *Vis. Neurosci.* 19.1, pp. 109–118. DOI: 10.1017/S0952523802191103. URL: https://www.researchgate.net/publication/11206241%20https://www.cambridge.org/core/product/identifier/S0952523802191103/type/journal%7B%5C_%7Darticle%20http://www.ncbi.nlm.nih.gov/pubmed/12180855.

Neitz, A. et al. (2020). "Effect of cone spectral topography on chromatic detection sensitivity". In: *J. Opt. Soc. Am. A* 37.4, A244–A254. DOI: 10.1364/josaa.382384. URL: /pmc/articles/PMC7231539/?report=abstract%20https://www.ncbi.nlm.nih.gov/pmc/articles/PMC7231539/.

Otazu, X., C. A. Parraga, & M. Vanrell (2010). "Toward a unified chromatic induction model". In: *J. Vis.* 10.12, pp. 1–24. DOI: 10.1167/10.12.5.

Patterson, S. S., M. Neitz, & J. Neitz (2019). "Reconciling Color Vision Models With Midget Ganglion Cell Receptive Fields". In: *Front. Neurosci.* 13. DOI: 10.3389/fnins.2019.00865.

Pinna, B., G. Brelstaff, & L. Spillmann (2001). "Surface color from boundaries: A new 'watercolor' illusion". In: *Vision Res.* 41.20, pp. 2669–2676. DOI: 10.1016/S0042-6989(01)00105-5.

Roorda, A. & D. R. Williams (1999). "The arrangement of the three cone classes in the living human eye". In: *Nature* 397.6719, pp. 520–522. DOI: 10.1038/17383. URL: http://www.ncbi.nlm.nih.gov/pubmed/10028967.

Rudd, M. E. & I. K. Zemach (2004). "Quantitative properties of achromatic color induction: An edge integration analysis". In: *Vision Res.* 44.10, pp. 971–981. DOI: 10.1016/j.visres.2003.12.004.

— (2005). "The highest luminance anchoring rule in achromatic color perception: some counterexamples and an alternative theory." In: *J. Vis.* 5.11, pp. 983–1003. DOI: 10.1167/5.11.5.

— (2007). "Contrast polarity and edge integration in achromatic color perception." In: *J. Opt. Soc. Am. A* 24.8, pp. 2134–56. DOI: 10.1364/JOSAA.24.002134. URL: http://www.ncbi.nlm.nih.gov/pubmed/17621319.

Sabesan, R. et al. (2016). "The elementary representation of spatial and color vision in the human retina". In: *Sci. Adv.* 2.9, e1600797. DOI: 10.1126/sciadv.1600797. URL: http://advances.sciencemag.org/.

Schmidt, B. P. et al. (2018). "Sensations from a single M-cone depend on the activity of surrounding S-cones". In: *Sci. Rep.* 8.1, pp. 1–10. DOI: 10.1038/s41598-018-26754-1. URL: www.nature.com/scientificreports/.

Sekiguchi, N., D. R. Williams, & D. H. Brainard (1993). "Efficiency in detection of isoluminant and isochromatic interference fringes". In: *J. Opt. Soc. Am. A* 10.10, pp. 2118–2133. DOI: 10.1364/josaa.10.002118. URL: http://www.ncbi.nlm.nih.gov/pubmed/8229351.

Shapley, R. & M. J. Hawken (2011). "Color in the Cortex: Single- and double-opponent cells". In: *Vision Res.* 51.7, pp. 701–717. DOI: 10.1016/j.visres.2011.02.012.

Shevell, S. K. & P. R. Martin (2017). "Color opponency: tutorial". In: *J. Opt. Soc. Am. A* 34.7, pp. 1099–1108. DOI: 10.1364/JOSAA.34.001099. URL: https://www.osapublishing.org/abstract.cfm?URI=josaa-34-7-1099.

Shevell, S. K. & P. Monnier (2006). "Color shifts induced by S-cone patterns are mediated by a neural representation driven by multiple cone types". In: *Vis. Neurosci.* 23.3-4, pp. 567–571. DOI: 10.1017/S0952523806233303.

— (2005). "Color shifts from S-cone patterned backgrounds: Contrast sensitivity and spatial frequency selectivity". In: *Vision Res.* 45.9, pp. 1147–1154. DOI: 10.1016/j.visres.2004.11.013.

Shevell, S. K. & J. Wei (1998). "Chromatic induction: Border contrast or adaptation to surrounding light?" In: *Vision Res.* 38.11, pp. 1561–1566. DOI: 10.1016/S0042-6989(98)00006-6.

Smith, G. & D. A. Atchison (1997). *The Eye and Visual Optical Instruments*. Cambridge University Press, p. 830. DOI: 10.1017/cbo9780511609541. URL: https://ui.adsabs.harvard.edu/abs/1997evoi.book.....S/abstract%20https://www.cambridge.org/core/product/identifier/9780511609541/type/book.

— (2000). *Optics of the human eye*. Butterworth-Heinemann. URL: https://ci.nii.ac.jp/ncid/BA47642570.bib.

Smith, V. C. & J. Pokorny (1975). "Spectral sensitivity of the foveal cone photopigments between 400 and 500 nm." In: *Vision Res.* 15.2, pp. 161–171. DOI: 10.1016/0042-6989(75)90203-5. URL: http://www.ncbi.nlm.nih.gov/pubmed/1129973.

Smith, V. C., P. Q. Jin, & J. Pokorny (2001). "The role of spatial frequency in color induction". In: *Vision Res.* 41.8, pp. 1007–1021. DOI: 10.1016/S0042-6989(01)00031-1.

Solomon, S. G., J. W. Peirce, & P. Lennie (2004). "The Impact of Suppressive Surrounds on Chromatic Properties of Cortical Neurons". In: *J. Neurosci.* 24.1, pp. 148–160. DOI: 10.1523/JNEUROSCI.3036-03.2004. URL: http://www.jneurosci.org/cgi/doi/10.1523/JNEUROSCI.3036-03.2004.

Stanley, P. A. & A. K. Davies (1995). "The effect of field of view size on steady-state pupil diameter". In: *Ophthalmic Physiol. Opt.* 15.6, pp. 601–603. DOI: 10.1046/j.1475-1313.1995.9400019v.x. URL: https://www.onlinelibrary.wiley.com/doi/full/10.1046/j.

1475-1313.1995.9400019v.x%20https://www.onlinelibrary.wiley.com/doi/abs/10.1046/j.1475-1313.1995.9400019v.x%20https://onlinelibrary.wiley.com/doi/10.1046/j.1475-1313.1995.9400019v.x%20http://www.ncbi.nlm.ni.

Suchkov, N., E. J. Fernández, & P. Artal (2019). "Impact of longitudinal chromatic aberration on through-focus visual acuity". In: *Opt. Express* 27.24, pp. 35935–35947. DOI: 10.1364/oe.27.035935.

Tailby, C. et al. (2008). "Transmission of blue (S) cone signals through the primate lateral geniculate nucleus". In: *J. Physiol.* 586.24, pp. 5947–5967. DOI: 10.1113/jphysiol.2008.161893. URL: /pmc/articles/PMC2655435/?report=abstract%20https://www.ncbi.nlm.nih.gov/pmc/articles/PMC2655435/.

Thibos, L. N., A. Bradley, et al. (1990). "Theory and measurement of ocular chromatic aberration". In: *Vision Res.* 30.1, pp. 33–49. DOI: 10.1016/0042-6989(90)90126-6.

Thibos, L. N., M. Ye, et al. (1992). "The chromatic eye: a new reduced-eye model of ocular chromatic aberration in humans". In: *Appl. Opt.* 31.19, p. 3594. DOI: 10.1364/ao.31.003594. URL: https://www.osapublishing.org/abstract.cfm?URI=ao-31-19-3594%20http://www.ncbi.nlm.nih.gov/pubmed/20725330.

Vladusich, T., M. P. Lucassen, & F. W. Cornelissen (2006). "Edge integration and the perception of brightness and darkness". In: *J. Vis.* 6.2006, pp. 1126–1147. DOI: 10.1167/6.10.12.

Wald, G. & D. R. Griffin (1947). "The change in refractive power of the human eye in dim and bright light". In: *J. Opt. Soc. Am.* 37.5, pp. 321–336. DOI: 10.1364/JOSA.37.000321. URL: https://www.osapublishing.org/viewmedia.cfm?uri=josa-37-5-321%7B%5C&%7Dseq=0%7B%5C&%7Dhtml=true%20https://www.osapublishing.org/abstract.cfm?uri=josa-37-5-321%20https://www.osapublishing.org/josa/abstract.cfm?uri=josa-37-5-321.

Wandell, B. A. (1995). *Foundations of vision*. Vol. 8. Sinauer Associates Sunderland, MA.

Wandell, B. A. & L. D. Silverstein (2003). "Digital color reproduction". In: *Sci. Color*. Ed. by S. K. Shevell. 2nd. Elsevier, pp. 280–315.

Watson, A. B. & J. I. Yellott (2012). "A unified formula for light-adapted pupil size". In: *J. Vis.* 12.10, pp. 1–16. DOI: 10.1167/12.10.12. URL: http://www.journalofvision.org/content/12/10/12.

Webster, M. A., E. Switkes, & K. K. De Valois (1990). "Orientation and spatial-frequency discrimination for luminance and chromatic gratings". In: *J. Opt. Soc. Am. A* 7.6, pp. 1034–1049. DOI: 10.1364/josaa.7.001034. URL: http://www.ncbi.nlm.nih.gov/pubmed/2362227.

Weitzman, D. O. & J. A. Kinney (1967). "Appearance of color for small, brief, spectral stimuli, in the central fovaea". In: *J. Opt. Soc. Am.* 57.5, pp. 665–670. DOI: 10.1364/JOSA.57.000665.

Werner, J. S. & J. Walraven (1982). "Effect of chromatic adaptation on the achromatic locus: The role of contrast, luminance and background color". In: *Vision Res.* 22.8, pp. 929–943. DOI: 10.1016/0042-6989(82)90029-3. URL: https://linkinghub.elsevier.com/retrieve/pii/0042698982900293.

Williams, D., N. Sekiguchi, & D. Brainard (1993). "Color, contrast sensitivity, and the cone mosaic". In: *Proc. Natl. Acad. Sci. U. S. A.* 90.21, pp. 9770–9777. DOI: 10.1073/pnas.90.21.9770.

Williams, D. R., D. H. Brainard, et al. (1994). "Double-pass and interferometric measures of the optical quality of the eye". In: *J. Opt. Soc. Am. A* 11.12, pp. 3123–3135. DOI: 10.1364/josaa.11.003123.

Williams, D. R. & N. J. Coletta (1987). "Cone spacing and the visual resolution limit". In: *J. Opt. Soc. Am. A* 4.8, pp. 1514–1523. DOI: 10.1364/josaa.4.001514.

Williams, D. R., N. Sekiguchi, et al. (1991). "The Cost of Trichromacy for Spatial Vision". In: *From Pigment. to Percept.* Springer, Boston, MA, pp. 11–22. DOI: 10.1007/978-1-4615-3718-2_2. URL: https://link.springer.com/chapter/10.1007/978-1-4615-3718-2%7B%5C_%7D2.

Willmer, E. N. (1944). "Colour of small objects." In: *Nature* 153.3895, pp. 774–775. DOI: 10.1038/153774b0. URL: http://www.nature.com/articles/153774b0.

Willmer, E. N. & W. D. Wright (1945). "Colour sensitivity of the fovea centralis". In: *Nature* 156.3950, pp. 119–121. DOI: 10.1038/156119a0.

Wool, L. E., J. D. Crook, et al. (2018). "Nonselective wiring accounts for red-green opponency in midget ganglion cells of the primate retina". In: *J. Neurosci.* 38.6, pp. 1520–1540. DOI: 10.1523/JNEUROSCI.1688-17.2017. URL: http://www.jneurosci.org/lookup/doi/10.1523/JNEUROSCI.1688-17.2017.

Wool, L. E., O. S. Packer, et al. (2019). "Connectomic identification and three-dimensional color tuning of S-OFF midget ganglion cells in the primate retina". In: *J. Neurosci.* 39.40, pp. 7893–7909. DOI: 10.1523/JNEUROSCI.0778-19.2019. URL: https://doi.org/10.1523/JNEUROSCI.0778-19.2019.

Xing, D. et al. (2015). "Brightness-Color Interactions in Human Early Visual Cortex". In: *J. Neurosci.* 35.5, pp. 2226–2232. DOI: 10.1523/JNEUROSCI.3740-14.2015. URL: http://www.jneurosci.org/cgi/doi/10.1523/JNEUROSCI.3740-14.2015%20https://www.jneurosci.org/lookup/doi/10.1523/JNEUROSCI.3740-14.2015.

Xu, X., A. B. Bonds, & V. A. Casagrande (2002). "Modeling receptive-field structure of koniocellular, magnocellular, and parvocellular LGN cells in the owl monkey (Aotus trivigatus)". In: *Vis. Neurosci.* 19.6, pp. 703–711. DOI: 10.1017/S0952523802196027. URL: https://doi.org/10.1017/S0952523802196027.

Zhang, C. et al. (2020). "Circuit Reorganization Shapes the Developing Human Foveal Midget Connectome toward Single-Cone Resolution". In: *Neuron* 108.5, pp. 905–918. DOI: 10.1016/j.neuron.2020.09.014. URL: https://doi.org/10.1016/j.neuron.2020.09.014.

Zlatkova, M. B., A. Vassilev, & R. S. Anderson (2008). "Resolution acuity for equiluminant gratings of S-cone positive or negative contrast in human vision". In: *J. Vis.* 8.3, pp. 1–10. DOI: 10.1167/8.3.9. URL: http://journalofvision.org/8/3/9/.

Appendix A

Color representation

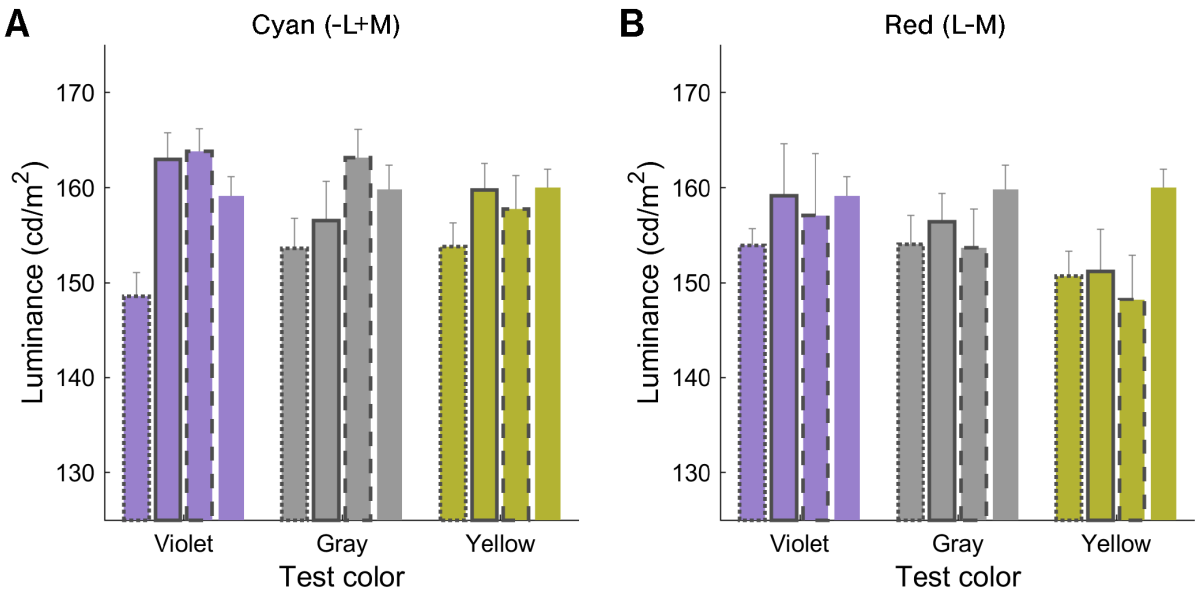

Figure A.1 The matched luminances to the test luminance
The format is the same as in **Fig. 4.5.**

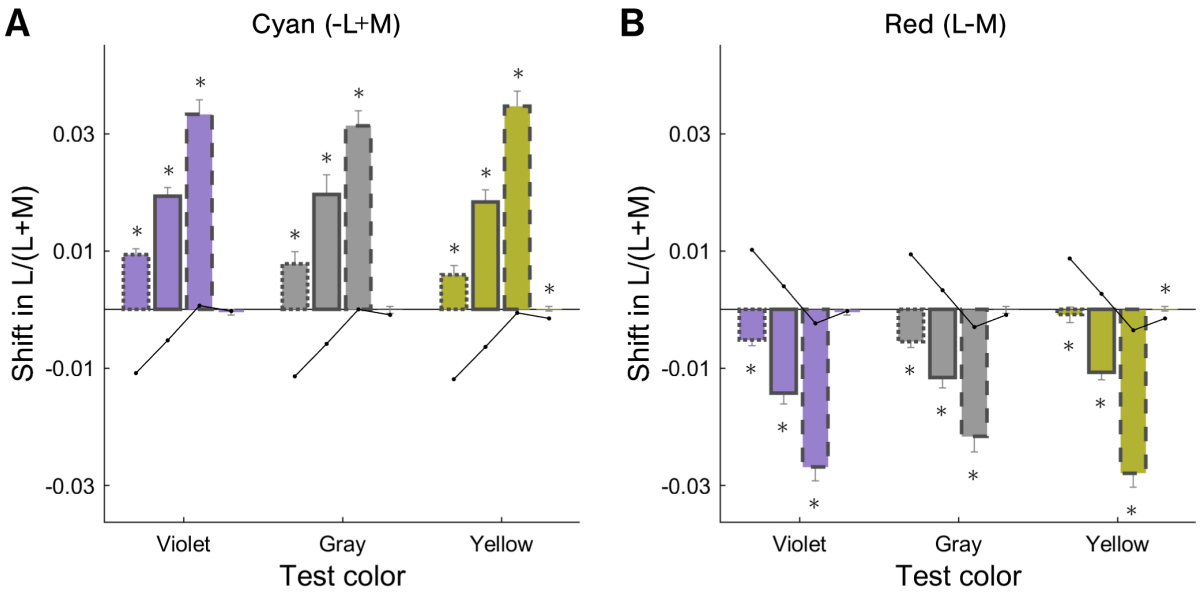

Figure A.2 Shifts in the l axis from the test chromaticity

The format is the same as in **Fig. 4.5.** Error bars are the same as the data in **Fig. 4.3** and **Fig. 4.4.**

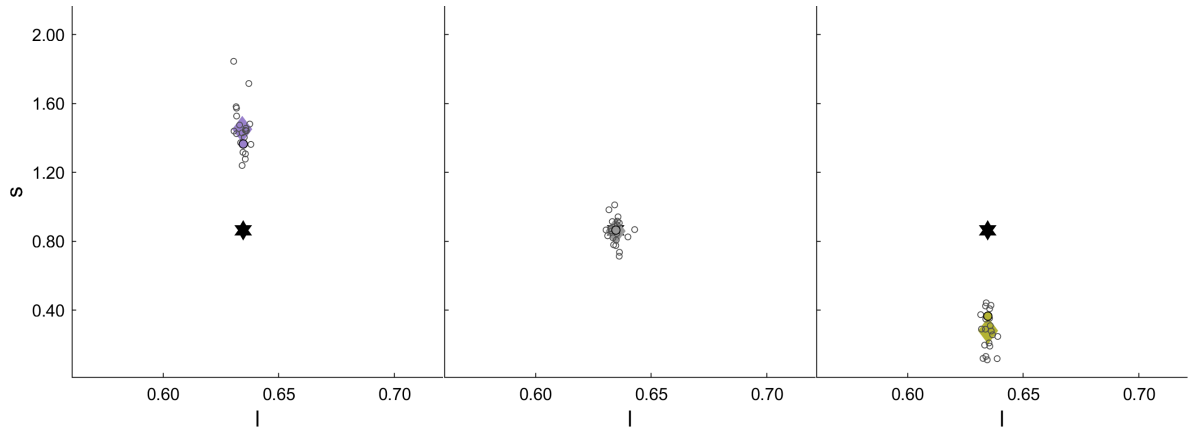

Figure A.3 Each matchings (void circles) of the baseline condition for the test lines (edged circles) on the gray surrounding (filled star)

The left, middle and right panel show matchings of the purple, gray and yellow test lines. The other format is the same as in **Fig. 4.3.**

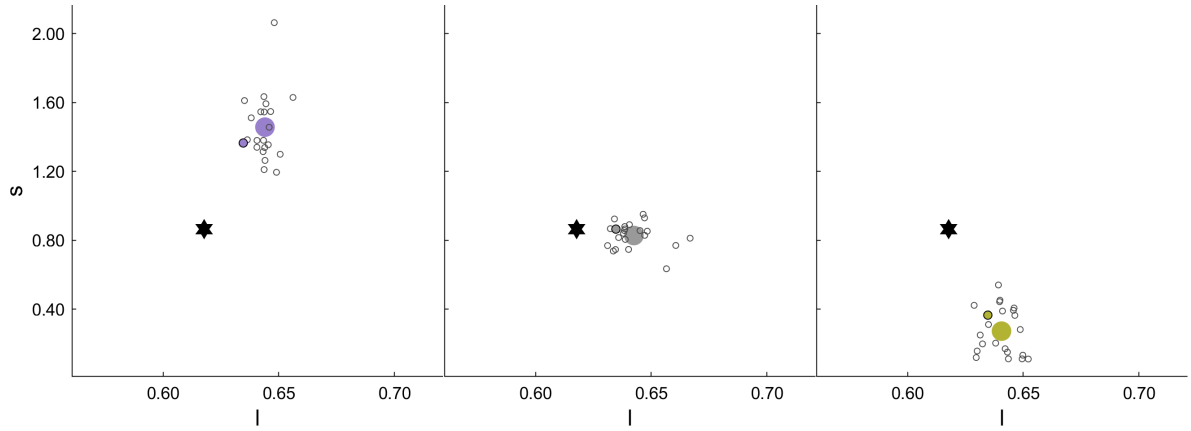

Figure A.4 Each matchings of the no-contour condition for the test lines on the cyan inducer

The other format is the same as in **Fig. 4.3** and **Fig. A.3.**

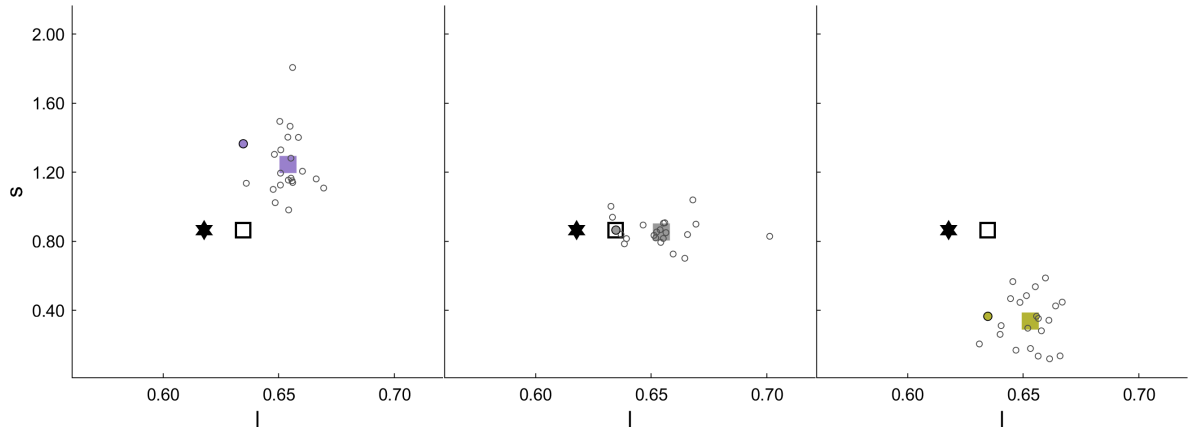

Figure A.5 Each matchings of the white-contour condition for the test lines on the cyan inducer

The other format is the same as in **Fig. 4.3** and **Fig. A.3.**

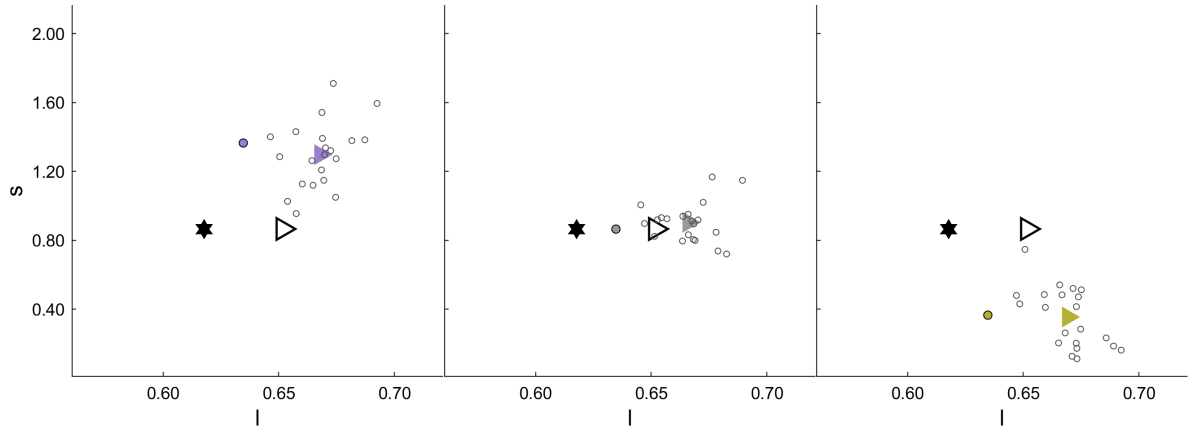

Figure A.6 Each matchings of the chromatic-contour condition for the test lines on the cyan inducer

The other format is the same as in **Fig. 4.3** and **Fig. A.3.**

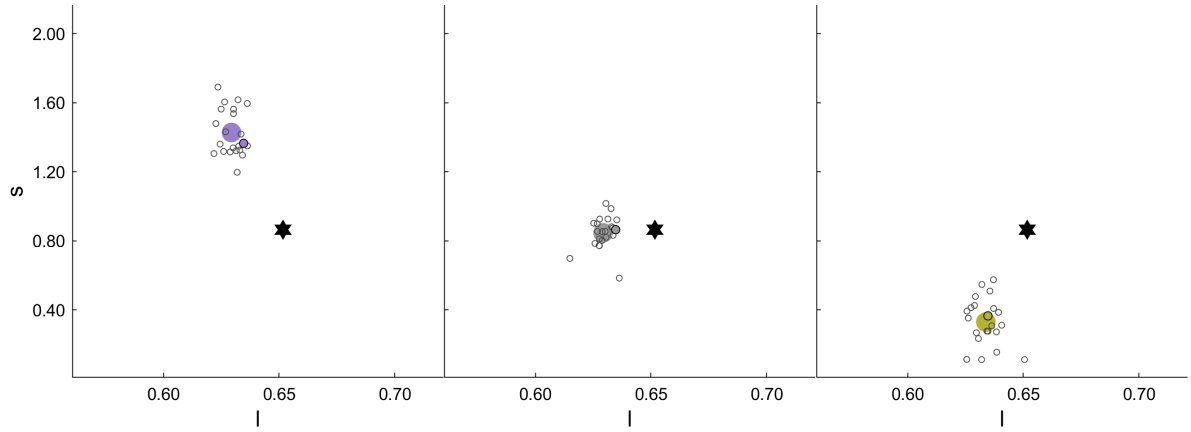

Figure A.7 Each matchings of the no-contour condition for the test lines on the red inducer

The other format is the same as in **Fig. 4.3** and **Fig. A.3.**

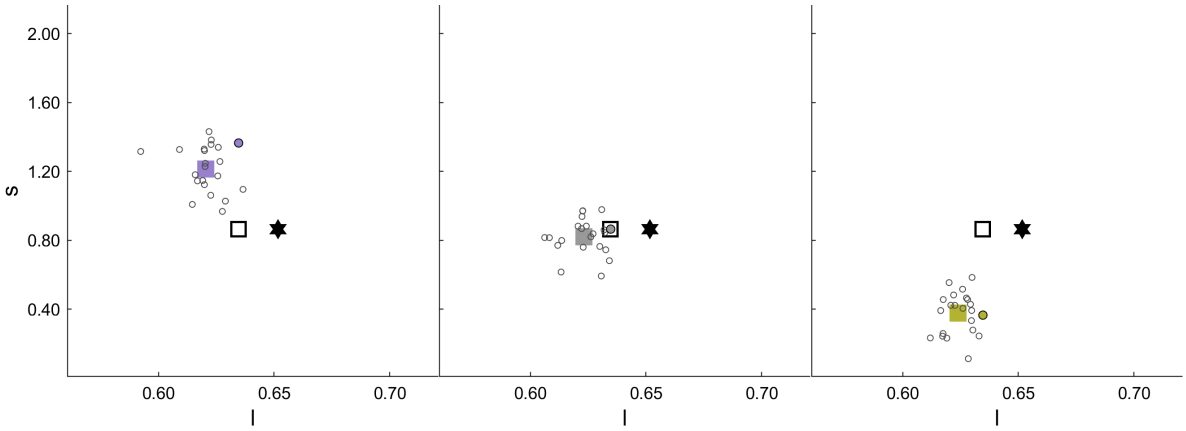

Figure A.8 Each matchings of the white-contour condition for the test lines on the red inducer

The other format is the same as in **Fig. 4.3** and **Fig. A.3.**

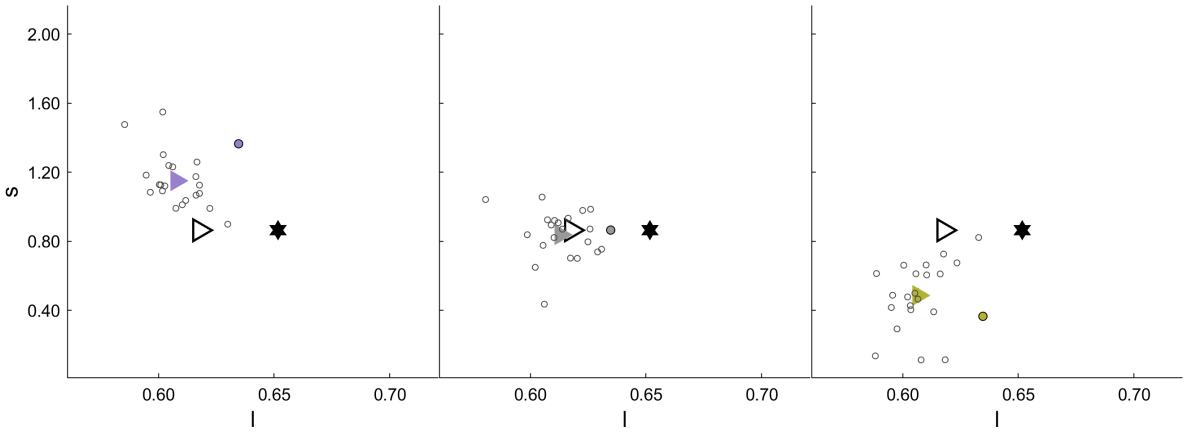

Figure A.9 Each matchings of the chromatic-contour condition for the test lines on the red inducer

The other format is the same as in **Fig. 4.3a**nd **Fig. A.3.**

Appendix B

Line width dependency

N/A responses

The participants were allowed to select the question mark if no suitable color existed on the palette or if they could not distinguish the color of the line (hereafter N/A response). **Fig. B.1** shows the number of N/A responses for all conditions. The maximum number of N/A responses was 2 (9.5% for the total responses; 21) for the dark-test line surrounded by a violet inducer. The N/A responses were frequently observed for the thin- and dark-test lines.

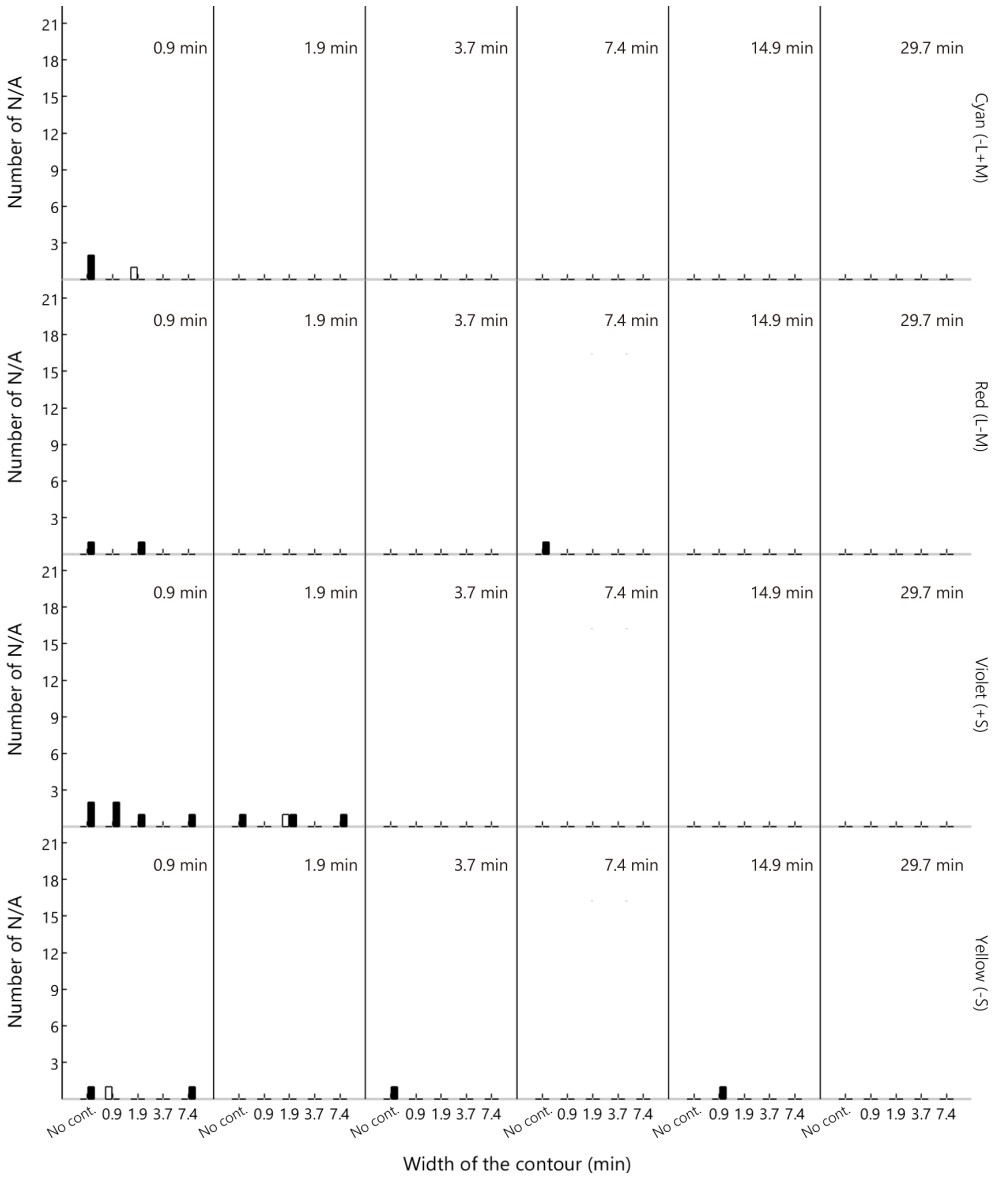

Figure B.1 The number of N/A responses

Panels are separated by the width of the test line from left to right (denoted in the upper right corner) and the color of the inducers from top to bottom (cyan, red, violet, and yellow). The horizontal axis indicates the width of the contour, and the vertical axis indicates the number of N/A responses. The white and black bars indicate the response for the pale- and dark-test lines, respectively.

Supplemental results

The matching and estimated artifacts are shown by the bubble plot in the main text. However, it is difficult to determine the specific value and variance of the bubble plot. Here, the data were plotted by the points for each width of the test line separately (**Fig. B.2** and **Fig. B.3**).

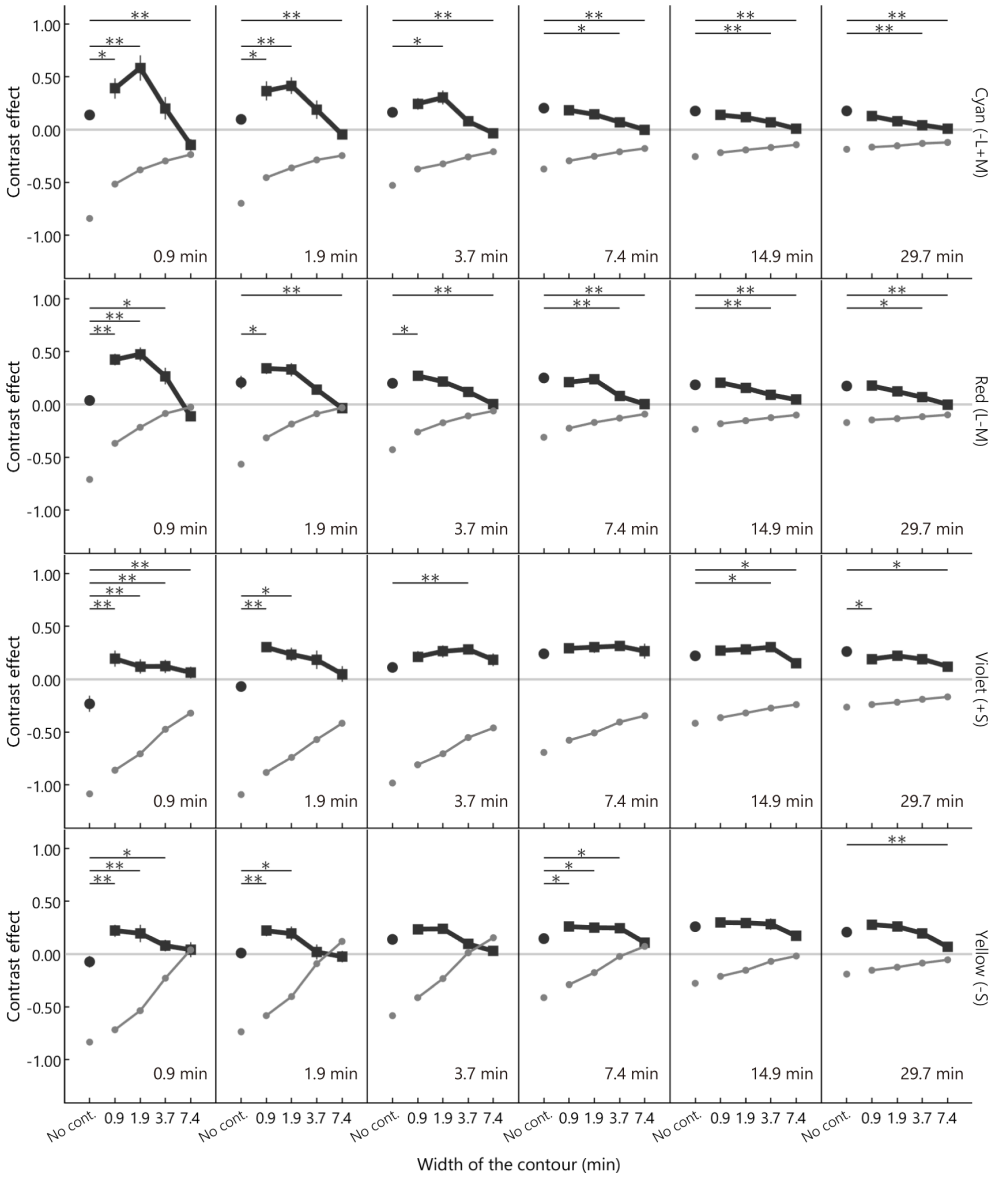

Figure B.2 The matching and the estimated artifact of the pale gray induced line

The horizontal axis of each panel indicates the contour width, which corresponds to the vertical axis in **Fig. 5.4** in the main text. The vertical axis indicates the contrast effect. The panels from left to right indicate the width of the test line. The thick square and circle indicate the matching of the contour and no-contour condition, respectively. Small gray dots indicate the estimated artifact. The error bar is the standard error of the mean. The asterisks indicate significant differences from the no-contour condition (**: p <0.01, * : p <0.05, sign test).

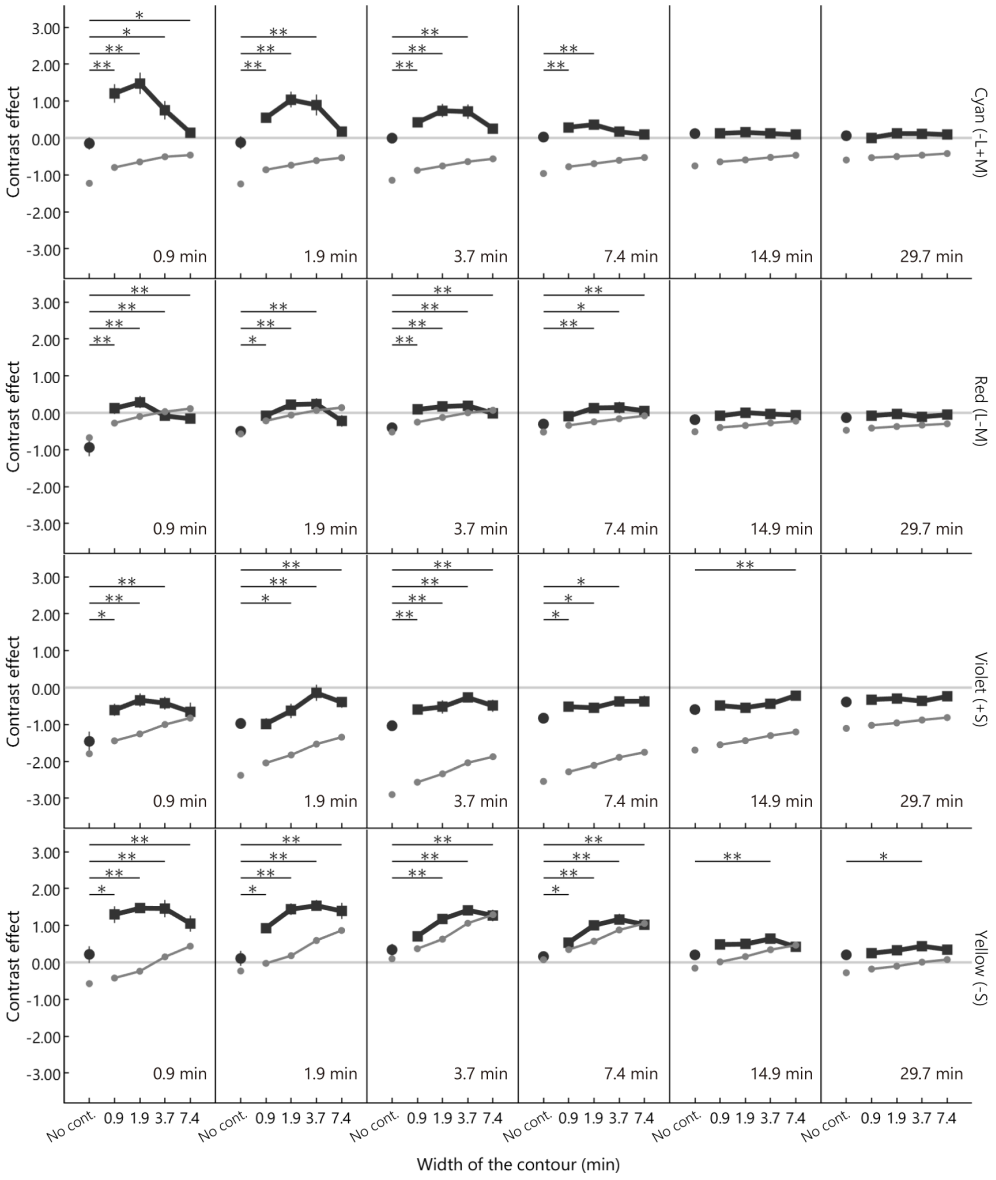

Figure B.3 The matching and estimated artifact of the dark-test line
The format is the same as that in **Fig. B.2.**

Statistics

Analysis of variance was performed on the within-subjects factor (ranova function, Statistics and Machine Learning Toolbox version 12.0, MATLAB R2020b, Mathworks). The complete results are shown in **Table B.1--Table B.4.**

Table B.1 Two way repeated measures ANOVA of Contour condition for the pale induced line (150 cd/m^2)

Inducer	Source	SS	df	MS	F	p
Cyan	Test-line width	2.58	5	0.52	6.87	0.00
	Contour width	7.30	3	2.43	34.44	0.00
	Test-line width x Contour width	3.30	15	0.22	7.25	0.00
	Error(Test-line width)	7.15	95	0.08		
	Error(Contour width)	4.03	57	0.07		
	Error(Test-line width x Contour width)	8.64	285	0.03		
Violet	Test-line width	1.25	5	0.25	5.24	0.00
	Contour width	0.84	3	0.28	4.98	0.00
	Test-line width x Contour width	0.50	15	0.03	1.06	0.40
	Error(Test-line width)	4.52	95	0.05		
	Error(Contour width)	3.19	57	0.06		
	Error(Test-line width x Contour width)	9.04	285	0.03		
Red	Test-line width	1.57	5	0.31	15.49	0.00
	Contour width	6.82	3	2.27	35.12	0.00
	Test-line width x Contour width	2.01	15	0.13	7.35	0.00
	Error(Test-line width)	2.02	100	0.02		
	Error(Contour width)	3.88	60	0.06		
	Error(Test-line width x Contour width)	5.46	300	0.02		
Yellow	Test-line width	1.31	5	0.26	3.11	0.01
	Contour width	2.67	3	0.89	18.48	0.00
	Test-line width x Contour width	0.44	15	0.03	1.06	0.39
	Error(Test-line width)	8.01	95	0.08		
	Error(Contour width)	2.75	57	0.05		
	Error(Test-line width x Contour width)	7.93	285	0.03		

SS: Sum of squares, df : degrees of freedom, MS: Mean squares

Table B.2 One way repeated measures ANOVA of No-contour condition for the pale induced line (150 cd/m^2)

Inducer	Source	SS	df	MS	F	p
Cyan	Test-line width	0.14	5	0.03	1.80	0.12
	Error(Test-line width)	1.61	100	0.02		
Violet	Test-line width	4.20	5	0.84	18.49	0.00
	Error(Test-line width)	4.54	100	0.05		
Red	Test-line width	0.56	5	0.11	4.99	0.00
	Error(Test-line width)	2.24	100	0.02		
Yellow	Test-line width	1.62	5	0.32	8.77	0.00
	Error(Test-line width)	3.69	100	0.04		

SS: Sum of squares, df : degrees of freedom, MS: Mean squares

Table B.3 Two way repeated measures ANOVA of Contour condition for the dark induced line (25 cd/m^2)

Inducer	Source	SS	df	MS	F	p
Cyan	Test-line width	45.40	5	9.08	17.16	0.00
	Contour width	16.46	3	5.49	11.02	0.00
	Test-line width x Contour width	18.78	15	1.25	5.43	0.00
	Error(Test-line width)	52.92	100	0.53		
	Error(Contour width)	29.88	60	0.50		
	Error(Test-line width x Contour width)	69.15	300	0.23		
Violet	Test-line width	2.64	5	0.53	1.47	0.21
	Contour width	5.16	3	1.72	3.96	0.01
	Test-line width x Contour width	7.47	15	0.50	1.79	0.04
	Error(Test-line width)	28.66	80	0.36		
	Error(Contour width)	20.87	48	0.43		
	Error(Test-line width x Contour width)	66.74	240	0.28		
Red	Test-line width	1.84	5	0.37	1.95	0.09
	Contour width	3.06	3	1.02	7.10	0.00
	Test-line width x Contour width	4.14	15	0.28	2.74	0.00
	Error(Test-line width)	17.94	95	0.19		
	Error(Contour width)	8.17	57	0.14		
	Error(Test-line width x Contour width)	28.69	285	0.10		
Yellow	Test-line width	66.26	5	13.25	27.35	0.00
	Contour width	10.12	3	3.37	11.44	0.00
	Test-line width x Contour width	6.84	15	0.46	1.83	0.03
	Error(Test-line width)	43.61	90	0.48		
	Error(Contour width)	15.92	54	0.29		
	Error(Test-line width x Contour width)	67.16	270	0.25		

SS: Sum of squares, df : degrees of freedom, MS: Mean squares

Table B.4 One way repeated measures ANOVA of No-contour condition for the pale induced line (25 cd/m^2)

Inducer	Source	SS	df	MS	F	p
Cyan	Test-line width	1.01	5	0.20	1.32	0.26
	Error(Test-line width)	13.77	90	0.15		
Violet	Test-line width	13.59	5	2.72	8.59	0.00
	Error(Test-line width)	28.48	90	0.32		
Red	Test-line width	5.24	5	1.05	6.05	0.00
	Error(Test-line width)	15.59	90	0.17		
Yellow	Test-line width	0.68	5	0.14	0.41	0.84
	Error(Test-line width)	31.85	95	0.34		

SS: Sum of squares, df : degrees of freedom, MS: Mean squares

Appendix C

Luminance dependency

Individual datas

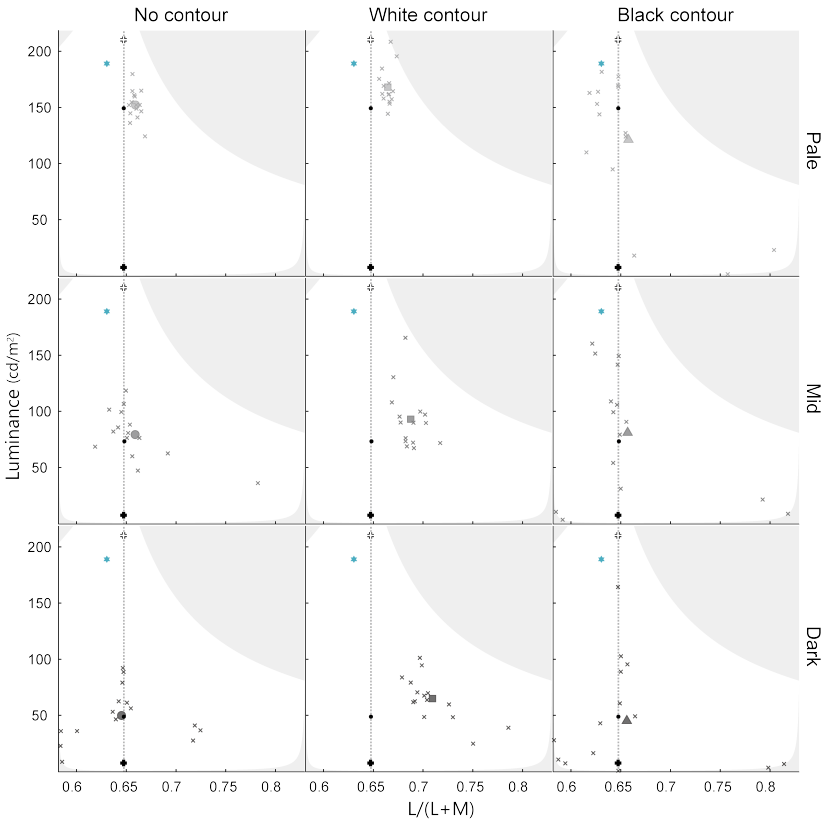

Figure C.1 Individual results of the appearance matching of the cyan inducer (5 observers × 3 repetitions).

Panels from left to right show the results of no-, white-, and black-contour conditions. Panels from top to bottom show the results of pale (150 cd/m^2), mid (75 cd/m^2), and dark (50 cd/m^2) test lines. Axes are the same as in figure 5E, F in the main text. The small black dot on the vertical line (D65) represents the levels of the test lines of the sample. The colored star represents the inducer of the sample. Small crosses represent each matching. Circles, squares, and triangles represent the mean of the no-, white-, and black-contour conditions, respectively. White and black crosses represent the color of the white and black contours of the sample stimuli, respectively.

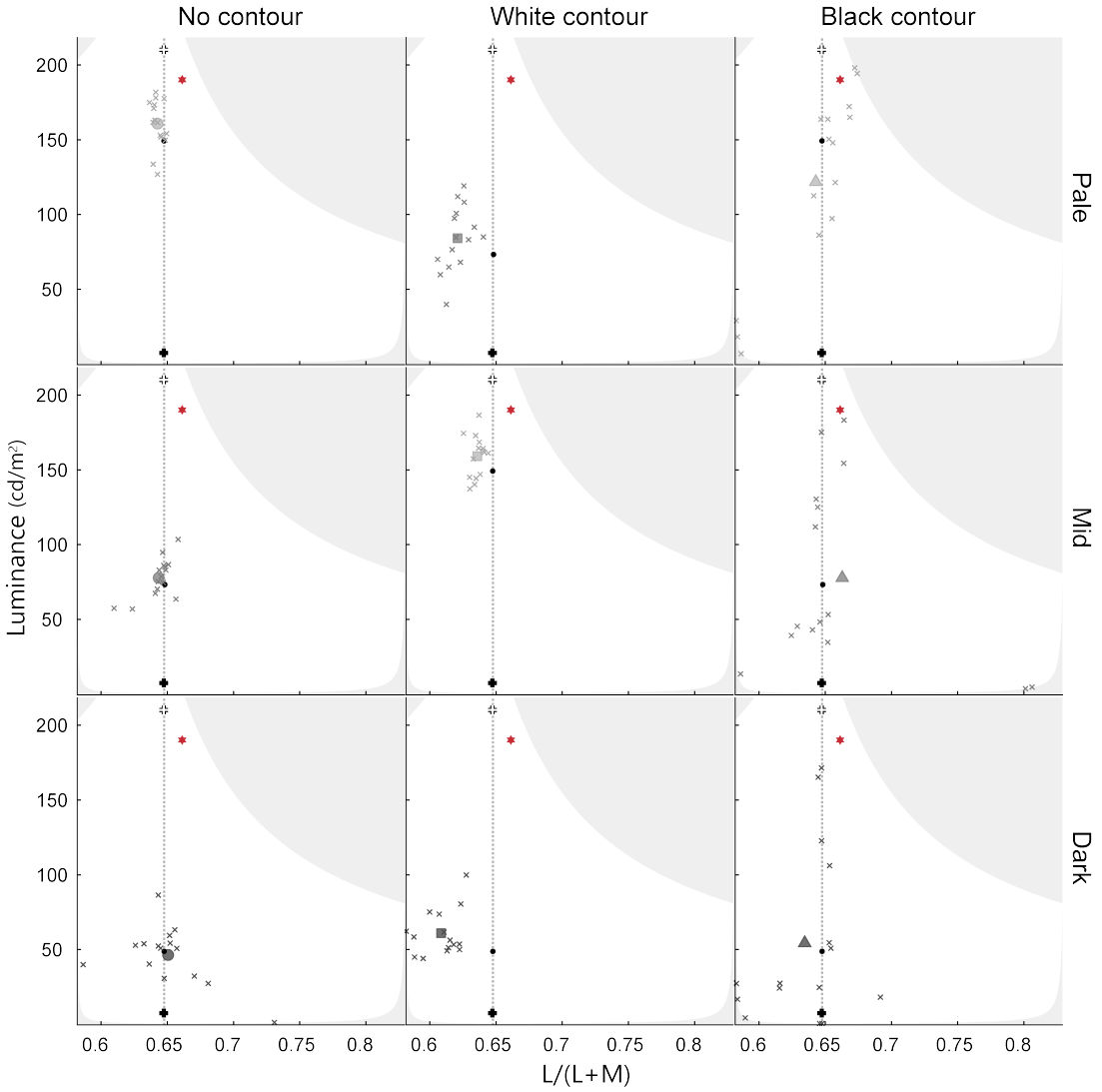

Figure C.2 Individual results of the appearance matching of the red inducer. The format is the same as **Fig. C.1.**

List of Research Results

• Publication

1. Tama Kanematsu & Kowa Koida, “Influence of stimulus size on simultaneous chromatic induction”, Frontiers in Psychology, 13, 818149, January 2022

2. Tama Kanematsu & Kowa Koida, "Large enhancement of simultaneous color contrast by white flanking contours", Scientific Reports, 10, 20136, November 2020

• Presentations in Conferences

3. Tama Kanematsu & Kowa Koida, Large color contrast effect induced by a thin white-gap; evidence for interaction between color and luminance, the 15th Asia-Pacific Conference on Vision (APCV 2019), PR0047, Osaka, Japan, August 2019, Poster

4. Tama Kanematsu & Kowa Koida, Remote simultaneous color contrast and assimilation effects across the L-M cone axis, The 25th symposium of the International Colour Vision Society (ICVS 2019), Poster#19, Riga, Latvia, July 2019, Poster

5. Tama Kanematsu & Kowa Koida, Large enhancement of simultaneous color contrast by surrounding white gap, but not by black gap, Vision Sciences Society 2019 Annual Meeting (VSS 2019), 63.306, Florida, USA, May 2019, Poster

6. Tama Kanematsu & Kowa Koida, Hyper color contrast illusion (HCC), large enhancement of simultaneous color contrast by bordering white line, The 24th symposium of the International Colour Vision Society (ICVS 2017), pp.34, Erlangen, Germany, August 2017, Aural

• Presentations in Japanese

7. 兼松圭 & 鯉田孝和、細かい輝度コントラストによる色情報の補完、日本視覚学会 2019 年冬季大会、3o03、東京、2019 年 1 月、 口頭

8. 兼松圭 & 鯉田孝和、白色境界線の付加による古典的色錯視からの色対比分離、日本視覚学会 2018 年夏季大会、2p05、茨城、2018 年 8 月、ポスター

9. 兼松圭 & 鯉田孝和、白色境界線の付加による色対比錯視の増強、日本視覚学会 2018 年冬季大会、3o02、東京、2018 年 1 月、口頭

• Awards

10. 兼松圭、2019 年度学生表彰 個人(学術研究活動)、豊橋技術科学大学

11. Tama Kanematsu, Student Travel Award, The 25th symposium of the International Colour Vision Society (ICVS 2019), Riga, Latvia, July 2019

12. 兼松圭、最優秀特別研究発表賞、修士研究発表会（豊橋技術科学大学大学院 情報・知能工学専攻)、2019 年 2 月

13. Tama Kanematsu & Kowa Koida, Worldwide Top 10 Finalist, "White + gray = red", Best

Illusion of the Year Contest 2018, Neural Correlate Society, December 2018

14. Tama Kanematsu, Student Travel Award, The 24th symposium of the International Colour Vision Society (ICVS 2017), Erlangen, Germany, August 2017

15. 兼松圭、最優秀特別研究発表賞、卒業研究発表会（豊橋技術科学大学 情報・知能工学課程)、2016 年 12 月